UNIVERSIDADE D
COIMBRA

Jorge Gabriel Oliveira Melo

Detection of Significant Blood Pressure Events in the Perioperative Care

VOLUME 1

Dissertação no âmbito do Mestrado Integrado de Engenharia Biomédica, orientada pelo Professor Doutor Paulo Fernando Pereira de Carvalho e apresentada ao CISUC/DEI.

Outubro de 2020

FACULDADE DE CIÊNCIAS E TECNOLOGIA
UNIVERSIDADE D COIMBRA

Jorge Gabriel Oliveira Melo

Detection of Significant Blood Pressure Events in the Perioperative Care

Dissertation submitted to the
University of Coimbra for the degree of
Master in Biomedical Engineering

Supervisors:
Prof. Dr. Paulo de Carvalho (CISUC/UC)
Prof. Dr. Jorge Henriques (CISUC/UC)
Dr. Jens Muehlsteff (Philips)

Coimbra, 2020

Resumo

Complicações cardíacas são comuns durante uma cirurgia, com uma estimativa de 30% dos pacientes submetidos a extensos procedimentos cirúrgicos devido à presença de comorbidades cardiovasculares e intervenções não cardíacas associadas a uma taxa de 7-11% de complicações, sendo que 42% dessas são causadas por problemas cardíacos. A hemodinâmica reflete a capacidade de perfusão de oxigénio e nutrientes em todos os órgãos, a fim de manter as funções orgânicas ideais e evitar complicações. Uma técnica fundamental para avaliação hemodinâmica é a monitorização da pressão arterial (PA), que pode ser realizada de forma invasiva com cateter arterial ou não invasiva com uma braçadeira. As técnicas invasivas fornecem monitorização contínua da PA "batimento a batimento", leituras precisas da PA em baixas pressões e formas de onda de pressão de pulso, mas são caras, demoradas e precisam de um operador treinado. Enquanto isso, os métodos baseados na braçadeira fornecem medições intermitentes (com intervalos de alguns minutos a várias horas) de pressão arterial sistólica (PAS), diastólica (PAD) e média (PAM) e são associadas à subestimação dos valores da PA hipertensiva e superestimação da PA hipotensiva, mas são baratos e fáceis de empregar. Na verdade, a monitorização intermitente da PA é realizada mesmo em pacientes gravemente doentes sob certas circunstâncias, como falta de equipamento técnico ou equipa clínica.
Sendo assim, este estudo aborda a oportunidade para o desenvolvimento de soluções de monitorização de PA contínuas e não invasivas com base em métricas relacionadas com a PA, como o tempo de chegada de pulso (PAT), que podem fornecer estimativas de PA em tempo real, sendo fáceis de empregar e exigindo apenas tecnologias amplamente disponíveis, como a fotopletismografia (PPG) e eletrocardiografia (ECG).
Os dados adquiridos de 9 pacientes submetidos a cirurgias cardíacas ou neurológicas incluem PA invasiva e sinais de ECG e PPG. Três modelos de regressão baseados nas equações de Moens-Korteweg e Bramwell-Hill são estudados e métodos para calibração sistemática são analisados. Os resultados são comparados com a PA (invasiva) e a amostragem intermitente dos valores originais da PA arterial como um processo de retentor de ordem zero (ZoH) para simular métodos baseados na braçadeira sem quaisquer erros comumente associados. Além disso, é proposta uma solução para amostragem não uniforme da PA, baseada na variabilidade da PA com o objetivo de aumentar a frequência de amostragem da PA quando a PA é instável e diminuir caso contrário. Os resultados sugerem que o uso de modelos de regressão, o modelo MK-BH mais especificamente, com um procedimento de amostragem e calibração uniforme com um intervalo de 5 minutos melhoraria muito a monitorização da PA no ambiente intraoperatório em comparação com o ZoH contra a PA "real", resultando numa redução do desvio padrão do erro e do erro absoluto médio de até 50% para a PAS. Estas melhorias tornam-se mais expressivas quando olhamos para os 5% e 1% maiores erros absolutos com uma redução de mais de 50%.

Em relação à abordagem de amostragem de PA não uniforme, pode-se identificar ligeiras melhorias nos modelos de regressão alimentados por essas amostras de PA para calibração em termos de ME ± SD e MAE em comparação com a amostragem e calibração uniforme anterior de 5 minutos. Olhando para os maiores 5% e 1% erros absolutos, a melhoria é visível para o modelo MK-BH, que melhora os maiores 1% de erros absolutos em até 30%, enquanto o ZoH melhora em até 30% para ambos.

Por último, um algoritmo para detecção e classificação de eventos rápidos de PA é proposto com base em métricas indiretas relacionadas com a PA. O algoritmo analisa os últimos 5 minutos de monitorização em cada instante e classifica como nenhum evento, evento pequeno, evento médio ou evento grande. Os resultados sugerem o potencial de desenvolvimento de uma ferramenta semelhante com base em métricas indiretas de avaliação da PA, a fim de criar um procedimento de amostragem de BP não uniforme e otimizado.

Abstract

Cardiac complications are common during a surgery, with estimated 30% of patients undergoing extensive surgical procedures in the presence of cardiovascular comorbidities and non-cardiac interventions being associated with 7-11% of complication rate while 42% of these are caused by cardiac issues. Hemodynamics reflect the ability for perfusion of oxygen and nutrient to all organs in order to maintain optimal organ functions and avoid complications. One fundamental technique for hemodynamics evaluation is the arterial blood pressure (BP) monitoring, which can be performed invasively with an arterial catheter or non-invasively with cuff-based methods. Invasive techniques provide continuous "beat-to-beat" BP monitoring, accurate BP readings at low pressures and pulse pressure waveforms, but are expensive, time-consuming and need a trained operator. Meanwhile, cuff-based methods provide intermittent measurements (from a few minutes to several hours intervals) of systolic (SBP), diastolic (DBP) and mean (MAP) arterial pressure, and are associated with underestimation of hypertensive BP values and overestimation of hypotensive BP, but are cheap and easy to employ. In fact, intermittent cuff-based BP monitoring is performed even in critically ill patients under certain circumstances, such as lack of technical equipment or clinical staff.

Being so, this study addresses the opportunity for development of non-invasive BP monitoring solutions based on BP surrogates such as the pulse arrival time (PAT) that might provide real-time BP estimations while being easy to employ and only requiring widely available technologies such as photoplethysmograpy (PPG) and electrocardiography (ECG).

Data acquired from 9 patients undergoing cardiac or neuro surgeries include invasive arterial BP, PPG and ECG signals. Three regression models based on Moens-Korteweg and Bramwell-Hill equations are studied and methods for systematic calibration are analyzed. Results are compared with ground truth BP (invasive) and intermittent sampling from the original arterial BP values as a zero-order hold (ZoH) process in order to simulate cuff-based methods without any commonly associated errors. Furthermore, a solution for non-uniform BP sampling is proposed, based on BP variability aiming to increase BP sampling frequency when BP is unstable and decrease otherwise. Results suggest that the use of regression models, the MK-BH model more specifically, with a uniform 5 minutes interval BP sampling and calibration procedure would highly improve the BP monitoring in the intraoperative environment comparing with the ZoH against ground truth BP, resulting in a reduction of the standard deviation of the error and the mean absolute error up to 50% for the SBP. These improvements become more expressive when one looks at the top 5% and 1% absolute errors with a reduction of more than 50%.

Regarding the non-uniform BP sampling approach, one could identify slight improvements from the regression models using these BP samples for calibration in terms of ME $\pm$ SD and MAE

comparing with the previous uniform 5 minutes BP sampling and calibration. Looking at the top 5% and 1% absolute errors, the improvement is visible for the MK-BH model which improves the top 1% absolute errors up to 30%, while the ZoH improves up to 30% for both top 1% and 5% absolute errors.
At last, an algorithm for fast BP events detection and classification is proposed based on BP surrogates. The algorithm analyzes the last 5 minutes of monitoring at each time instance and classifies it as no event, small event, medium event or large event. The results support the potential for developing such tool based on BP surrogates in order to create a non-uniform BP sampling procedure.

Acronyms

5-CV 5-fold Cross Validation.

ABP Arterial Blood Pressure.
ACE Angiotensin-converting Enzyme.
Ach Acetylcholine.
ADH Antidiuretic Hormone.
AI Augmentation Index.
ANS Authonomic Nervous System.
AoP Aortic Pressure.
AV Atrioventricular.

CCC Cardiovascular Control Centers.
cNIBP Continuous Non-Invasive Blood Pressure.
CNS Central Nervous System.
CO Cardiac Output.

DBP Diastolic Blood Pressure.

E Epinephrine.
ECG Electrocardiogram.

FT Feature.

HR Heart Rate.

ICG Impedance Cardiography.
ICU Intensive Care Unit.

LAP Left Atrial Pressure.
LDA Linear Discriminant Analysis.
LVET Left Ventricular Ejection Time.
LVP Left Ventricular Pressure.
LVV Left Ventricular Volume.

MAE Mean Absolute Error.

MAP Mean Arterial Pressure.

ME Mean Error.

MLR Multinomial Logistic Regression.

NE Norepinephrine.

NIBP Non-Invasive Blood Pressure.

NO Nitric Oxide.

OR Operative Room.

PAT Pulse Arrival Time.

PEP Pre-Ejection Period.

PNS Parasympathetic Nervous System.

PPG Photoplethysmography.

PTT Pulse Transit Time.

PWV Pulse Wave Velocity.

RAA Renin-Angiotensin-Aldosterone.

RI Reflection Index.

SA Sinoatrial.

SBP Systolic Blood Pressure.

SD Standard Deviation.

SI Stiffness Index.

SNS Sympathetic Nervous System.

ThR Threshold.

TVR Total Vascular Resistance.

VSMCs Vascular Smooth Muscle Cells.

ZoH Zero-order Hold.

List of Figures

List of Tables

Contents

1

Introduction

This thesis addresses the problem of evaluation of the cardiovascular function in the operative room (OR) and intensive care unit (ICU) covering the perioperative care and later focusing in the intraoperative period and the blood pressure monitoring using non-invasive techniques. Several surrogates were extracted from electrocardiograms (ECG) and photoplethysmograms (PPG) from patients during surgical interventions and their capability of describing changes in the cardiovascular system function is analyzed. State-of-the-art models for blood pressure estimation from surrogates are analyzed and, finally, an algorithm for blood pressure events detection is proposed.

1.1 Motivation

Recent studies show that major operations worldwide happen at the pace of 4% of the global population annually. Estimated 30% of patients undergo extensive surgical procedures when cardiovascular comorbidities are present. Non-cardiac interventions are associated with 7-11% complication rate while 42% of those are caused by cardiac complications. Regarding to Europe, these numbers translate into at least 167 000 cardiac complications annually because of non-cardiac surgical procedures, of which 19 000 threat lives [72]. The cardiovascular homeostatic state is what clinicians commonly define as hemodynamics and reflects the ability for perfusion of oxygen and nutrients to all organs so that optimal organ functions are maintained and complications are avoided. Hemodynamic instability is recognized to create a crucial impact in surgical patient's outcome, ultimately resulting in an increase of organ failures and mortality rates [3, 4]. Monitoring hemodynamic variables during surgeries enables clinicians to identify any organ disfunction which can be correlated with a surgical procedure or patient's comorbidities. It's known that a proactive hemodynamics management strategy within the perioperative period may reduce morbidity and mortality for high-risk surgical patients [53].

Traditional hemodynamic evaluation includes the simplest form of monitoring: the health care professionals inspect the patients to see if they are conscious, agitated or in distress, breathing regular or labored, in presence or absence of central and peripheral cyanosis; touching of the skin of a patient to notice if it's cool and moist, and if capillary refill is quick or not; palpation of the central and peripheral pulses to evaluate rate and firmness [128]. Other evaluation metrics include arterial blood pressure (ABP), heart rate (HR), pulse oximetry, central venous oxygen saturationand lactate concentration [116]. A survey from 2011 revealed that most of the anesthesiologists from USA and Europe agree that their current hemodynamic management could be improved, stating that their institutions lack written protocols, care guides or statements concerning the hemodynamic management [17]. Also, this survey reveals that the majority of the anesthesiologists try to

optimize the patient's arterial blood pressure (ABP) during most of high-risk surgeries. In fact, ABP monitoring is the most common hemodynamic evaluation measure in acutely or critically ill patients, but there are several alternative ways to try and do it and therefore the clinician choice has direct impact in the clinical decision-making and also the patient's surgical outcomes. The clinical reference method for BP monitoring in high-risk surgical and critically hill patients is the continuous invasive ABP measurement using an arterial catheter (A-line) because it detects almost twice as much intraoperative hypotension episodes than intermittent non-invasive measurements using oscillometry and triggers vasopressor therapy in adults having non-cardiac surgery [112]. Although it's considered the gold standard for ABP measurements, this technique has it's pitfalls and is just recommended if there's a requirement for continuous BP monitoring, impracticality of non-invasive BP measurements, the necessity for repeated arterial blood sampling or more advanced invasive hemodynamic monitoring (pulse wave analysis, transpulmonary thermodilution) [148]. Intermittent non-invasive measurements using oscillometry are easy to undertake but are related to BP overestimation during hypotension episodes and underestimation during hypertension episodes [181].
A non-invasive, continuous and reliable BP measuring device would help monitor patients without pain and the risk of infection in emergency situations like an accident, in ambulance transfer or within the emergency room. It could also be applied safely and easily to patients undergoing surgery, and moreover, it might be especially beneficial for unconscious patients under continuous monitoring for an extended period by reducing infection. For this reason, photoplethysmograph-based, ultrasound-based, and tactile-sensor-based approaches are under investigation, but further development is required in order to enable this technology to be reliable, accurate and user-friendly [109].

1.2 Contributions and Relevance

This thesis is focused on the analysis of different continuous non-invasive BP inference algorithms based on BP surrogates during intraoperative care compared with A-line measurements (ground truth) and intermittent BP sampling. The studied algorithms are based on the analysis of non-invasive signals that are affordable and commonly used in hospital care, such as ECG and PPG. The extraction of cardiovascular parameters in a continuous basis (beat-by-beat) is a fundamental requisite of the present thesis, as well as the robustness of the proposed algorithms in highly unstable patients undergoing critical surgical interventions (e.g.: cardiac surgeries). This work analyzes cardiovascular parameters known to characterize the chronotropic (heart rate - HR), inotropic (left ventricular ejection time - LVET), vascular tone and blood pressure (pulse arrival time - PAT, stiffness index – SI – and reflection index - SI, respectively).
Since most of the recently proposed algorithms in the literature are highly complex, not available for simple implementation and require further testing in order to validate the results, it was chosen to evaluate the most simple non-invasive continuous BP (cNIBP) estimation algorithms based on the pulse wave velocity. Given that these models only monitor the velocity at which the blood pressure pulse propagates through the arterial systemic circulation and this parameter is influenced by only some of the mechanisms that regulate the peripheric BP, re-calibration is required. Different re-calibration process definitions are tested, from simple fixed interval re-calibration to dynamic re-calibration based on BP variability.
In the current dissertation, an approach for cNIBP monitoring in the OR is proposed based on

the detection of BP events using BP surrogates (e.g.: pulse arrival time), defined as fast and wide BP changes, that trigger BP samples (e.g.: cuff measurements). The proposed algorithm provides a personalized and dynamic solution for NIBP monitoring that adapts to each patient condition at any time, increasing the sample rate (e.g.: BP sampling) in the presence of BP events and avoiding unnecessary measurements when BP is steady. This solution would improve both patient's comfort (in the absence of significant BP changes) and NIBP monitoring, including earlier detection of critical events. At last, combining the events detection algorithm with known cNIBP estimation algorithms highly improves their performance, opening doors for future clinical applications.

1.3 Dissertation Outline

The content of this dissertation is organized as follows: Chapter 2 describes the anatomy and physiology of the different human mechanisms involved in hemodynamic regulation. Starting by describing the different structures of the cardiovascular system, including the heart and blood vessels and finishing with known multi-system interactions that influence hemodynamics, outlining the complexity of these interactions is the main focus of this dissertation.
Chapter 3 consists of a review of hemodynamic management in critical care, more specifically the blood pressure monitoring in the operative room. It starts with an analysis of the difficulties for defining BP targets for different patients in different settings exposed by several clinicians and is followed by an overview of different blood pressure techniques, from invasive to non-invasive. It ends with the presentation and detailed description of different proposed BP surrogates obtained non-invasively using PPG and ECG signals.
Chapter 4 analyzes different BP surrogates and how simple regression models based on PWV would perform under critical circumstances like the operative room with patients undergoing cardiovascular or neuro surgeries. The process of calibration is described and the impact of different BP sampling intervals for calibration is addressed against ground truth BP (invasive) and intermittent sampling. A non-uniform BP sampling strategy based on BP variability categorization is proposed and the results improve.
Chapter 5 proposes an algorithm for fast events detection based on the variability of BP surrogates, using a multinomial logistic regression that fits the input data to the BP variability categories defined previously. The results suggest the potential to use BP surrogates in order to create an optimized non-uniform BP sampling technique that improve the BP monitoring in clinical practice.

2

Physiological Background

In order to grasp the issue of hemodynamics monitoring and management, one needs to fully understand the cardiovascular system and how different mechanisms affect the cardiovascular function. In this chapter the anatomy and physiology of this system is described.

2.1 The Cardiovascular System

The cardiovascular system consists of the heart and the circulatory system. The heart acts as an efficiently designed pump that pushes the blood through a complex network of arteries, arterioles and capillaries up to the organs, tissues, and cells of the body in order to meet it's hematologic requirements. The heart is actually divided in two separate pumping systems that throw blood into the systemic and pulmonary circulation. The right side of the heart receives oxygen-poor blood (venous blood) from the superior and inferior vena cava and pumps it with the right ventricle to the lungs, where the gas exchanges between the blood and alveoli takes place. The oxygen-rich blood (arterial blood) comes back to the heart, through the pulmonary veins and the pulmonary circulation is completed. The systemic circulation starts with the contraction of the left ventricle that pumps the blood into the aortic artery. The systemic circulation supplies the oxygenated blood to all tissues of the body and picks up carbon dioxide and waste products from the cells activity. The venous blood comes back to the right side of the heart and this process repeats. The Figure 2.1 illustrates the aforementioned processes.

2.1.1 Heart and Its Electro-Mechanical Activity

The heart is a cavernous, muscular organ consisting of 4 chambers: the right atrium, that receives blood from the veins and pumps it to the right ventricle, the right ventricle, that receives blood from the right atrium and pumps it to the lungs, where it is charged with oxygen; the left atrium receives oxygenated blood from the lungs and pumps it to the left ventricle; and the left ventricle (the strongest chamber) pumps oxygen-rich blood to the rest of the body. The left ventricle's strong contractions create our blood pressure. [59]
One-way valves situated at the entrance and exit of both ventricles channel the blood circulation in the correct direction. The atrioventricular valves are situated at the entrance of the right and left ventricles (the tricuspid valve and mitral (bicuspid) valve, respectively) and are mainly accountable for the flow of blood from the atria to the ventricles during diastole and shut during the beginning of the systolic contraction, producing the known first heart sound. The semilunar valves are located at the outlet of the right and left ventricles (pulmonic and aortic valves, respectively)

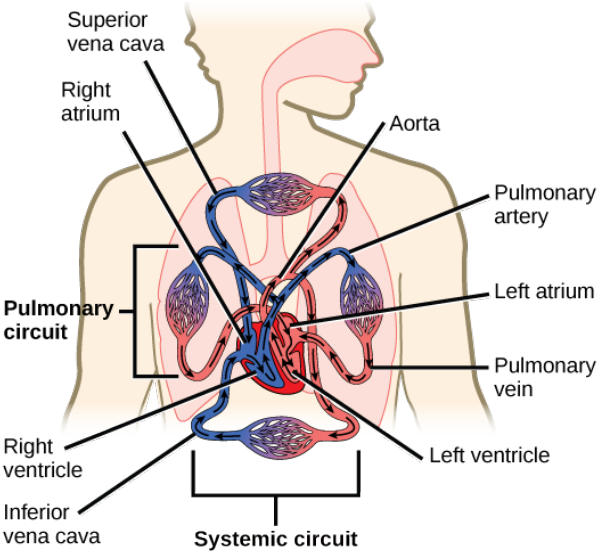

Figure 2.1: Illustration of systemic and pulmonary circuits. Adapted from [117]

and are mainly accountable for the flow of blood to the outside of the heart during systole and close during the beginning of the ventricular relaxation (diastole), creating the second heart sound. These valves open and close in response to pressure changes inside and outside the ventricles and play an important role in preventing blood regurgitation to the atria and ventricles. [94]
The coronary arteries run along the surface of the heart and provide oxygen-rich blood to the heart muscle. A web of nerve tissue also runs through the heart, conducting the complex signals that govern contraction and relaxation. Surrounding the heart is a sac called the pericardium. [182]

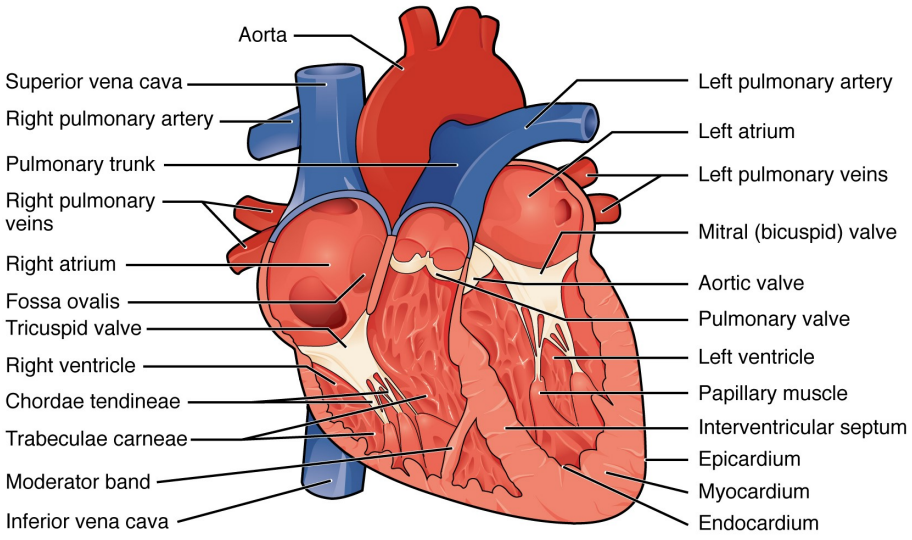

Figure 2.2: Illustration of the anatomy of the heart that shows the four chambers, the major vessels and their early branches, as well as the valves. From [117]

The cardiac muscle has the particular ability to induct an electrical potential at a fixed rate that propagates quickly from cell to cell to trigger the contractile mechanism - known as autorhythmicity. Although it's called autorhythmicity, the heart rate is, in fact, modulated by the endocrine and nervous systems. Two main types of cardiac muscle cells compose the heart tissue: myocardial contractile cells and myocardial conducting cells. The myocardial contractile cells represent 99% of the cells in the atria and ventricles. As the name suggests, this cells are responsible for producing impulses and contractions that pump blood into the arteries. The myocardial conducting cells act similarly in many aspects to neurons, although they're specialized muscle cells, forming the conduction system of the heart. These cells are responsible for starting and conducting the electrical impulse (action potential) that propagates throughout the heart and triggers the contractions.
The cardiac conduction system includes the sinoatrial (SA) node, the atrioventricular (AV) node, the AV bundle, the AV bundle branches, and the Purkinje fibers.

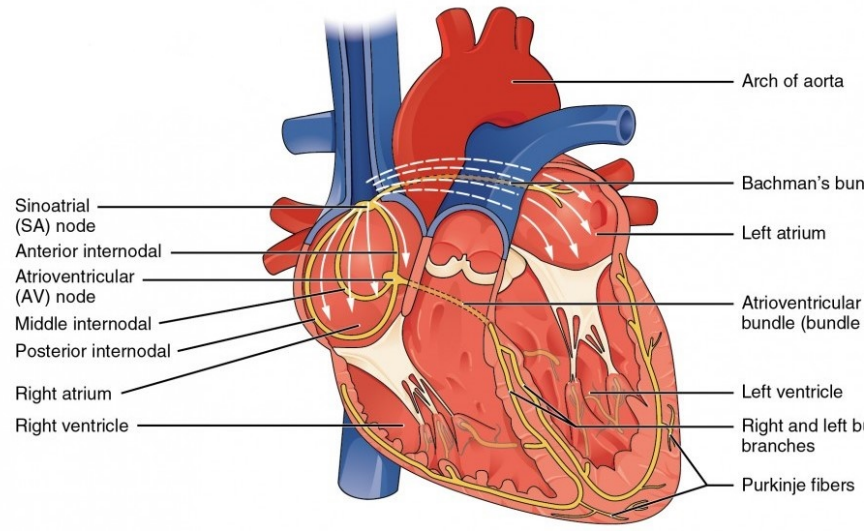

Figure 2.3: Illustration of the anatomy of the heart with specialized conducting components including the sinoatrial node, the internodal pathways, the atrioventricular node, the atrioventricular bundle, the right and left bundle branches, and the Purkinje fibers. Adapted from [1]

The SA node consists of a clump of specialized myocardial conducting cells found in the superior and posterior walls of the right atrium near the cavoatrial junction. The SA node has the highest inherent rate of depolarization and is recognized as the pacemaker of the heart. It initiates the standard electrical pattern followed by the contraction of the heart [117]. The impulse is transmitted throughout the atria by specialized internodal pathways, to the atrial myocardial contractile cells and reaches the atrioventricular node. The connective tissue of the cardiac skeleton prevents the impulse from spreading into the myocardial cells in the ventricles except at the AV node. Additionally, a specialized pathway called Bachmann's bundle or interatrial band leads the impulse directly from the right atrium pathway to the left atrium.[117]
The AV node also consists of a bunch of specialized myocardial conductive cells, located in the inferior portion of the right atrium within the atrioventricular septum, that provoke a delay in the electric impulse transmission. This pause before the AV node depolarizes and conducts the signal to the atrioventricular bundle is fundamental to the heart activity, because it allows the atrial cadiomyocytes to complete their contraction that pumps blood into the ventricles before the

impulse is transmitted to the cells of the ventricle. [117]
The impulse is then conducted by the AV bundle, or bundle of His, throughout the interventricular septum before dividing into two branches that supply each ventricle. These branches reach the apex of the heart and link with the Purkinje fibers, which are accountable for propagating the impulse from the myocardial conductive fibers to the myocardial contractile cells. These cells cover the inner ventricular walls of the heart and transmit the impulse from the apex of the heart, progressing upwards to eject blood into the great arteries.

Pressure and volume variations inside the heart are some of the most relevant characteristics when analyzing the cardiac muscle physiology. Systole (contraction and ejection) and diastole (relaxation and filling) are the main stages of the cardiac cycle. These mechanical events are accountable for pressure fluctuations inside the ventricles, which cause the heart valves to open and the blood to flow from high to low-pressure areas. Thus, we can describe the cardiac cycle by monitoring changes in pressure and volume inside each heart chamber. Figure 2.4 represents the cardiac cycle of the left part of the heart in terms of ventricular volume (LVV), ventricular pressure(LVP), atrial pressure (LAP) and aortic pressure (AoP) as a function of time. It also correlates with electrocardiogram (ECG) and phonocardiogram (PCG) signals and known events.

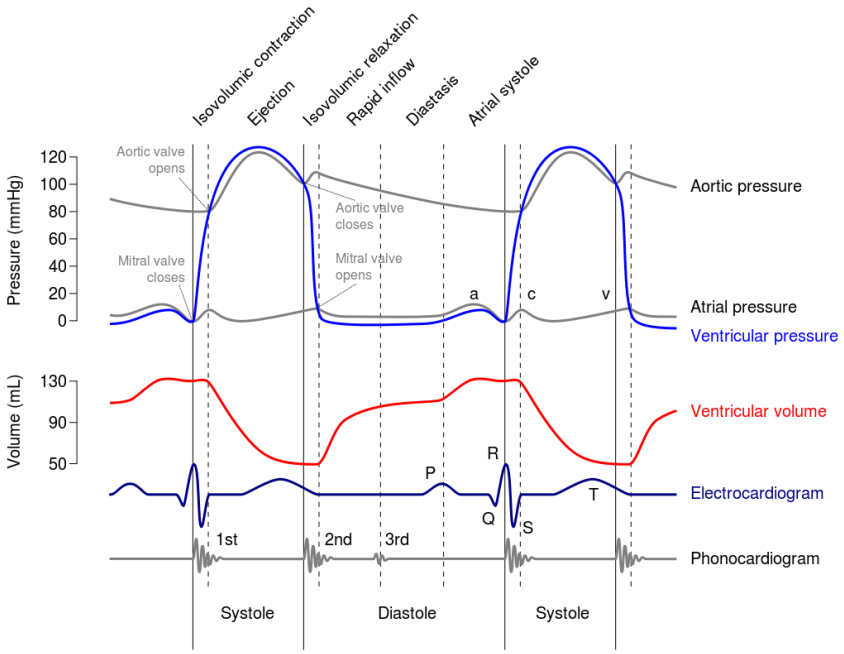

Figure 2.4: Wiggers Diagram, showing the cardiac cycle events occurring in the left atria and left ventricle. Adapted from [20]

During the filling stage, the LVP and LVV are relatively uniform and AoP is gradually decreasing. Meanwhile, the heart is in its relaxed state (diastole); The isovolumic contraction initiates with the electrical impulse arriving to the ventricles and pressure increases within the chamber. Early after contraction starts, LVP increases to be bigger than the left atrial pressure and the mitral valve closes. Since LVP is less than AoP, the aortic valve keeps itself closed. As the name suggests, during this phase the ventricle is contracting isovolumically (i.e., at a constant volume). Eventually, LVP surpasses AoP and the aortic valve opens. The ejection phase begins and blood is pumped from the

ventricle into the aorta and LVV decreases. While the contraction process of the cardiac muscle gets to its maximal effort, ejection slows down and ultimately, as the muscles begin to relax, LVP drops below AoP provoking the aortic valve to close and initiating the isovolumic relaxation phase. During this stage all valves are closed and LVP drops owing to the repolarization. Eventually, LVP drops below LAP and the mitral valve opens, initiating the filling stage again and the process repeats [117].
Another way for visualizing these events is to display LVP as a function of LVV on a "pressure-volume loop diagram" (presented in Figure 2.5). The same mechanical events previously described are represented in this diagram.

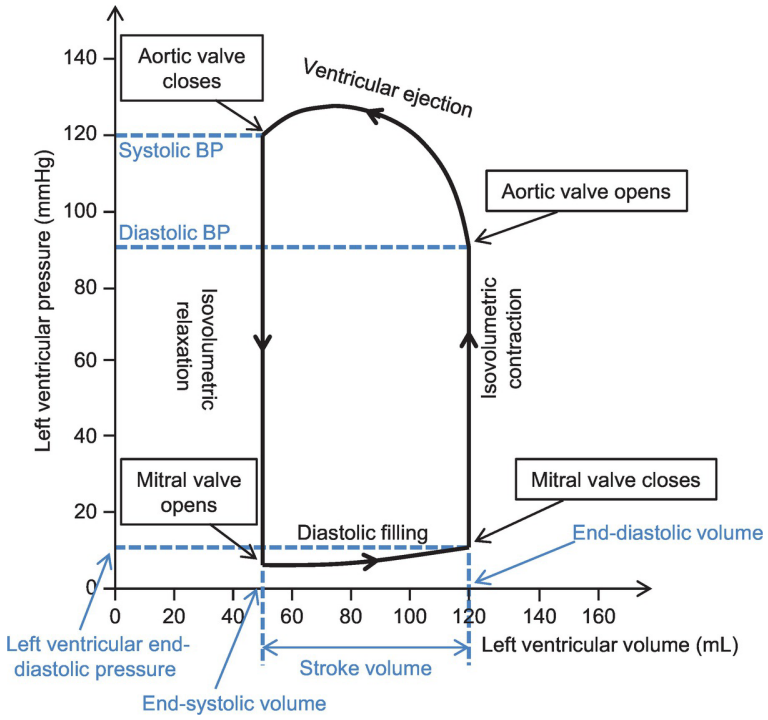

Figure 2.5: The left ventricular pressure–volume loop through the cardiac cycle. Adapted from [20]

2.1.2 Blood Vessels and the Arterial Blood Pressure Waveform

Blood vessels are the channels through which blood flows until it reaches body tissues. These vessels make up two closed systems of tubes that start and finish in the heart. The pulmonary circulation transports blood from the right ventricle to the lungs and back to the left atrium and the systemic circulation carries blood from the left ventricle to the tissues in all parts of the body and back to the right atrium. Based on their structure and function, blood vessels are classified as arteries, capillaries or veins.
The systemic circulation starts with the aorta artery at the exit of the left ventricle and branches into smaller arteries along the path until the branching results in microscopic arteries called arterioles. Arterioles play a key role in regulating blood flow into the tissue capillaries. Capillaries are the smallest and most numerous of the blood vessels and form the connection between the vessels that bring blood from the heart (arteries) and the vessels that return blood to the heart (veins). Their primary function is the exchange of gases and materials between the blood and tissue cells.

Veins carry blood towards the heart after it passes through the capillaries. The smallest ones are called venules and from here, blood flows into progressively larger veins until it reaches the heart through the superior and inferior vena cava.
The achievement of the primary functions of the circulatory system is guaranteed by anatomical arrangements of the vasculature and by control mechanisms that act directly in the vessels, including local, neural and humoral mechanisms. They can work independently of each other, but there are also interactions among them. These systems will be further described in more detail.

Every heartbeat creates an impact with the stroke volume ejected into the arteries, that create a wave of vascular distention and results in the arterial pulse wave. The wave is reflected back mostly by the arteriole, which provides the majority of the peripheral vascular resistance [120]. Peak aortic blood flow acceleration produces the initial rise of the pressure pulse, while the ejection of the ventricular volume fills out and upholds the pulse waveform [105]. Understanding the arterial blood pressure waveform from the central arterial tree to the periphery has been the focus of several studies [15, 134, 164, 177, 88, 68, 78, 169, 75].
Studies [169, 75, 78] confirmed the existence of two major reflection sites in the central arteries. The first reflection site is the juncture between thoracic and abdominal aorta, which is marked by a significant decrease in diameter and a change in elasticity, and the second site arises from the juncture between abdominal aorta and common iliac arteries. These reflection sites cause reflected arterial pressure pulses that counter-propagate to the direction of the single arterial pressure pulse, due to left ventricular contraction, that gave rise to them. As these reflected pressure pulses reach the aortic arch from below, they enter the subclavian arteries and head into the arterial periphery of the arm, following the first pressure pulse that, besides traveling down the aorta, also entered the arm complex arteries. Figure 2.6 illustrates the process described, where a main pressure wave (P1) passes the aortic arch and propagates both downwards and upwards. Upwards, the pulse travels through the subclavian artery, the axillary artery until it reaches the brachial artery where blood pressure measurements are commonly extracted. Eventually, the pulse reaches the radial artery and, finally, the digital artery where it is usual to place a light sensor - photoplethysmograph. Downwards, the pressure wave meets two major reflection sites in the arterial pathway that exhibit significant changes in arterial resistance and compliance. The first site, at the juncture between descending thoracic and abdominal aorta, causes the pressure wave to be reflected upwards, causing the first reflection wave (P2). The second reflection site, located between the abdominal aorta and the common iliac arteries, creates the second reflection wave (P3). These waves travel upwards, in the opposite direction of the main pulse (P1) and eventually reach the brachial, radial and digital arteries. It is possible to decompose the obtained arterial blood pressure waveform at the radial artery in these different identified pulses.
The arterial pulse provides important information on the cardiovascular prognosis. There is substantial evidence that the aortic pulse wave velocity (PWV) and augmentation index predict cardiovascular morbidity and mortality in a variety of populations, as confirmed by recent meta-analysis studies [175, 176]. The vascular properties of the central and peripheral arteries can cause pulse abnormalities and cardiovascular disease progression including elevated central pressure leading to an increase in cardiac afterload [55, 138] and widened pulsatile pressure causing circumferential tensile stress that damages the vulnerable microvasculature in brain and kidney [121, 142, 165].

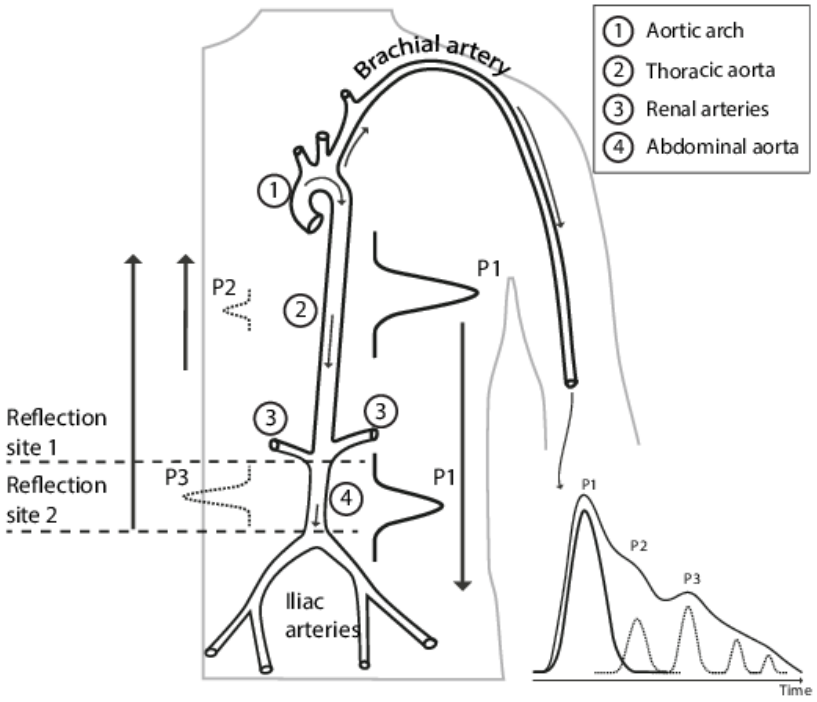

Figure 2.6: Sketch of the aorta/arm complex arterial system and its effect on the arterial pressure pulse wave shape that is observed at the radial/digital artery. Two reflection sites, one at the height of the renal arteries (3), the other one in the vicinity of the iliac bifurcation, give rise to the first and second reflected pulses (P2 and P3, respectively) that trail the primary left ventricular ejection (P1). Adapted from [7]

2.2 Multi-system interactions and Blood Pressure Regulation Mechanisms

The control of hemodynamics requires a complex system to maintain an "optimal" arterial blood pressure in order to ensure the perfusion of blood in the tissues, meeting their metabolic requirements. Arterial Blood Pressure (BP) is often considered to be directly proportional to the product of cardiac output (CO) and total vascular resistance (TVR). Acute regulatory mechanisms are coordinated in the cardiovascular control centers in the brainstem, which, in turn, are influenced by other neural centers that include sensors both intrinsic and extrinsic to the circulation. Figure 2.7 illustrates the processes involved in BP regulation.

2.2.1 Cardiovascular Control Centers

The cardiovascular control centers of the central nervous system (CNS) are found in the medulla oblongata and have two major subdivisions that innervate the heart and the peripheral vasculature. The cardiac control center can be further subdivided into the cardioinhibitory center and the cardiostimulatory centre. The cardioinhibitory center has parasympathetic vagal efferents to reduce heart rate (HR) and, to a lesser extent, atrial contractility. Activation of the cardiostimulatory center increases myocardial contractility (inotropy) and HR (chronotropy) via activation of the sympathetic nervous system (SNS) [155]. The vasomotor centre has both vasoconstrictor and

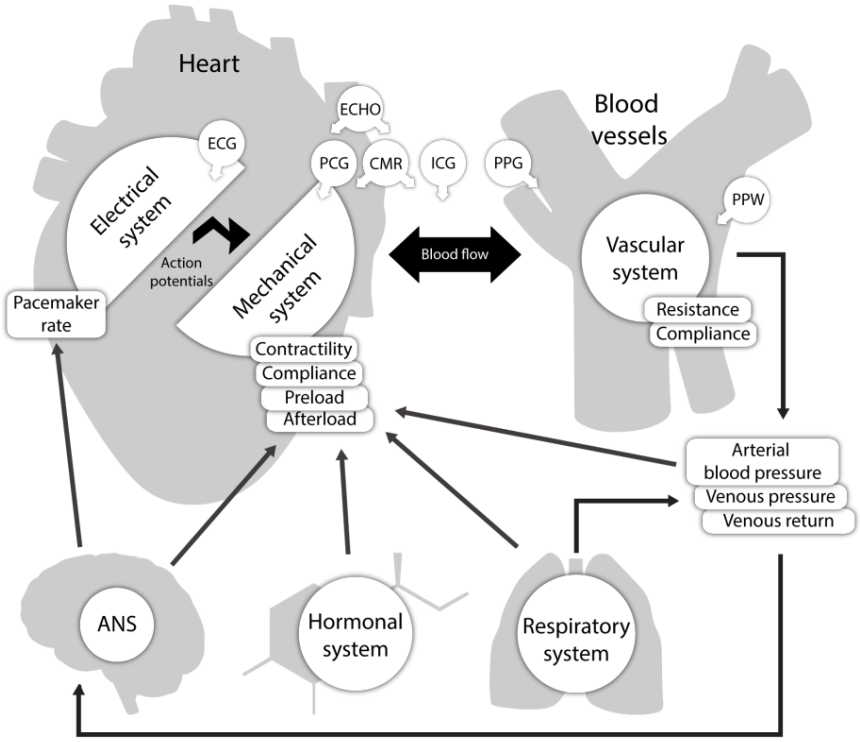

Figure 2.7: Schematic representation of interactions between the subsystems involved in cardiac activity and different monitoring technologies. ECG (electrocardiography), PCG (phonocardiography), ECHO (echocardiography), CMR (cardiac magnetic resonance), ICG (impedance cardiography), PPG (photoplethysmography) and PPW (pulse pressure wave). Adapted from [32]

vasodilator areas: the first containing a high concentration of neurons secreting noradrenaline [52], that is sent to the periphery via the sympathetic nervous system; the second inhibits the activity of the vasoconstrictor area. A sensory area receives input from cranial nerves IX and X, and efferent neurons project to vasoconstrictor and vasodilatory areas and hence modulate the output.
The cardiovascular control centers also receive modulatory neural input from other regions within the brain, including the motor cortex, frontal cortex and limbic system.

2.2.2 Vasomotor Tone

The vasomotor tone is the sum of the muscular forces intrinsic to the blood vessel opposing an increase in vessel diameter [92]. Vascular smooth muscle cells (VSMCs) located in the vessels walls mediate the vasomotor tone. VSMCs contain larger numbers of actin filaments and lower numbers of myosin filaments, compared with skeletal muscle, which gives them the ability to contract more slowly but generating higher forces with sustainable activity [60]. The conduction of the action potential between VSMCs is done via gap junctions like in the myocardium.
Just like any other muscle, the interaction between actin and myosin is regulated by intracellular calcium concentrations, but VSMCs lack toponin and fast sodium channels [13]. Voltage-gated channels and receptor-mediated channels in the sarcolemma, and the sarcoplasmic reticulum change the concentration of intracellular calcium with influence of several agents such as nitric oxide (NO), acetylcholine (Ach), catecholamines and angiotensin II [5]. The free calcium binds to calmodulin, which in turn binds to myosin light chain kinase. This activated complex phosphorylates myosin

cross bridges and initiates contraction. Dephosphorylation of cross bridges and reductions in intracellular calcium provoke relaxation.
The authonomic nervous system (ANS), humoral agents (e.g., angiotensin) and autacoids (e.g., NO, kinins and vasodilator eicosanoids) have the ability to regulate the vasomotor tone [135]. Basal vascular tone is mediated by low level, continuous impulses from the SNS (1 per seconds, approximately) and partial arteriolar and venular constriction via VSMCs contraction, complemented by circulating adrenaline from the adrenal medulla. Basal tone is maintained at around 50% of maximum constriction, meaning that vasodilatation can be caused by a reduction in tonic SNS activity without a direct influence of increased parasympathetic nervous system (PNS) activity. Considering that the blood flow in the venules faces little resistance compared with arteries, one can conclude that the ANS effects mediate capacitance which has direct effects on venous return and preload [14].

2.2.3 Autonomic Nervous System

As stated, the cardiovascular control centers modulate the ANS which innervates the cardiac muscle and VSMCs. The pre-ganglionic neurons originate in the brainstem or the spinal cord and connect to the autonomic ganglions of the ANS, releasing Ach, while the post-ganglionic neurons connect the autonomic ganglions with effector organs and release NA for the SNS and Ach for the PNS.
In the heart, the ANS regulates chronotropy, inotropy and coronary perfusion. The SNS has greater innervation of the ventricular myocardium, mediated via the left stellate ganglion [42] and the stimulation of SNS results in increased HR via β1-adrenergic receptors, and increased stroke volume (SV) via the stellate ganglion. Normal basal sympathetic activity maintains cardiac contractility around 20% greater than that of a denervated heart. PNS fibers are present mainly in the SA and AV nodes, and the atria. Stimulation results in a decreased SA/AV nodes excitability, hence decreasing HR. PNS has little influence on inotropicity, since it lacks efferent distribution to the ventricles.
Regarding the influence of the ANS in the peripheral circulation, it was shown that the SNS has the greater importance in regulation of vascular tone. In fact, the distribution of parasympathetic nerves is limited and PNS effects mediate dilatation mainly via endothelial mechanisms, while the SNS causes vasoconstriction by stimulation of α-1 adrenergic receptors.

2.2.4 Baroreflex Mechanism

The baroreflex mechanism provides a quick negative feedback loop that helps maintaining the blood pressure values constant. Pressure-responsive nerve endings, known as baroreceptors, are located at the atria of the heart and vena cava, but the most sensitive baroreceptors are in the walls of the aortic arch and internal carotid artery and relay to the CCC, in the medulla oblongata. While the carotid sinus baroreceptor axons travel within the cranial nerve IX, the aortic arch baroreceptor axons travel within the cranial nerve X. When the receptor endings detect an elevated BP, by induced stretching of the blood vessel, action potential generation rates increase proportionally to the BP change and results in negative chronotropic and inotropic effects, in addition to a reduction in vasoconstriction. The effects of the baroreflex mechanism is evident in the acute setting such as when standing from a sitting position. The performance of this mechanism can be influenced by age, hypertension and coronary disease.

2.2.5 Humoral Control Mechanism

Humoral mechanisms act to control blood pressure through vasodilatation, vasoconstriction and alteration of blood volume.
Cathecolamines are produced in large quantities by the sympathetic adrenal system in response to stimulation and released by two effector subunits constituted by the sympathetic neurons and the adrenal medulla. These two structures are not always activated to the same extent. Some stimuli cause preferential activation of the sympathetic neurons, mainly driven by the nervous activity of higher centers, (e.g., posture change), while others that of the adrenal medulla, mainly driven by splanchnic nerves, (e.g., emotion, hypoglycemia) [136]. Norepinephrine (NE) is a neurotransmitter released by sympathetic-nerve endings and stimulates post-synaptic receptors, while epinephrine (E) is mainly produced by the adrenal medulla and is released directly into the blood stream. The cardiovascular response to this mechanism depends on the balance between α- (vasoconstrictor) and β- (vasodilating) receptors, since both NE and E can activate these receptors. Catecholamines are associated with increased heart rate and blood pressure, increased blood going to major organs such as the brain, heart and kidneys and lower amount of blood going to the skin and intestines.

The Renin-angiotensin-aldosterone (RAA) system is another hormone system that regulates blood pressure. When renal blood flow is reduced, juxtaglomerular cells in the kidneys convert the precursor prorenin (already present in the blood) into renin and secrete it into circulation. Plasma renin then carries out the conversion of angiotensinogen, released by the liver, to angiotensin I. Angiotensin I is subsequently converted to angiotensin II by the angiotensin-converting enzyme (ACE) found on the surface of vascular endothelial cells, predominantly those of the lungs. Angiotensin II is a potent vasoconstrictive peptide that causes blood vessels to narrow, resulting in increased blood pressure. Angiotensin II also stimulates the secretion of the hormone aldosterone from the adrenal cortex. Aldosterone causes the renal tubules to increase the reabsorption of sodium which in consequence causes the reabsorption of water into the blood, while at the same time causing the excretion of potassium (to maintain electrolyte balance). This increases the volume of extracellular fluid in the body, which also increases blood pressure [6]. Angiotensin II also activates the secretion of antidiuretic hormone (ADH), known as vasopressin, which induces translocation of aquaporin-2 channels in collecting ducts to enhance free water permeability and resolption (anti-diuresis) and also has direct vasoconstrictory effects.

Nitric oxide (NO) is considered on of the most important mediators of vascular hearth. Within the vascular endothelium, the production of NO is responsibility of the activated endothelial nitric oxide synthase and requires the amino acid L-arginine as the main subtrate for synthesis. Once synthesized, NO diffuses across the cell membrane of endothelial cells and enters VSMCs where activation of guanylate cyclase occurs, known to elicit vascular smooth muscle relaxation through several mechanisms [89].

Atrial natriuretic peptide is another hormone involved in hemodynamics control. It's synthesized by atrial myocytes in response to chamber distension and hormones such as adrenaline and ADH [90]. It directly relaxes VSMCs and inhibits renin, therefore having an overall natriuretic effect to reduce BP.

2.3 Conclusion

In this chapter, the main anatomic and physiological aspects that are relevant for the understanding of the objective of this thesis were outlined. It started with a brief description of the anatomy and physiology of the cardiac system, including a picture of the heart and blood vessels. It ended up with an overview of the different mechanisms that affect and regulate the hemodynamics in different ways, outlining the complexity of actions and interactions of these systems. This knowledge is crucial for understanding the problems of hemodynamics management in critical care addressed in the next chapters.

3

Blood Pressure Monitoring In Critical Care: Review

Monitoring the blood pressure (BP) is among the foremost procedures for hemodynamic evaluation in acutely or critically ill patients. The principles for routine and regular BP monitoring in perioperative care is predicated on the subsequent arguments: BP can be exceptionally volatile, abnormal BP and unfavorable outcomes are associated, BP may be promptly treated, and protocol-guided BP management improves outcomes supported by some randomized controlled trials [10]. Although systematic BP monitoring is mandatory in perioperative care, the appropriate BP target for a specific patient receiving anesthesia and surgery is not consensual [98]. As an example, a systematic literature review of 130 studies found 140 different definitions of intraoperative hypotension [10].

It is known that hypotension and hypertension in intraoperative environments can impair the function of important organs, like the brain [9], the heart [172], and the kidneys [178]. Also, intraoperative hypotension and hypertension seems to be correlated with higher morbidity and mortality rates [9, 11, 103] with special attention to the depth of hypotension and the cumulative time spent on hypotension influencing the outcomes. Some studies suggest that minor but prolonged and major but brief BP changes can both impact the surgery outcomes [98]. In 1990, Charlson et al. showed that prolonged changes in MAP of more than 20 mmHg or 20% from the patient's preoperative levels were associated with postoperative complications [24]. More recently, Monk et al. found that intraoperative SBP $<$ 67 mmHg for more than 8.2 minutes, mean arterial pressure (MAP) $<$ 49 mmHg for more than 3.9 minutes and diastolic blood pressure (DBP) $<$ 33 mmHg for more than 4.4 minutes were associated with 30-day mortality [103]. But most up-to-date studies present different definitions for BP targets and existing controversy raises the question whether patients with different baseline BP (e.g., Normotensive vs Hypertensive) would equally benefit from identical BP targets (e.g., MAP $<$ 60 mmHg for hypotension).

A recent survey analyzed the best available evidence and clinical experience and suggests that intraoperative hemodynamic management should consider the baseline BP of each patient, classifying patients as low baseline BP (SBP $<$ 90 mmHg or DBP $<$ 50 mmHg), normal baseline BP (SBP 90–129 mmHg and DBP 50–79 mmHg) and high baseline BP (SBP $>$ 130 mmHg or DBP $>$ 80 mmHg) [98]. Baseline BP is obtained as the average of multiple measurements taken with the patient unstressed, pain free, and awake (or lightly sedated). Then, reckoning on the sort of surgery and risks of hypotension-related organ ischemia and hypertension-related bleeding, different BP targets are defined in order to improve the surgery outcomes, as shown in figure 3.1.

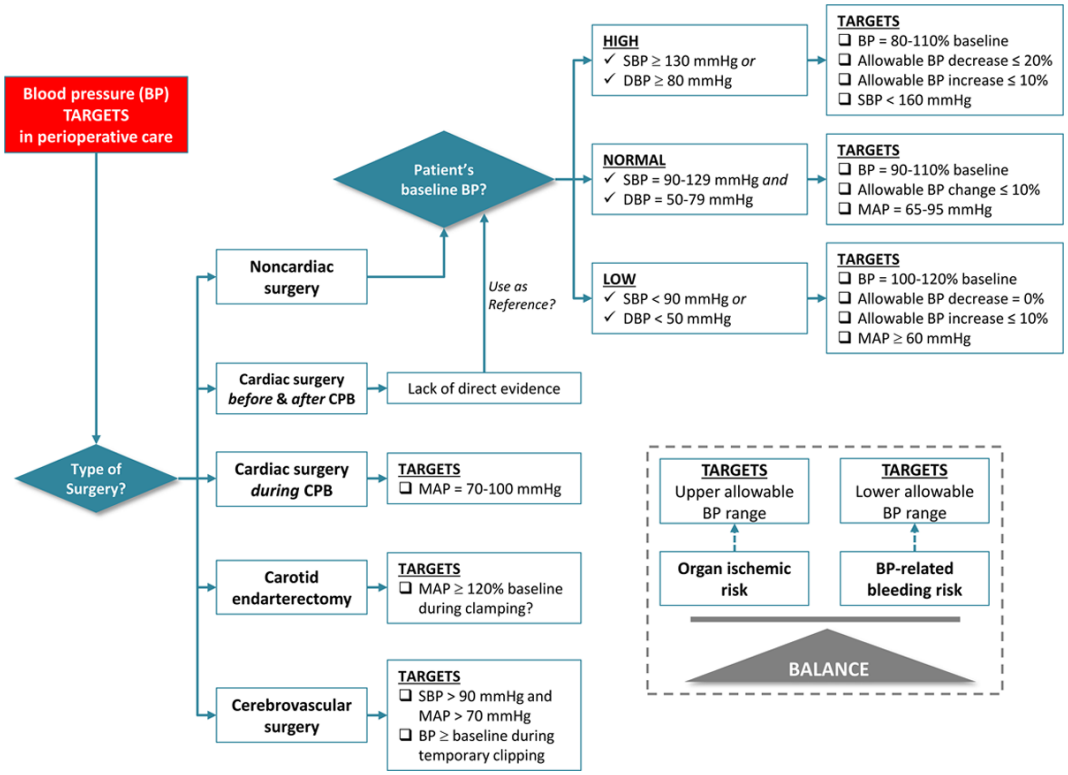

Figure 3.1: Considerations during the determination of BP targets in perioperative care based on the available evidence and clinical experience. The main considerations are type of surgery, patient's baseline BP, and risks of organ ischemia and surgical bleeding. CPB indicates cardiopulmonary bypass. From [98]

3.1 Blood Pressure Monitoring Techniques

Intraoperative Blood Pressure (BP) measurements can be either intermittent or continuous, invasive or non-invasive [18]. Most anesthesiology societies recommend BP monitoring at worst once every 5 min in anesthetized subjects undergoing surgical procedures while invasive BP monitoring is usually indicated only within the case of high-risk patients or in complex surgical procedures [119].

The direct measurement of BP via arterial cannulation is considered the clinical reference method. This technique has several critical advantages like continuous 'beat-to-beat' BP monitoring, accurate BP reading at low pressures (p.e.: shocked patients), possibility to estimate intravascular volume status from the contour of the ABP signal, accurate measurements in specific patients where non-invasive technologies fail (p.e.: patients with gross peripheral edema in ICU or morbidly obese patients) and permits blood sampling through the arterial catheter [51]. In clinical routine, it is usually performed during high-risk surgery and in intensive care medicine. The cannulation of an artery, however, might be time-consuming, is expensive, has to be done by a trained operator, and is associated—although very rarely—with potential major complications like embolism, lesion of nerves or vessels, or ischemia [51, 149]. For these reasons, BP is commonly measured non-invasively.

Intermittent non-invasive BP (NIBP) monitoring is considered to be the standard-of-care during

low and intermediate risk anesthesia, yet commonest devices using the oscillometric method tend to overestimate hypotensive BP values and to underestimate hypertensive BP values and could result in delayed recognition of BP fluctuations [181, 80]. Despite this, a survey from 2010 reported that the employment of oscillometric NIBP measurements in critically ill patients is common despite the paucity of evidence validating its accuracy in critically ill patients [25]. These results could also be justified by the fact that cuff based NIBP measurements are inexpensive, easy and fast to use.

Continuous NIBP monitoring is a long-awaited solution that will join the best of both worlds: 'beat-to-beat' BP readings and high accuracy while being easy and fast to deploy, cheap and without the requirement of special trained operators. Most of the research in this area is predicated on two different approaches: arterial applanation tonometry, the volume clamp method and pulse wave velocity. The first one was addressed by Pressman and Newgard [131], who obtained the arterial pulse wave with a transducer strapped to an artery with a bone underneath. Most recently, this system has been refined and results suggest that it allows the accurate reading of mean arterial pressure (MAP) and diastolic blood pressure (DBP) [95]. Also, it's been tested in cardiology to assess central vascular pressures [113], where the pulse wave obtained by applanation tonometry was analysed. A device using this system for BP prediction is the T-Line system (Tensys Medical, San Diego, CA, USA) [147, 40].

The second technique for non-invasive continuous BP measurement - volume clamp method (or vascular unloading technology) - relies on the work of Penaz et al. [127]. The BP is measured at the finger with an inflatable cuff combined with a photodiode. The volume fluctuation within the finger is caused by blood flow and is detected by the photodiode; the pressure in the cuff is adjusted to keep the diameter constant [127]. From the pressure changes in the cuff, a BP curve may be calculated. Devices based on this technique are ClearSight (Edwards, Irvine, CA, USA) and CNAP (CNSystems Medizintechnik AG, Graz, Austria). In case of severe vasoconstriction, peripheral vascular disease, or distorted fingers as a result of arthritis, clinical trials have shown that it can be difficult to obtain a valid waveform using finger cuffs. Additionally, compared to standard intermittent devices for NIBP measurement, this solutions for continuous BP monitoring are relatively expensive [96].

In 2014, a review of several available devices, including CNAP and T-line, suggests that they might not satisfy the standards of the AAMI guidelines, but also addresses the necessity of a better definition of how these devices should be evaluated and what should be their purpose [69].

Nowadays, many research projects are focused on the photoplethysmography (PPG) and its relationship with BP. PPG technology is becoming more readily available, inexpensive, convenient and easily integrated into portable devices, like smartphones and smart watches. With the advancement of digital sensors, signal processing techniques, machine-learning algorithms and improved physiologic models, the usage of PPG's pulse waveform for the assessment of BP has become more feasible [83, 84, 79, 23].

3.2 Photoplethismography and BP Surrogates

Hertzman and colleagues first introduced the term "photoplethysmography" in 1938 and suggested that it represented the volumetric changes within the dermal vasculature [57, 58]. Since the early 1990s, the pulse oximetry – obtained via PPG – is a global standard for monitoring during anes-

thesia [118].

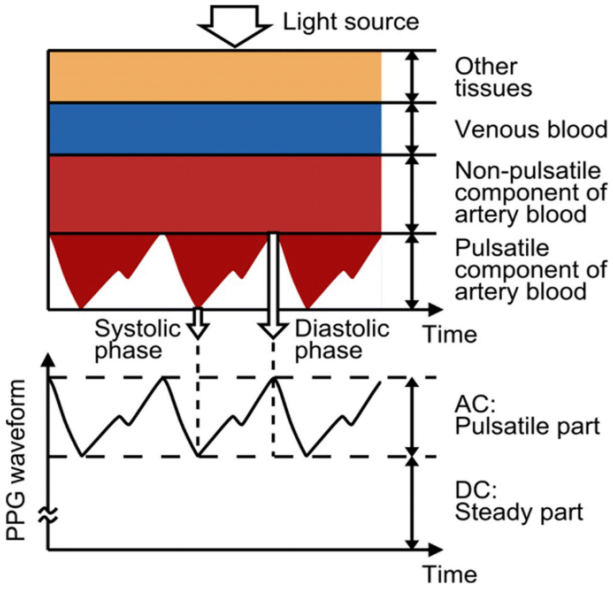

Figure 3.2: Illustration of PPG signal AC and DC components. From [161].

The PPG device consists of a light emitting diode (LED) and a photodiode and is often placed in the patient's finger. By measuring the amount of light that's absorbed or reflected by the blood that exists in the optical path, the PPG signal becomes responsive to changes in the volume of blood in that area. The PPG signal ends up being a complex mixture of the blood flow in veins, arteries and capillaries, with a pulsatile and a non-pulsatile component. The first component is related to changes in blood volume inside arteries and is synchronous with the heartbeat, while the non-pulsatile component is related to the basic blood volume, respiration, the sympathetic nervous system and thermoregulation [171].
In clinical practice, PPG is routinely used to track cardiac-induced blood volume fluctuations within microvascular beds at peripheral body sites, like the finger, forehead, earlobe, and toe [41]. The red (680 nm) or near-infrared (810 nm) light is commonly used for transmissive PPG devices, with the infrared emission having the deepest penetration [86, 145]. Given that the absorption of light by hemoglobin is a function of oxygenation and optical wavelength, the use of PPG at multiple wavelengths is also routinely employed in pulse oximetry [41].
The research with PPG technology suggests its potential for the monitoring of blood oxygen saturation, heart rate, blood pressure, cardiac output, respiration, arterial aging, endothelial function, microvascular blood flow and autonomic function [4, 100, 123]. Also, the PPG signal produces pulse waveforms that are very similar to pressure waveforms obtained with tonometry.

3.2.1 Pulse Wave Velocity

The focus of several recent studies on continuous non-invasive blood pressure (cNIBP) monitoring is the analysis of the pulse wave travelling from the heart to peripheral sites and the electromechanical timings of the heart [115, 47, 44, 129, 30, 87, 167, 106, 185, 187, 132, 76, 183, 26, 97, 45, 77, 111, 188, 35]. Regarding the analysis of the pulse wave, the main approaches rely on the estimation

of the pulse wave velocity (PWV) or, inversely, pulse transit time (PTT), that represents the time taken by the pulse wave to propagate through a certain length of the arterial tree and is correlated with BP. It is important to note that this procedure does not account for changes in the vascular structure properties, since it assumes that the pulse wave travels through an homogeneous arterial segment, resulting in a constant need of external calibration procedures. This characteristic is of great importance when we're estimating the BP during transient events (e.g.: physical exercise, administration of vaso-active drugs and posture changes).

The definition of PTT presented above would make it hard to measure this metric, since it would need two sensors positioned in two locations of the analyzed arterial segment that would record the pulse wave [35, 76, 37]. In practice, having two sensors at a small distance apart would be difficult and uncomfortable, leading to alternative approaches. The most common approach is to assess PTT based on the simultaneous detection of the electrocardiogram (ECG) R-peaks and the beginning of the pulse wave inflection measured at a peripheral site (PPG), representing the pulse wave travelling through arteries with significantly different elastic properties [132]. Also, this metric corresponds to an approximation of PTT, called pulse arrival time (PAT) and its relation to PTT is described by equation (3.1):

$$PAT = PEP + PTT \tag{3.1}$$

where PEP represents the Pre-Ejection Period, the time between the electrical depolarization of the left ventricle and the beginning of ventricular ejection and cannot be measured with pulse propagation approaches. PEP can be estimated with the time distance between the ECG R-wave and a reference point in the Impedance Cardiography (ICG), as shown in figure 3.3

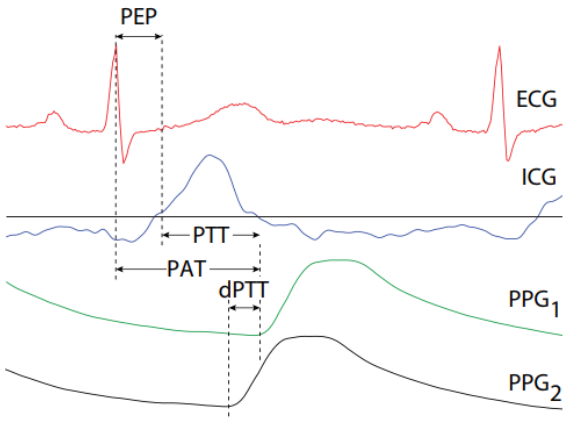

Figure 3.3: Illustration of PAT, PTT, dPTT and PEP. PPG_1 and PPG_2 refer to different arterial segments. From [32].

PAT-based approaches are the most common [115, 44, 76, 183, 26, 97, 45, 77, 111, 188, 189, 129, 30, 87, 167, 35, 106, 186, 187], but different techniques have been proposed to extract additional BP surrogates. Some researchers used impedance cardiography (ICG) for the assessment of PEP and then an estimation of PTT is obtained subtracting the extracted PEP from the PAT measurements [186, 187, 132, 126, 124, 34]. Other approaches include the subtraction of two PAT measures

(DPTT – differential pulse transit time) from distinct arterial pathways [47, 132], or in the same arterial pathway [46, 173, 191]. Furthermore, PAT and PTT have been defined using different characteristic points in the PPG pulse wave (e.g.: onset of the pulse wave, or the systolic inflection point, or the peak of the pulse wave) [30, 87, 187, 76, 45, 77, 111, 188] and the identification of this reference points has been done with different methods (e.g.: Hilbert-Huang transform [27], time delay methods [174] and multi-gaussian fitting [33]). It was expected that changes in BP would affect PTT/PAT extracted measures which was indeed observed by many researchers [115, 47, 132, 76, 183, 26, 97, 45, 77, 188, 189, 91, 185, 44, 129, 30, 87, 167, 35, 106, 187]. However, PTT and PAT only reflect a part of a more complex integrated system that regulates BP and assuming a linear relationship between PTT/PAT and BP leads to contrasting results, with correlation coefficients ranging from -0,1 to -0,99 [38], which can be due to different measuring conditions and physiological properties of the patient. The Moens-Korteweg equation aims to represent the non-linear relationship between PTT and BP by linking the velocity of the pulse wave and the elastic and geometric properties of a short elastic vessel. Many BP surrogates using PTT/PAT employ this equation and it is given by (3.2):

$$\mathrm{PWV} = \frac{\mathrm{distance}}{\mathrm{PTT}} = \sqrt{\frac{\mathrm{Eh}}{\rho 2\mathrm{r}}} \tag{3.2}$$

where E is the Young elasticity modulus of the vessel's wall, ρ is the blood density, h is the wall thickness and r is the vessel radius. It is assumed that ρ, r *and* h suffer changes small enough to be ignored and the main variations are expected to come from the elasticity modulus. The following equation (3.3) was proposed by Hughes [62] and represents the relationship between PWV and BP:

$$\mathrm{E} = \mathrm{E}_0 \mathrm{e}^{\alpha \mathrm{P}} \tag{3.3}$$

where $\alpha \approx 0.017 mmHg^{-1}$ and P is the mean arterial pressure (MAP). The combination of the equation (3.2) with the linearization of the equation (3.3) ($E \approx E_0(1+\alpha P)$) provides the quadratic dependency that relates PTT with MAP:

$$P = A(\frac{1}{PTT})^2 + B \tag{3.4}$$

Bramwell and Hill [16] derived yet another expression (Bramwell-Hill equation), from the Moens-Korteweg equation, which relates the velocity of the pulse wave with the vessel compliance and is given by (3.5):

$$\mathrm{PWV} = \sqrt{\frac{\mathrm{A}}{\rho \mathrm{C_A}}} = \sqrt{\frac{\mathrm{V} \cdot \Delta \mathrm{P}}{\rho \cdot \Delta \mathrm{V}}} \tag{3.5}$$

where A is the lumen area, $C_A = \frac{\nabla A}{\nabla P}$ is the compliance area and ρ is the blood density. Modeling the pressure-volume relationship with a sigmoidal curve [151, 61] provided a link between BP and

PWV. Following this relationship, Shaltis et al. [151] proposed the following equation:

$$V = \frac{a}{1 + e^{-bP}} \tag{3.6}$$

Where a and b are parameters needing for fitting during a training phase with experimental data. Substituting the volume (V) in (3.5) with equation (3.6) and rearranging the equation with Taylor's expansion, one obtains the following equation:

$$\mathrm{PWV} = \sqrt{\frac{\mathrm{e}^{-\mathrm{bP}} + 1}{\rho \mathrm{b}}} \approx \frac{1}{\sqrt{\rho \mathrm{b}}} \frac{\sqrt{2}}{\left(1 - \frac{\mathrm{bP}}{4}\right)} \equiv \frac{1}{\mathrm{cP} - \frac{\mathrm{c}}{4}} \leftrightarrow \mathrm{PTT} = \mathrm{L}(\mathrm{cP} - \frac{\mathrm{c}}{4}) \tag{3.7}$$

Where L is the distance travelled by the pulse and c is obtained by fitting the algorithm with experimental data.
Both Moens-Korteweg and Bramwell-Hill equations are the basis for several research work relating BP and PWV. Different authors derived calibration functions that differ on the number of unknown parameters, linearity vs non-linearity and additional parameters. Chen et al. [26] combines two separately obtained components to predict the systolic blood pressure (SBP), one higher frequency component obtained with a specific frequency band of PAT and other lower frequency component obtained with cuff measurements intermittently. The equation describing the process is the following:

$$P_e = P_b - \frac{2}{\gamma T_b} \Delta T \tag{3.8}$$

Where P_e is the estimated SBP, P_b is the last measured SBP, T_b is the PAT corresponding to P_b, ∇T is the change in PAT and γ is an unknown fitting parameter. Poon et al. [129] proposed two dependent functions, one for SBP and the other for DBP estimations:

$$\begin{aligned} DBP &= \tfrac{SBP_o}{3} + \tfrac{2DBP_o}{3} + A \ln\left(\tfrac{PTT_{W_o}}{PTT_W}\right) - \tfrac{(SBP_o - DBP_o)}{3} \tfrac{PTT_W^2}{PTT_W^2} \\ SBP &= DBP + (SBP_o - DBP_o) \tfrac{PTT_{W_o}^2}{PTT_W^2} \end{aligned} \tag{3.9}$$

Where SBP_0, DBP_0, PTT_{W_0} are measured SBP, DBP and PTT values and PTT_W is a weighted PTT. A is the unknown parameter that is fitted to experimental data. Gesche et al. [49] proposed a calibratton function with 3 terms: : (1) an exponential term, (2) a second non-linear term, and (3) a correction constant:

$$\mathrm{BP_{PTT}} = P1 \times \mathrm{PWV} \times \mathrm{e}^{(P3 \times \mathrm{PWV})} + P2 \times \mathrm{PWV}^{P4} - (\mathrm{BP_{PTT,cal}} - \mathrm{BP_{cal}}) \tag{3.10}$$

Where $P1$, $P2$ and $P3$ are unknown fitting parameters, $\mathrm{BP_{PTT,cal}}$ is the predicted BP in the calibration instance and $\mathrm{BP_{cal}}$ is the value obtained with the cuff in the same instance. PWV is estimated from PTT, patient's height and a body correlation factor.

These models don't consider continuous changes in the vascular properties, like the diameter of blood vessels, which implies an intermittent re-calibration of the model parameters in long term measurements [187]. Poon et al. [130] and McCombie et al. [93] addressed this issue by mapping

PTT changes associated with changes in the hydrostatic pressure provoked by the lifting of the hand above the level of the heart. The discussion whether PAT may be a reliable parameter to describe BP variations has led researchers to gauge the influence of PEP and PTT during transient events such as physical exercise [35, 186, 132, 107], posture change [44, 106, 108] and administration of vaso-active drugs [126]. Muehlsteff et al. [108], Deb et al. [35], Wong et al. [186] and Proenca et al. [132] concluded that BP is most consistently correlated to PAT rather than PTT or DPTT during intermittent short-term physical exercises. Moreover, Proenca et al. [132] showed that an accurate estimation for PEP was required to estimate PTT precisely and that wasn't possible. Regarding the context of posture changes, Muehlsteff et al. [106] proved that PAT-based models were not suitable for the prediction of BP changes, showing that PAT is strongly affected by posture changes at almost constant values of SBP and DBP. The determination of BP through PAT during vaso-active drugs administration was addressed by Payne et al. [126], who showed that PAT is comparatively unaffected by different drugs within the overall studied population and obtained a better correlation with SBP than DBP and MAP. The author states in conclusion that PAT should be avoided as a purely vascular function surrogate but did not reject its potential in the assessment of BP variability and rapid pressure changes. Baruch et al. [7] proposed a novel pulse decomposition analysis (PDA) of the pulse pressure that assumes that the peripheral arterial pressure pulse is a superposition of 5 individual component pressure pulses, the first of which is due to the left ventricular ejection from the heart while the remaining component pressure pulses are reflections and re-reflections that originate from only two reflection sites within the central arteries. From the PDA, the authors extracted several parameters that were then compared with SBP and PP, from which two were highlighted: $P2P1$ (the amplitude ratio of the first reflection wave and the main pulse) and $T13$ (the time span between the main pulse and the second reflection wave) that were strongly correlated with aortic SBP and PP.

3.2.2 Other Vascular Function Surrogates

A few more cardiovascular function surrogates have been proposed in literature, which include the augmentation index (AI), the stiffness index (SI), the reflection index (RI) and the left ventricular ejection time (LVET). In order to extract this metrics, Takazawa et al. [159] proposed the identification of five consecutive waves, located at the systolic (a, b, c and d waves) and at the diastolic (e wave) phases of the PPG pulse.

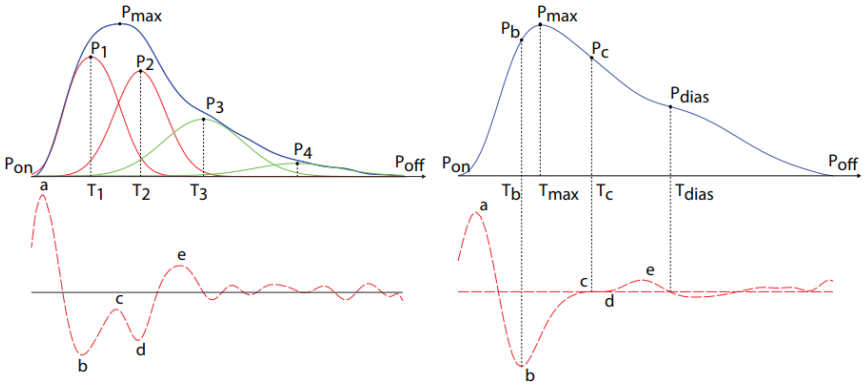

Figure 3.4: Reference points proposed by Takazawa et al. From [160].

The augmentation index (AI) is a recognized parameter for evaluating arterial stiffness and wave reflection. It corresponds to the percentage of central pulse pressure imputable to the secondary systolic pressure increase resulting from the overlap of the forward and reflected pressure waves [102]. Three main factors affect wave reflections: the distance to the reflecting site, the speed of wave transmission, and the magnitude of the reflection coefficient [102]. Takazawa et al. defined AI as the ratio between the late and early systolic components ($AI_{tak} = \frac{P_c}{P_b}$) derived from the PPG second derivative [159], while Rubins et al. proposed two definitions of AI depending on the PPG morphology (type A: $AI_{rub} = 1 - \frac{P1}{P_{max}}$ and type C: $AI_{rub} = 1 - \frac{P2}{P_{max}}$) [139]. AI is commonly associated with ageing [122]. Stiffness index (SI) is a measure of the timing of the diastolic component relative to the systolic component of PWV in the large arteries [100] and was defined in [29] as the time delay between the direct and the reflection waves ($SI = T_{dias} - T_{max}$). Millesseau et al. [100] proposed the correction of SI with relation to the subject height h ($SI = \frac{h}{T_{dias} - T_{max}}$) and suggested that this index increases with age. In [7], it was shown that SI also correlates with PP. The reflection index (RI) has been associated with small artery stiffness [101, 36] and changes in vascular tone and is determined by the ration between the height of the diastolic wave to the maximum pulse height ($RI = \frac{P_{dias}}{P_{max}}$) [29, 101]. The left ventricular ejection time (LVET) is defined by the time between opening and closing of the aortic valve during the cardiac cycle. In an unhealthy heart, the LVET will change during disease progression as previously demonstrated in patients with ischemic heart disease, heart failure, hypertension and aortic stenosis [54, 74, 70]. Chan et al. [21] proposed a method to ascertain the LVET based on the analysis of successive derivatives of the PPG. In this study, several characteristic points are extracted in each derivative based on waveform features (e.g., amplitude, slope and curvature). Using these characteristic points, three estimations of LVET are extracted which are then used to assess a final LVET estimation based on a rule-based decision logic approach. More recently, Couceiro et al. proposed a new method for the estimation of LVET based on the analysis of the systolic model of the decomposed PPG pulse [33]. The PPG pulse is decomposed into multiple Gaussian functions corresponding to the systolic and diastolic phases of the PPG pulse, and the LVET is assessed from the 3rd derivative of the functions corresponding to the systolic phase. The analysis of the systolic model rather than the whole PPG pulse was motivated by the need of reducing the influence of noise and pulse wave reflections in the estimation of LVET. Also, the relative heights of the proposed pulse wave reference points (b/a, c/a, d/a and e/a ratios), particularly the c/a ratio, have been related to arterial stiffness and aging [160, 65] and essential hypertension [154]. All these ratios were used to propose an "ageing index" $(b-c-d-e)/a$ [160].

3.3 Conclusion

In this chapter, the problem of BP monitoring in critical care was addressed starting with the difficulty of defining BP targets (e.g.: hypotension/hypertension) and the need for personalized BP management for patients with different baseline BP, hypotension-related organ ischemia and hypertension-related bleeding, and different types of surgeries. The work presented by Meng et al. [98] helps understanding the difference between primary care and perioperative care BP management, citing relevant randomized and nonrandomized studies that helped defining new and more accurate BP targets that positively affect surgeries outcomes.
Moreover, different BP monitoring were presented including the arterial cannulation, intermittent NIBP (cuff-based methods) and recently proposed techniques for continuous NIBP: arterial appla-

nation tonometry, the volume clamp method and the pulse wave velocity. It ends with a detailed description of BP surrogates extracted from the PPG and ECG signals with the main focus on the pulse wave velocity and the pulse arrival time (PAT).

4

Evaluation of Continuous Non-Invasive Blood Pressure Estimation Algorithms Based on Photoplethysmography and Electrocardiography

4.1 Introduction

Different BP monitoring techniques available in the ICU include intermittent NIBP (e.g., oscillometry) and continuous invasive BP monitoring (e.g., radial arthery catheterization). The intermittent NIBP is the most common procedure during low and intermediate risk anesthesia, since it's readily available and inexpensive, but has been widely used in high-risk surgeries also [25]. The direct BP measurement via arterial cannulation is regarded as the clinical reference method and is mainly used in high-risk surgeries and in intensive care medicine, but it is expensive, time-consuming and requires a trained operator [51]. Another BP monitoring technique is expected to become widely available soon by using continuous non-invasive technologies such as the volume clamp method, the arterial applanation tonometry and the pulse wave velocity.

The most suitable method of BP monitoring for patients undergoing surgical procedures should be identified using a perioperative cardiovascular risk stratification. Several types of hypotension have been identified during general anaesthesia and surgery (e.g., post-induction hypotension, early intraoperative hypotension and late intraoperative hypotension) [156]. Walsh et al. showed that hypotension events lasting just a few minutes could adversely affect organ function [179]. Therefore, it is of utmost importance for the clinician to maintain the BP steady and continuous monitoring would help a lot. Benes et al. demonstrated that continuous BP monitoring outperformed intermittent NIBP measurements taken every 5 minutes helping to keep BP stable during surgery [8]. Ilies et al. presented improvements in the detection of hypotensive episodes using continuous monitoring in patients undergoing planned cesarean section against intermittent NIBP [63].

In the perioperative setting, the likelihood for intraoperative hypotension and the patient's risk

to develop hypoperfusion-induced organ failure should be considered when choosing which BP monitoring to use, according to [96]. The idea is illustrated in figure 4.1.

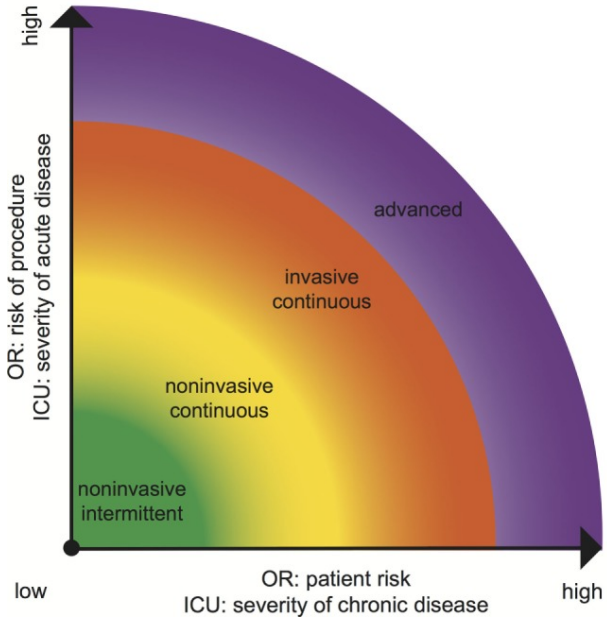

Figure 4.1: Choice of adequate blood pressure monitoring equipment in ICU and OR according to patient and procedural risk (OR) (45) or chronic and acute disease (ICU). From [96].

Currently, the arterial tonometry method, vascular unloading technique, pulse wave velocity (PWV) method, and pulse waveform characteristics method are the main non-invasive continuous BP measurement methods being developed. The arterial tonometry method is applicable to superficial arteries like the radial artery [131, 95, 113, 147, 40] and calibration isn't needed whenever, making it possible to achieve long-term BP monitoring. However, the sensor is sensitive to displacement and pressure [39]. The vascular unloading technique is able to estimate BP using the mechanical properties of the blood vessel [127], but long-term monitoring may cause venous congestion and affect the estimations accuracy.
The PWV method relies on the Moens–Korteweg equation (3.2). Gribbin tested the variation of the arterial dilatation pressure of the limb in a large range by applying external pressure, monitored the PWV, and observed that PWV was correlated to blood pressure [50]. In 1984, Tanaka estimated the BP values from the PWV for the first time; however, the predicted values had big standard errors [162]. Suchlike the idea of PWV, Payne et al. verified that the pulse wave transit time (PTT) was associated with blood pressure [126] and the correlation between PTT and systolic blood pressure (SBP) was stronger than that between PTT and diastolic blood pressure (DBP).
More recently, different studies address features of the pulse wave signals within the time and frequency domains and analyzed multivariate regression models [144, 153, 81, 166]. The regression models weren't much different than the PTT-based models, while the features changed from univariate to multivariate and the accuracy improved. With the development of machine learning, the characteristic parameters of models were further enriched, including the amplitude, phase characteristics of pulse waves calculated with fast Fourier transform [190], spectral characteristics [180], and the features of the photoplethysmography (PPG) waveform and related first and second (time) derivatives [140, 141]. Additionally, scholars used more complex machine learning models, such as neural networks [65], [180, 140, 141, 137], support vector machines [193], adap-

tive boosting regression [104], and random forest algorithm [56]. Although machine learning and big data covered more BP information and improved the performance for BP estimation, various factors that affect blood pressure were not properly covered. During modeling, coming up with an appropriate feature set can undoubtedly reduce the complexity of the BP estimation models and contribute to a comprehensive real-time monitoring of blood pressure device. Table A.1 shows the most relevant BP estimation models studied during the elaboration of this thesis. It is clear that there is inconsistency in approaching this challenge, in terms of sample size, number and type of features, reported evaluation metrics, estimation models (linear regression, ANNs, etc...), BP data acquisition (A-line vs sphygmomanomether), recalibration/no recalibration, environment (ICU, lab tests) and training/testing settings. However, despite these challenges, this line of research seems encouraging with many different approaches available for analysis.
This thesis focuses on BP monitoring of patients during different types of surgery. Thus, our goal for this chapter is to analyze how state-of-the-art BP estimation models based on PPG and ECG signals perform under these specific conditions. A detailed analysis is employed in order to extract useful information about the pros and cons of these models in a real world intraoperative application. Since most of the recently proposed algorithms in the literature are highly complex, not available for simple implementation and require further testing for validation, an approach similar to [152] was taken in order to evaluate different more simple mathematical models.

4.2 Methods

4.2.1 Data collection

The MEC-U ethical committee approved the data collection for this study (St. Antonius Ziekenhuis, Koekoekslaan 1, 3430 EM Nieuwegein, NL. Approval W19.046), and it was carried out at the Elisabeth-Tweesteden Ziekenhuis hospital in Tilburg, NL. All patients gave their written informed consent for the investigation. Data was collected from 9 patients during surgery in the OR with an arterial line as standard of care.
These patients had an age range from 23 to 91 years ($\mu = 59.1, \sigma = 20{,}0$). The surgeries were vascular (5) and neuro (4) with lengths between 1.97 and 7.29 hours ($\mu = 4.26, \sigma = 1.89$). The ABP waveform was obtained at the radial site with an Edwards Lifesciences TruWave disposable pressure transducer (Edwards Lifesciences, Irvine, CA) and a Philips MP50 patient monitor (Philips Medizin Systeme, Böblingen, Germany). The data were recorded at a sampling rate of 125Hz on a laptop with custom data logger software. The recordings were started immediately after the arterial line was placed, when the patient was fully anesthetized and ventilated. The ABP waveforms span the duration of the entire surgery until the patient is either woken up, extubated, undraped, or prepared for transport to the recovery room, whichever occurred first.

4.2.2 Pre-processing

The PPG is known for considerable advantages, but it is prone to certain well-known sources of error which may lead to inaccurate readings: the introduction of ambient light at the photoreceptor, wearing nail polish, poor blood perfusion of the peripheral tissues and motion artifacts [157]. In order to deal with this limitation, a pre-processing stage is required. At this stage, high frequency and low frequency components of the acquired signal were removed using a bandpass Chebyshev

II filter with a 18 Hz and 0.5 Hz high and low cut-off frequencies [85], ensuring the preservation of the physiological relevant information (usually below 15 Hz [157]).
During surgery, several major sources of error may occur and affect the readings of ECG, PPG and A-line devices independently. Also, our setup includes cuff measurements that are triggered frequently, and the cuff is placed in the same arm as the A-line's catheter and the PPG sensor. In order to ensure integrity between these 3 different signals, a simple quality assessment tool was designed. First, systolic peaks are extracted from the ECG signal, using the Pan and Tompkins algorithm [125], then a similar approach is taken in order to extract the systolic peaks from the PPG signal. Then, using a 20 seconds sliding window, the heart rate (HR) is calculated inside the given window ($\mathrm{HR}[t-20s:t]$) for each time instance t using the PPG and ECG systolic peaks previously detected. If the heart rates obtained with the PPG and ECG differ for more than 30%, the given instance t is discarded. Figure 4.2 shows an example of this tool in action.

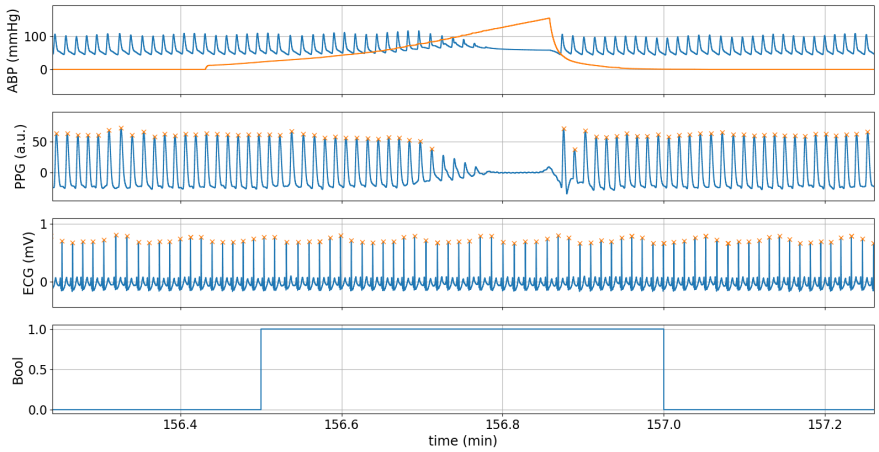

Figure 4.2: Plot showing the quality assessment tool (bottom sub-plot) triggering the impairment between ECG and PPG signals during cuff inflation (represented as the orange line in the top sub-plot).

4.2.3 Segmentation

The main objective in this step is to segment the PPG signals into individual PPG pulses per heartbeat. From each PPG pulse, several features will be extracted afterwards. To detect the PPG pulses, an approach similar to [158] was applied. Initially, the PPG signal is differentiated using a five-point digital differentiator [2] (from (4.1) to (4.4)), resulting in first to fourth order derivatives ($d1_{ppg}$, $d2_{ppg}$, $d3_{ppg}$ and $d4_{ppg}$).

$$d1_{ppg} = f'(t) = \frac{f(t-2h) - 8f(t-h) + 8f(t+h) - f(t+2h)}{12h^2} \tag{4.1}$$

$$d2_{ppg} = f''(t) = \frac{-f(t-2h) + 16f(t-h) - 30f(t) + 16f(t+h) - f(t+2h)}{12h^2} \tag{4.2}$$

$$d3_{ppg} = f'''(t) = \frac{-f(t-2h) + 2f(t-h) - 2f(t+h) + f(t+2h)}{2h^3} \tag{4.3}$$

$$d4_{ppg} = f''''(t) = \frac{f(t-2h) - 4f(t-h) + 6f(t) - 4f(t+h) + f(t+2h)}{2h^3} \tag{4.4}$$

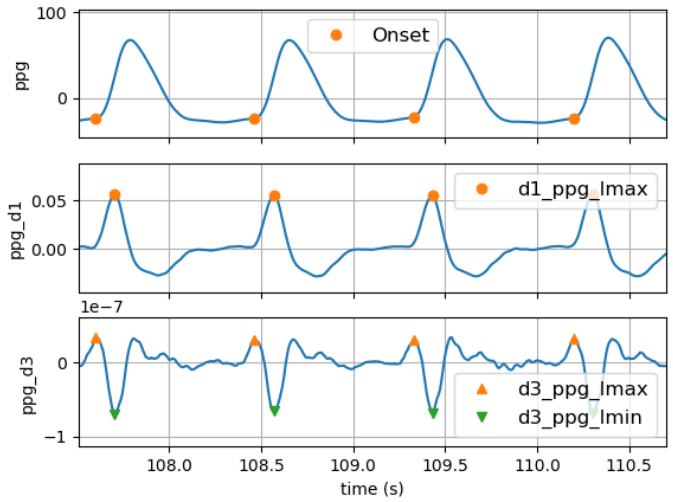

Figure 4.3: Plot of PPG signal and 1st and 3rd derivatives (order top to bottom) with characteristic points for the detection of the onset of each individual pulse.

From the analysis of the d1ppg, the local maxima (d1_ppg_lmax) with absolute amplitude greater than a threshold (ThR) are detected. Here, the ThR is selected based on an adaptive thresholding of the d1ppg data cumulative histogram (calculated within 10 seconds time windows) and was defined as the greater value bellow which 90% of the observations are found. Following the work proposed by Chan et al. [22], the PPG pulse onset was considered to be the point d1ppg presenting a rapid inflection (just before d1_ppg_lmax), which corresponds to a maximum in the d3 ppg (d3_ppg_lmax). The motivation behind this approach was firstly reported by L.B. Cook [184, 31], who observed a significant resemblance between the PPG signal first derivative and the arterial flow waveform. The detection of the d3_ppg_lmax characteristic point was accomplished in two phases: 1) detection of the d3ppg local minima (d3_ppg_lmin) corresponding to the d1ppg local maxima (see 4.3) and; 2) identification of the peak with greater amplitude (d3_ppg_lmax) prior to the previously identified most relevant valley.

4.2.4 Features Extraction

One of the goals of this chapter is to analyze the relationship between different proposed cardiovascular surrogates and blood pressure, thus it is described which features are being considered and how they are calculated.
The pulse arrival time (PAT) is perhaps the most studied feature in this field and has been commonly assessed with a few location definitions, including the diastolic minimum time [27, 3, 114], (b) intersecting tangent method [126], (c) times of maximum derivatives with respect to time [186, 49, 168, 64], and (d) time to reach a fraction of the pulse height [27, 168]. The studied PAT definitions are shown in Figure 4.4:

The left ventricular ejection time (LVET) is commonly associated with stroke volume and has been indicated as a valuable prognostic parameter related to hypovolemia [48]. Using the PPG

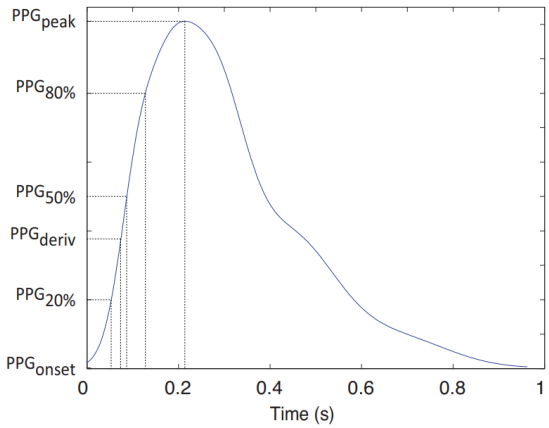

Figure 4.4: Plot of PPG pulse and different reference points for PAT definition and extraction.

waveform, LVET inference was firstly introduced in a study on the analysis of the ear densitogram [133], were it was suggested that the onset and offset of the systolic ejection could be recognized in the morphology of the first derivative. Based on this study, Chan et al. [22] proposed an algorithm for the assessment of LVET based on a rule-based combination of three LVET measures extracted from a multi-derivative analysis of the finger photoplethysmogram. However, some problems can be found on these high-order derivatives-based analysis, where noise can be a critical factor [22]. Later, Ricardo et al. [33] proposed a method for the assessment of cardiovascular surrogates, including LVET, based on the decomposition of the PPG pulse into its forward and reflection waves, using a multi-gaussian (MG) model formulation. The proposed methodology resorts on the segmentation of the PPG pulse into systolic and diastolic phases and consequent modeling of the segmented phases into a sum of three and two Gaussian functions motivated by the underlying physiology of the PPG pulse. For this study, we consider the LVET definition by Chan et. al. as represented in Figure 4.5.

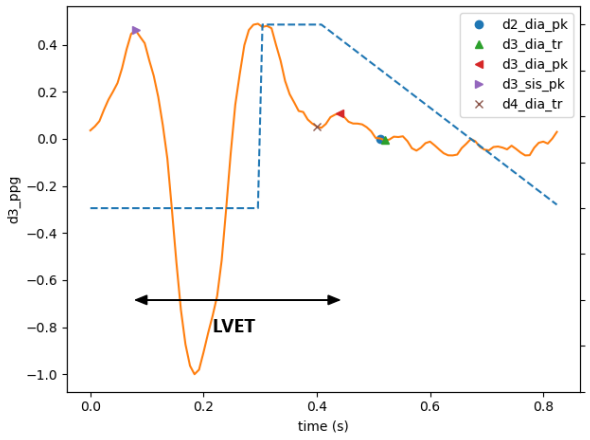

Figure 4.5: Plot of PPG pulse reference points for LVET definition and extraction.

The stiffness index (SI) is associated with the velocity of a pulse wave in large arteries [36], large artery stiffness [101] and it also correlates with pulse pressure [7]. The reflection index (RI) is associated with small artery stiffness [36] and changes in vascular tone [29]. Ricardo et al. [33]

also proposed a definition of RI with the time span between the forward (Ps) and reflected waves (Pd), using his MG model: SI = Bd – Bs. In the same article, a definition for the RI is proposed as the ratio between the amplitudes of the forward and reflected waves: RI = Ad/As. The heart rate (HR) is also studied.
The rationale for studying all this features is the different mechanisms affecting the regulation of BP and that can be identified with these features. It would be expected that chronotropic (HR), inotropic (LVET), vascular blood pressure (PAT, SI, RI) changes would be represented by changes in each of these features.

4.2.5 Features Post-processing

In order to ensure the data integrity, a post-processing step is needed, and it consists of an outlier removal approach similar to [143, 99]. The difference between each feature (FT_i) and its correspondent smoothed version (FTs_i), calculated using a moving median filter (5 minutes window), is defined by (4.5):

$$FT_i(t) = FTs_i(t) - FT_i(t) \tag{4.5}$$

Let $FT_i^w(t) = FT_i(t-w), \ldots, FT_i(t+w)$ be a temporal sliding window over the derived time series FT_i with length $2 * w + 1$ and centered in the instant t, for the i^{th} feature. For each window, the lower quartile (Q1: 25^{th} percentile), the upper quartile (Q3: 75^{th} percentile) and the interquartile range (IQR = Q3 – Q1) are identified and the measurement of $FT_i(t)$ is classified as an outlier if the following condition is satisfied:

$$FT_i(t) < Q1 - 3 * IQR \vee FT_i(t) > Q3 + 3 * IQR \tag{4.6}$$

The rationale behind this approach is that the sporadic parameter values resulting from artifacts and noise can be detected as outliers, which greatly differ from the parameter main trend. Finally, the parameters time-series were linearly interpolated at a 1Hz frequency.

4.2.6 Features Evaluation

In order to evaluate the different features, first one looks at the distributions and correlation between these features and the different targets (SBP, DBP and MAP) for all the data points. After, the Pearson's correlation coefficient is calculated inside 10 minutes windows with 50% overlap between each surrogate (HR, PAT, RI, SI, LVET) and blood pressure (SBP, DBP and MAP). The goal with this analysis is to address the problem of generalization and the conditional correlation between these features and blood pressure as noted by [38]. From this analysis, the best features are selected. The correlation coefficient is given by (4.7):

$$r = \frac{\sum(x - \bar{x})(y - \bar{y})}{\sqrt{\sum(x - \bar{x})^2 \sum(y - \bar{y})^2}} \tag{4.7}$$

4.2.7 Mathematical Models

Arterial pressure varies on a beat-to-beat basis and directly corresponds to cardiac output, arterial elasticity, and peripheral vascular resistance. Physiologically, it's regulated by vasomotion, neural regulation and arterial mechanisms [150]. Given the fluid is contained within an elastic conduits system, energy is transmitted predominantly to the arterial wall rather than through the in-compressible blood. The material properties, thickness, and lumen diameter of the arterial wall thus become the main determinants of the pressure wave velocity (PWV). Vascular elasticity models assume that the Moens–Korteweg equation [110] models a relationship between the wave speed or PWV and the incremental elastic modulus (a coefficient of elasticity) of the arterial wall [71]. Combining it with an exponential arterial elasticity model [26, 62], a BP-PAT model, called the MK-EE model, is obtained. It gives a logarithmic relationship between BP and the PAT. For the MK-EE model, assuming there's a negligible change in the arterial thickness and diameter with pressure variations, BP and the PAT can be linearly related by differentiating the M-K equation, called the L-MK model [26]. To get over the bad linear correlation of DBP in the L-MK model, the Bramwell–Hill equation [194] is introduced in estimating BP to make it have a high correlation, which is named the MK-BH model [163]. Recently, Poon et al. established a mathematical relationship between MAP and a factor that the change in elasticity is caused by pressure wave variations. It could be regarded as the development model of MK-BH, called the dMK-BH model [130].
The mathematical models are described in table 4.1.

Models	**SBP**	**DBP**	**Category**
MK-EE [193]	$a_1 = \ln PAT + b_1$	$a_1' * \ln PAT + b_1'$	Non-Linear
L-MK [26]	$a_2 + b_2 * \mathrm{PAT}$	$a_2' + b_2' * \mathrm{PAT}$	Linear
MK-BH [163]	$\mathrm{SBP}_0 - (2/(\gamma * \mathrm{PAT}_0)) * (\mathrm{PAT} - \mathrm{PAT}_0)$	$\mathrm{SBP} - \mathrm{PP}_0 \cdot (\mathrm{PAT}_0/\mathrm{PAT})^2$	Non-Linear

Table 4.1: Note: γ denoted a vascular information parameter which might be altered with age and the development of cardiovascular diseases. For the healthy subjects, it was set as $0.031 mmHg^{-1}$. SBP_0, PAT_0, PP_0 are measured samples for calibration. $a_1, a_1^{'}, a_2, a_2^{'}, b_1, b_1^{'}, b_2, b_2^{'}$ are fitting parameters.

4.2.8 Model's Performance

In this chapter, a comparison between the aforementioned mathematical models and BP is done by assuming the ABP-line signal as the ground BP values. Also, a comparison between these models and a 5 minutes sampling interval zero-order hold (ZoH) is performed in order to evaluate the usefulness of these models against intermittent NIBP, assuming that this modality only provides the value of the last measurement between the measurements. Intermittent NIBP is usually performed with cuff-based methods, such as oscillometry, that are associated with a certain degree of error compared with ABP-line measures, but this analysis is focused on the intermittent characteristics and different sampling definitions and not on cuff-associated errors.
During the training phase, training data is down sampled in order to obtain 1 sample per minute. This is done in order to simulate real-life applications where the ABP line wouldn't be available and measurements are taken with a cuff. The overall process is described in figure 4.6.

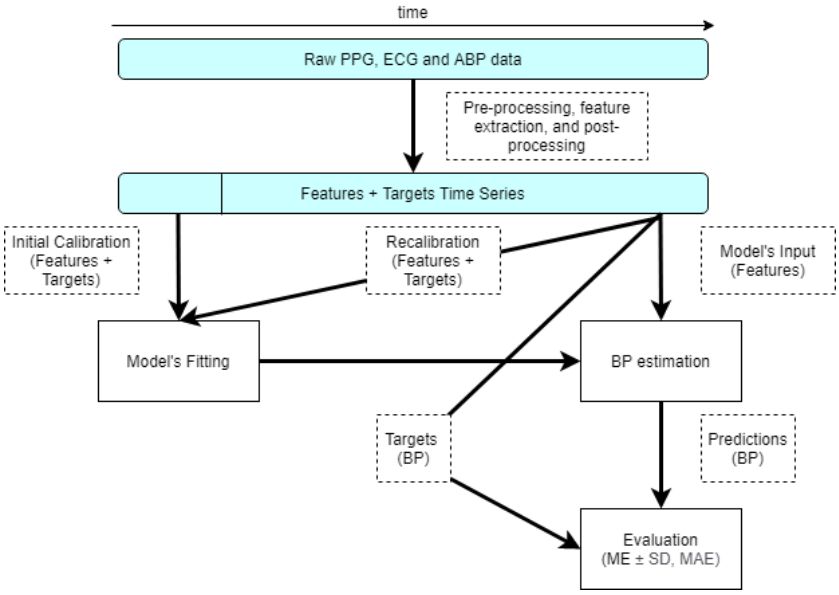

Figure 4.6: Diagram illustrating the analysis of BP estimation algorithms.

Initially, one performs the analysis of the given mathematical models with an initial calibration lasting 10 and 20 minutes. The goal is to analyze the impact of calibration conditions and the effect on long-term predictions. Secondly, static recalibration is performed, with time intervals ranging from [5, 10, 15, 20, 30] minutes. At last, a dynamic recalibration is proposed.
The dynamic recalibration process is based on the variability of true SBP, where a threshold is defined in order to trigger the recalibration process. Although there's no clear definition of a BP event, some studies showed that minor but prolonged and major but brief BP changes can both impact the surgery outcomes [98]. In 1990, Charlson et al. showed that prolonged changes in MAP of more than 20 mmHg or 20% from the patient's preoperative levels were associated with postoperative complications [24]. More recently, Monk et al. found that intraoperative SBP < 67 mmHg for more than 8.2 minutes, mean arterial pressure (MAP) < 49 mmHg for more than 3.9 minutes and diastolic blood pressure (DBP) < 33 mmHg for more than 4.4 minutes were associated with 30-day mortality [103]. Regarding the impact of a dynamic recalibration procedure in the mathematical model's outcomes, Chen suggested that a proper calibration interval should be a trade-off between patient comfort and estimation error and that no calibration should be triggered when BP shows no significant changes [26]. Assuming that minor and prolonged BP changes can be identified with current intermittent NIBP monitoring, one searches for sharp BP changes inside the most common 5 minute sampling interval. One proposes a simplified BP instability evaluation tool where the intervals for recalibration are defined based on the SBP $max - min$ difference, decreasing when SBP instability increases. The intervals were chosen in order to maintain approximately the same total number of samples comparing with the 5 minutes static recalibration for all of the patient's data.
At each instance t we look at the SBP for the last 5 minutes ($w = 5minutes$) and the process is performed as described in Algorithm 1.

Algorithm 1 Adaptive Recalibration Procedure

```
for t in range(SurgeryDuration) do
  if max(SBP[t − w : t]) − min(SBP[t − w : t]) > 20 then
    recalibration each 2.5 minutes
  else if 15 < max(SBP[t − w : t]) − min(SBP[t − w : t]) < 20 then
    recalibration each 5 minutes
  else if 10 < max(SBP[t − w : t]) − min(SBP[t − w : t]) < 15 then
    recalibration each 10 minutes
  else
    recalibration each 20 minutes
  end if
end for
```

The chosen evaluation metrics are the mean error (4.8) ± standard deviation (4.9) ($ME \pm SD$) and the mean absolute error (4.10) (MAE).

$$ME = \frac{1}{n}\Sigma(y - \hat{y}) \tag{4.8}$$

$$SD = \sqrt{\frac{\Sigma\left((y - \hat{y}) - ME\right)^2}{n}} \tag{4.9}$$

$$MAE = \frac{1}{n}\Sigma(|y - \hat{y}|) \tag{4.10}$$

4.3 Results and Discussion

4.3.1 Data Analysis and Feature Selection

In order to evaluate the relationship between HR, LVET, SI, RI and different definitions of PAT, and BP, one looks at the global and local correlation between these features and the targets. Tables 4.2 and 4.3 show the Pearson's correlation coefficients obtained within all the data points and tables 4.4 and 4.5 show the local Pearson's correlation coefficients. The results show that higher correlation between PAT appear when one looks at local correlation inside 10 minutes windows with 50% overlap, confirming the conditional correlation between PAT and BP that results in the need for initial calibration for each patient and continuous recalibration.
The relation between features other than PAT and BP is not linear, since the values swing between positive and negative values, so it's difficult to build a simple mathematical model that relies on these features. PAT_{onset} has the best overall local correlation (R = -0.743 ± 0.220 for SBP, R = -0.730 ± 0.214 for MAP and R = -0.721 ± 0.228 for DBP), meaning that this PAT definition is the most appropriate to infer BP. Figure 4.10 shows a more detailed distributions of the local correlation values that support this idea. Therefore, PAT_{onset} was chosen for future BP estimation algorithms implementation.

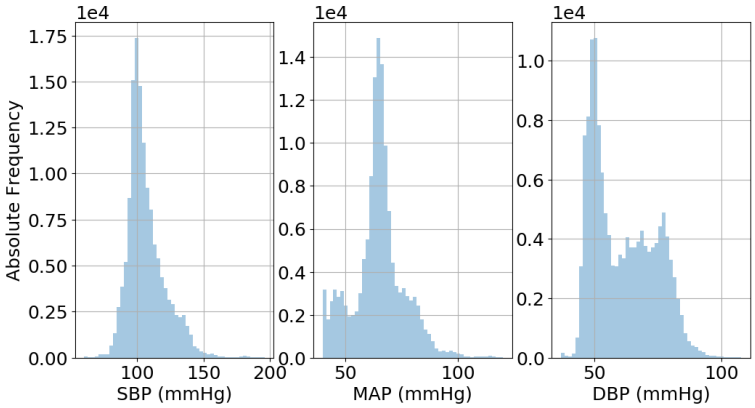

Figure 4.7: Blood pressure distributions with SBP ($\eta = 106.2, \sigma = 15.3$); MAP ($\eta = 70.7, \sigma = 9.0$);DP ($\eta = 52.9, \sigma = 6.9$).

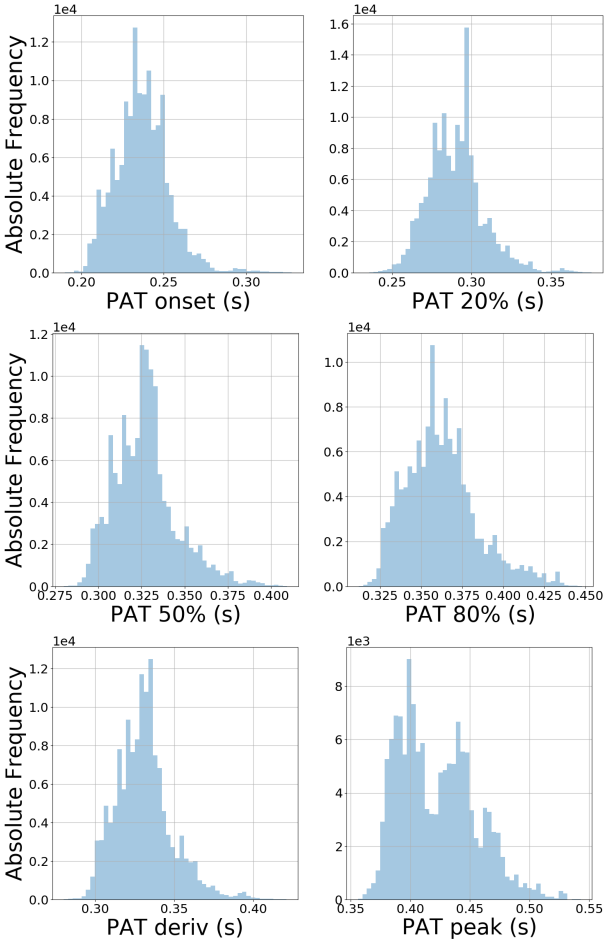

Figure 4.8: Pulse arrival time distributions with PAT_{onset} ($\eta = 0.23, \sigma = 0.02$); $PAT_{20\%}$ ($\eta = 0.29, \sigma = 0.01$); $PAT_{50\%}$ ($\eta = 0.32, \sigma = 0.02$); $PAT_{80\%}$ ($\eta = 0.36, \sigma = 0.02$); PAT_{deriv} ($\eta = 0.33, \sigma = 0.02$); PAT_{peak} ($\eta = 0.41, \sigma = 0.03$) (s).

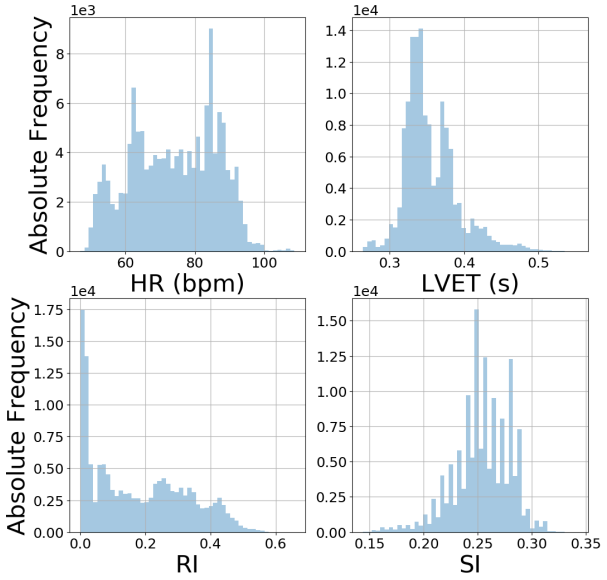

Figure 4.9: Other features distributions with HR; LVET, RI and SI.

	PATonset	PAT20	PAT50	PAT80	PATderiv	PATpeak
SBP	-0,359	-0,266	-0,095	0,077	-0,147	0,259
MAP	-0,191	-0,135	-0,202	-0,238	-0,223	-0,252
DBP	0,091	0,092	0,164	0,225	0,145	0,297

Table 4.2: Global correlation values between PAT and BP.

	HR	LVET	RI	SI
SBP	-0,360	0,230	0,448	-0,231
MAP	0,212	-0,498	-0,123	-0,227
DBP	-0,178	0,242	0,324	0,014

Table 4.3: Global correlation values for HR, LVET, RI and SI, and BP.

	PATonset	PAT20	PAT50	PAT80	PATderiv	PATpeak
SBP	-0.743± 0.220	-0.517 ± 0.377	-0.632 ± 0.308	-0.577 ± 0.372	-0.727 ± 0.238	-0.398 ± 0.506
MAP	-0.730 ± 0.214	-0.463 ± 0.402	-0.601 ± 0.319	-0.550 ± 0.380	-0.703 ± 0.240	-0.389 ± 0.498
DBP	-0.721 ± 0.228	-0.449 ± 0.405	-0.582 ± 0.326	-0.537 ± 0.376	-0.691 ± 0.254	-0.382 ± 0.489

Table 4.4: Local correlation values for PAT and BP, calculated inside 10 minutes windows with 50% overlap and displayed as mean ± standard deviation.

	HR	LVET	RI	SI
SBP	0.039 ± 0.513	-0.061± 0.419	0.210 ± 0.508	-0.045 ± 0.465
MAP	0.141 ± 0.510	-0.127 ± 0.402	0.234 ± 0.512	-0.096 ± 0.453
DBP	0.190± 0.516	-0.144 ± 0.401	0.226 ± 0.506	-0.112 ± 0.449

Table 4.5: Local correlation between HR, LVET, RI and SI, and BP. Displayed as mean ± standard deviation.

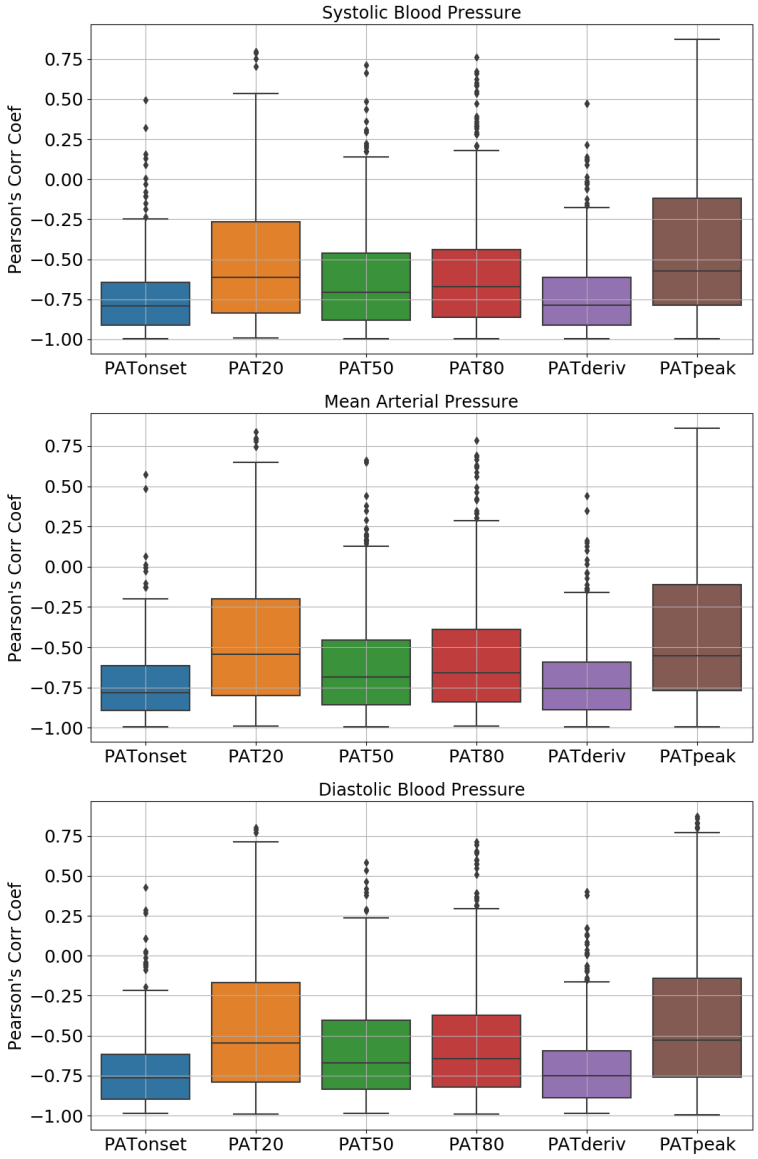

Figure 4.10: Boxplots for each PAT definition showing correlation coefficient's distribution.

4.3.2 Model's Performance

4.3.2.1 No Recalibration

The first step for the analysis of the different addressed models (MK-EE, L-MK and MK-BH) includes an analysis of the importance of initial calibration for each patient in the model's ability to fit the target values. For the initial calibration process, a number of samples are taken from the data (PAT and BP) and these samples are obtained with the past 30 seconds averaged and in such way that we obtain 1 sample per minute, in order to simulate real-world applications where the ABP line isn't available. Two approaches were taken, the first with an initial calibration lasting 10 minutes, consisting of 10 samples, and the second with an initial calibration lasting 20 minutes, consisting of 20 samples. The results shown in tables 4.6 and 4.7 support the need of a long enough initial calibration process so that the BP dynamics are captured by the aforementioned mathematical models. Therefore, the 20 minutes initial calibration duration was chosen for the

following analysis.

	Systolic BP		Diastolic BP	
	ME ± SD	**MAE**	**ME ± SD**	**MAE**
MK-EE	17.05 ± 18.78	19.83	9.63 ± 11.56	10.92
L-MK	17.85 ± 19.46	20.52	10.06 ± 12.07	11.29
MK-BH	18.38 ± 20.24	20.85	15.66 ± 17.98	18.29

Table 4.6: Performance of each model (MK-EE, L-MK and MK-BH) with 10 mins (10 samples) initial training and no recalibration.

	Systolic BP		Diastolic BP	
	ME ± SD	**MAE**	**ME ± SD**	**MAE**
MK-EE	5.41 ± 10.53	8.60	3.33 ± 5.93	4.91
L-MK	5.63 ± 12.97	8.63	3.47 ± 5.90	4.97
MK-BH	11.63 ± 11.58	13.83	8.91 ± 9.15	10.62

Table 4.7: Performance of each model (MK-EE, L-MK and MK-BH) with 20 mins (20 samples) initial training and no recalibration.

4.3.2.2 Fixed Time Interval Recalibration

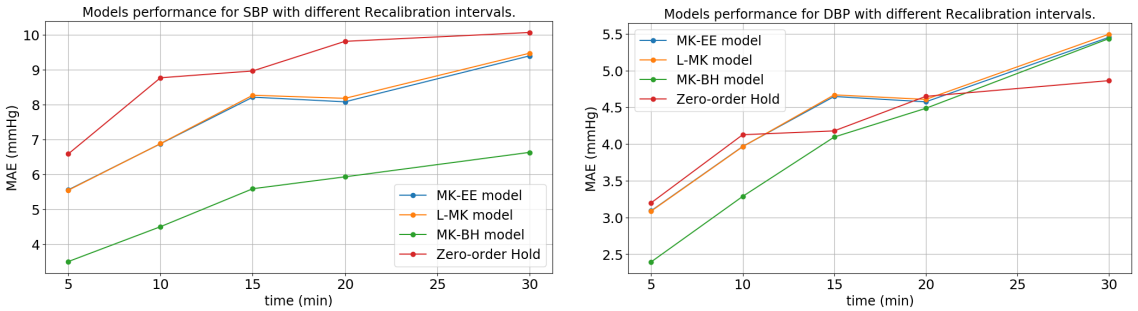

Figure 4.11: Performance in terms of MAE for each model and different fixed time interval recalibrations with SBP (top) and DBP (bottom) as targets.

In order to evaluate different fixed time interval recalibration processes with different frequencies, one starts by looking at the global MAE for SBP and DBP estimation as a function of different time intervals ranging from 5 to 30 minutes, including the Zero-order Hold (ZoH) that represents the intermittent NIBP, as shown in figure 4.11. It is noticeable that the mathematical models clearly outperform the ZoH when they are recalibrated each 5 minutes, and the results are presented in table 4.8, with the MK-BH model achieving ME values of 0.55 ± 5.94 for SBP and 0.42 ± 4.17 for DBP while the ZoH achieved 0.10 ± 11.66 for SBP and -0.01 ± 5.44 for DBP. In terms of MAE, the MK-BH model achieved 3.50 for SBP and 2.39 for DBP while the ZoH obtained 6.58 for SBP and 3.20 for DBP.

Figure 4.15 provides useful information about the dispersion of ME and MAE for the different models and ZoH estimating SBP and DBP, showing that the MK-BH model achieves less error dispersion for both SBP and DBP estimation than the other models and ZoH and further supporting that this model is the best solution for BP estimation. In order to further investigate the applicability of these models in practice, one looks also at the number of samples extracted during the process for the mathematical models and ZoH and the results show an increase of 30% with the use of these models, caused by the number of samples for the initial calibration.

Only 5% of the MK-BH model SBP estimates have absolute errors above 11.9 mmHg while this number rises to 24.6 mmHg for the ZoH; 99% of the MK-BH model SBP predictions have absolute errors below 24.2 mmHg while the ZoH achieves 50.2 mmHg. This numbers suggest that the ZoH is much more prone to bigger outliers than the MK-BH model, which highly affects the detection of relevant BP changes in critical settings.

Figures 4.12 and 4.13 show one patient's ground truth SBP and predictions achieved with the MK-BH model and ZoH. Here, the advantage of having a mathematical model predicting SBP in real-time against ZoH is highlighted, since it can successfully describe SBP dynamics inside the 5 minutes sampling interval that wouldn't be possible with the intermittent NIBP solution. Zooming in one specific segment (280 - 320 minutes, figure 4.14), this example suggests how the use of the MK-BH model in this specific conditions could identify in real-time a quick and sharp drop in SBP leading to hypotension (SBP $<$ 90 mmHg) and how ZoH (intermittent measurements) could completely miss an hypotension episode.

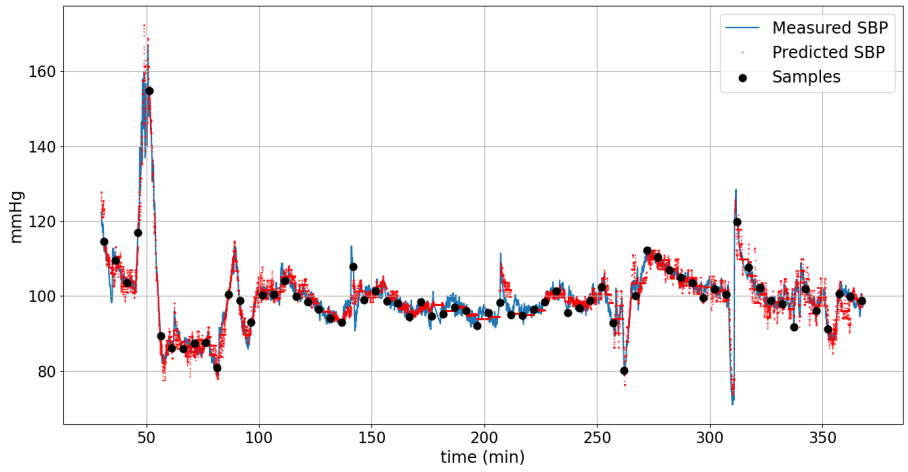

Figure 4.12: Example of one patient comparing ground truth SBP (blue) with MK-BH model's predictions with recalibration performed each 5 minutes (red) with the samples identified with black dots. First 20 minutes correspond to the intial calibration.

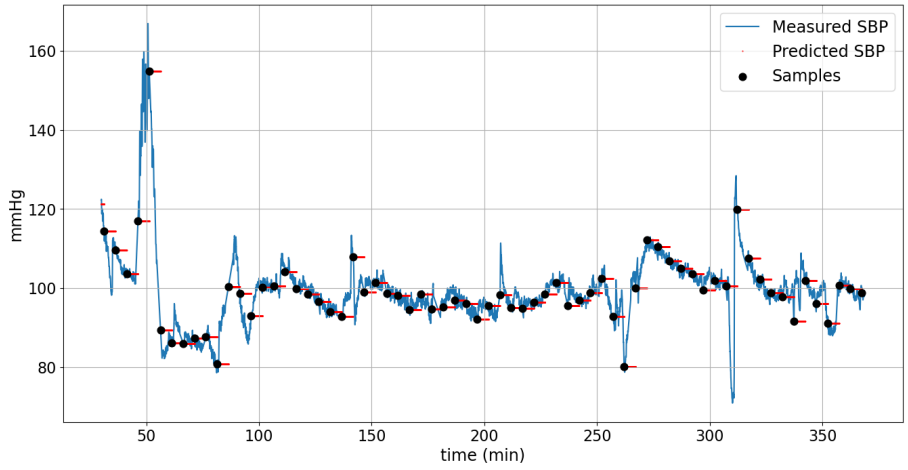

Figure 4.13: Example of one patient comparing ground truth SBP (blue) with ZoH predictions with samples extracted each 5 minutes (red) with the samples identified with black dots.

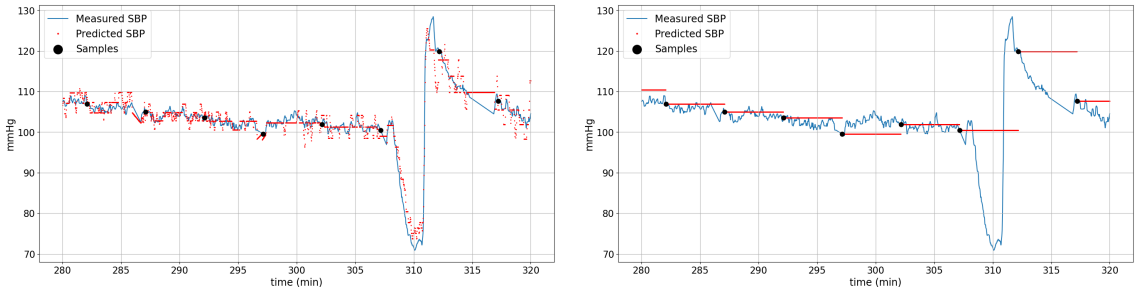

Figure 4.14: Zoom in specific segment of one of the patients. Left: MK-BH model predictions (red) on top of ground truth SBP (blue) with samples identified with black dots. Right: ZoH (red) on top of ground truth SBP (blue) with samples identified with black dots.

	Systolic BP		Diastolic BP		
	ME +- SD	**MAE**	**ME +- SD**	**MAE**	**No. Samples**
MK-EE	2.40 +- 7.95	5.55	1.89 +- 4.54	3.09	599
L-MK	2.49 +- 7.90	5.54	1.23 +- 4.53	3.09	599
MK-BH	0.55 +- 5.94	3.50	0.42 +- 4.17	2.39	599
ZoH	0.10 +- 11.66	6.58	-0.01 +- 5.44	3.20	464

Table 4.8: Performance of each model (MK-EE, L-MK, MK-BH and Zero-order Hold (ZoH)) with 20 mins (20 samples) initial training and recalibration performed each 5 minutes. The last (right) column shows the number of samples extracted from the time-series data.

Another analysis represented in table 4.9 shows the performance that these models achieve when they are recalibrated every 15 minutes, and compares with the ZoH performed each 5 minutes. While decreasing the number of samples by 47%, the MK-BH models was able to outperform the ZoH model in terms of ME and MAE for SBP, obtaining ME values of 0.47 ± 8.94 versus the 0.10 ± 11.66 obtained by the ZoH and a slight loss of the MK-BH model against ZoH in terms of DBP, obtaining 0.76 ± 6.83 versus -0.01 ± 5.44. The same thing for MAE values. This results are corroborated by the error dispersion shown in figure 4.16 where the MK-BH model outperforms the ZoH for SBP estimation, but is overtaken by the ZoH for DBP estimation. Only 5% of the MK-BH model SBP estimates have absolute errors above 20.8 mmHg while this number rises to 24.6 mmHg for the ZoH; 99% of the MK-BH model SBP predictions have absolute errors below 34.0 mmHg while the ZoH achieves 50.2 mmHg. This numbers support that the ZoH is much more prone to bigger outliers than the MK-BH model, even with less recalibrations performed.

	Systolic BP		Diastolic BP		
	ME ± SD	**MAE**	**ME ± SD**	**MAE**	**No. Samples**
MK-EE	4.47 ± 10.20	8.21	2.67 ± 5.99	4.64	316
L-MK	4.61 ± 10.22	8.27	2.73 ± 6.02	4.67	316
MK-BH	0.47 ± 8.94	5.59	0.76 ± 6.83	4.09	316
ZoH	0.10 ± 11.66	6.58	-0.01 ± 5.44	3.20	464

Table 4.9: Performance of each model (MK-EE, L-MK, MK-BH and Zero-order Hold (ZoH)) with 20 mins (20 samples) initial training and recalibration performed each 15 minutes. The last (right) column shows the number os samples extracted from the time-series data.

These results show the potential for improving the NIBP monitoring with simple mathematical models while slightly increasing the number of cuff measurements. Also, reducing the number of cuff measurements, thus increasing the patient's comfort, it is possible to achieve similar performance with these models.

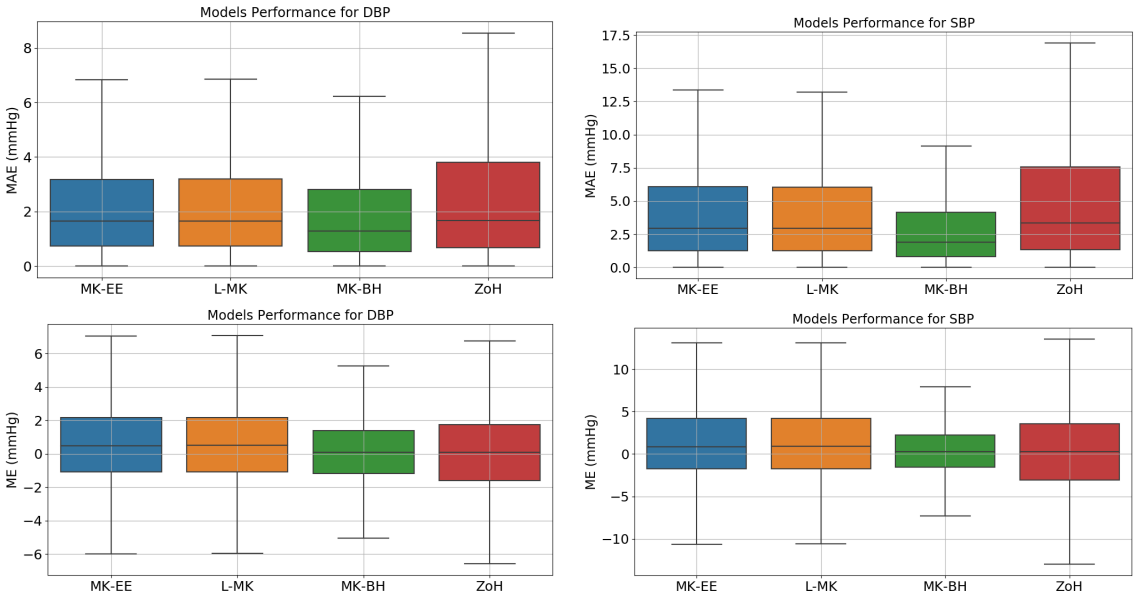

Figure 4.15: Boxplots showing distributions of absolute error (top) and error (bottom) for DBP (left) and SBP (right) for models with fixed time interval recalibration of 5 minutes.

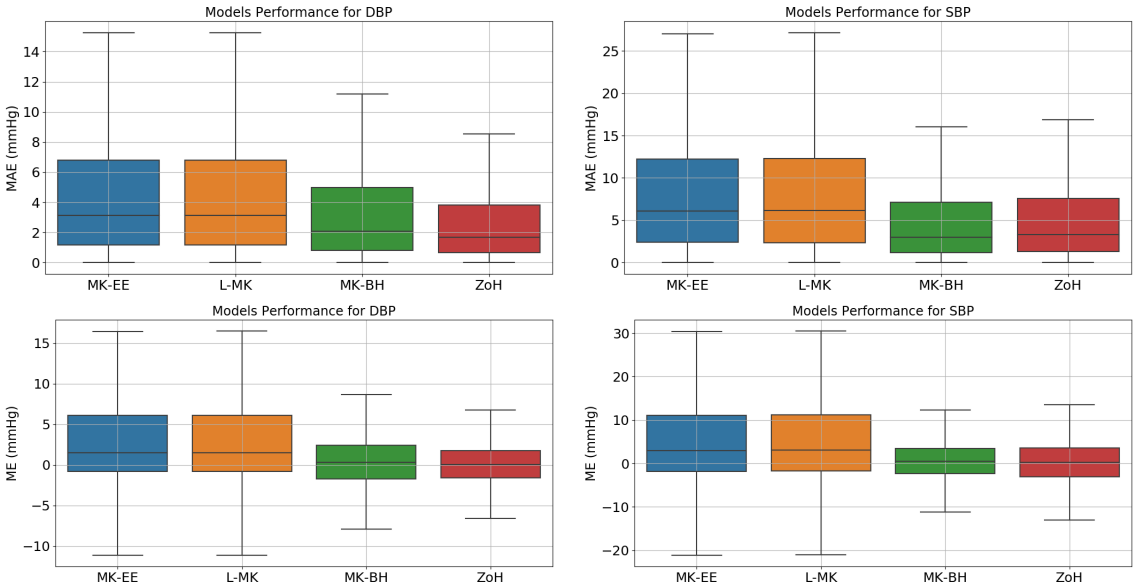

Figure 4.16: Boxplots showing distributions of absolute error (top) and error (bottom) for DBP (left) and SBP (right) for models with fixed time interval recalibration of 15 minutes.

4.3.2.3 Dynamic Recalibration

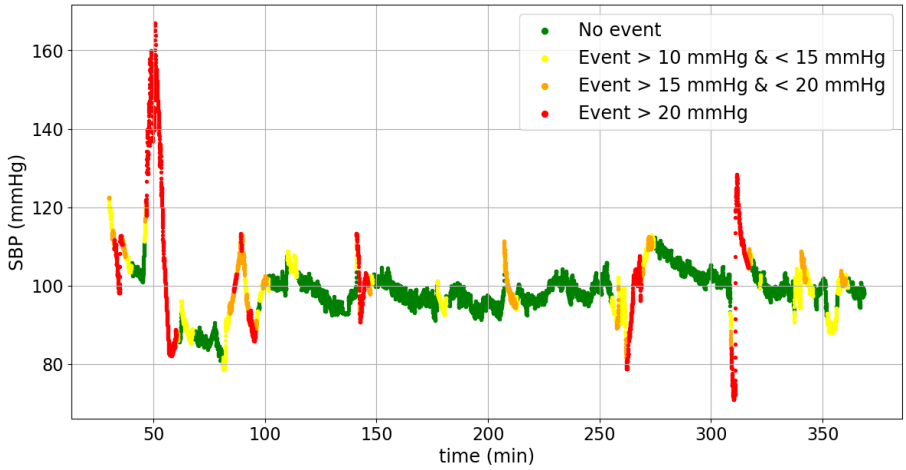

Figure 4.17: Example of one patient's categorical definition of BP events using SBP $max - min$ difference inside 5 minutes windows

In this section, an approach for dynamic recalibration (Algorithm 1) is analyzed. Since the criticality in BP monitoring refers to the events that happen during surgeries that lead to highly increased or decreased BP in short periods of time, one tests the performance of the aforementioned mathematical models and ZoH with dynamically defined sampling frequencies against state-of-the-art 5 minute fixed interval ZoH. Figure 4.17 shows an example of the events definition proposed here and one can identify different relevant BP events categorized based on the amplitude of the change that will trigger different sampling intervals.

The results shown in table 4.10 suggest that this approach would improve the performance of

	Systolic BP		Diastolic BP		
	ME +- SD	**MAE**	**ME +- SD**	**MAE**	**No. Samples**
MK-EE	2.90 +- 8.14	6.05	1.52 +- 4.58	3.32	571
L-MK	2.94 +- 8.07	6.02	1.54 +- 4.55	3.30	571
MK-BH	0.68 +- 4.88	3.23	0.46 +- 3.86	2.40	571
ZoH*	0.10 +- 11.66	6.58	-0.01 +- 5.44	3.20	464
ZoH	0.69 +- 8.67	5.72	0.35 +- 4.28	2.88	391

Table 4.10: Performance of each model (MK-EE, L-MK, MK-BH and Zero-order Hold (ZoH)) with 20 mins (20 samples) initial training and recalibration performed dynamically. The last (right) column shows the number os samples extracted from the time-series data. * ZoH performance from 5 minutes fixed sampling interval.

both MK-BH model and ZoH against state-of-the-art 5 minute fixed sampling interval in terms of MAE and ME, while increasing the number of samples by 23% (180 initial calibration samples + 391 recalibration samples). Figure 4.18 shows the error dispersion for the different models, further supporting that the MK-BH model clearly outperforms the other methods in both SBP and DBP estimation. Comparing the error dispersion of the MK-BH model and ZoH dynamically recalibrated with the 5 minutes static recalibration, as shown in figure 4.19, one can identify a slight increase in the error dispersion for the dynamic recalibration approach, except for the SBP estimation MAE metric.

Only 5% of the MK-BH model SBP estimates have absolute errors above 10.0 mmHg while the number rises to 16,6 mmHg for the ZoH. Also, 1% of absolute errors are above 16.9 mmHg for the MK-BH model and 34.0 mmHg for the ZoH, once again suggesting that the MK-BH model is also able to avoid relevant outliers with the dynamic solution compared with the ZoH. Comparing these results with the 5 minutes fixed recalibration interval, one identifies relevant improvements, with top 5% of absolute errors decreasing from 11.9 mmHg to 10.0 mmHg for the MK-BH models and from 24.6 mmHg to 16.6 mmHg for the ZoH. Looking at the top 1% the errors, it decreased from 24.2 mmHg to 16.9 mmHg for the MK-BH model and from 50.2 mmHg to 34.0 mmHg for the ZoH. This results suggest that the dynamic recalibration approach would highly improve both MK-BH model and ZoH performance, avoiding major outliers.

Figures 4.20 and 4.21 show how the MK-BH model and the ZoH behave in one of the patients regarding the estimation of SBP. It's noticeable that the BP samples are mostly triggered in the presence of relevant BP events and avoided when BP is steady. The advantages of having a dynamic sampling solution are highlighted and the MK-BH model proves to be a good solution for non-invasive BP monitoring, capturing relevant BP dynamics between samplings.

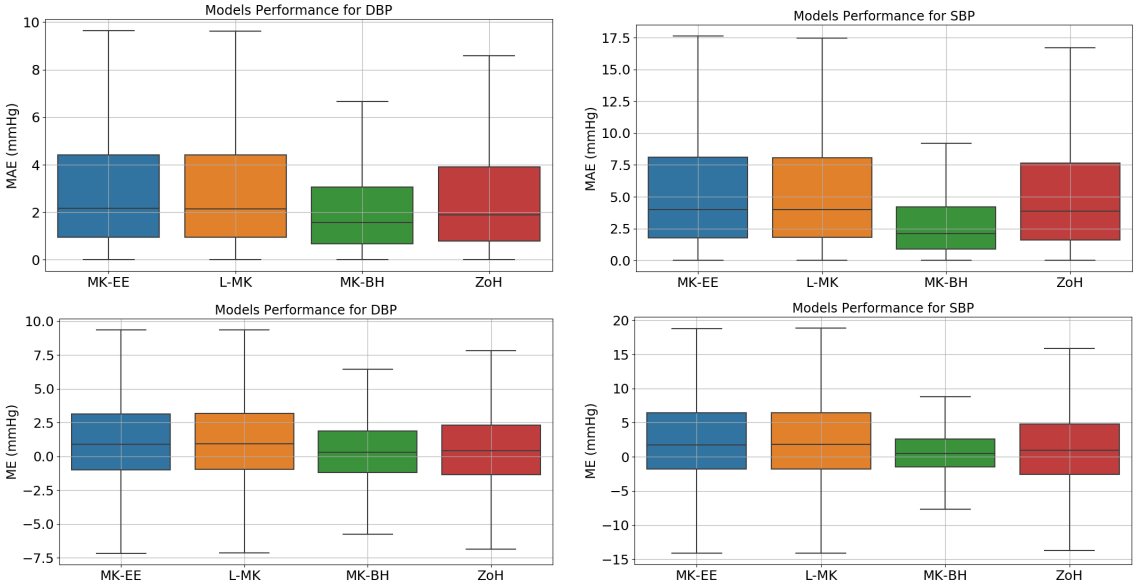

Figure 4.18: Boxplots showing distributions of absolute error (top) and error (bottom) for DBP (left) and SBP (right) for models with dynamic recalibration.

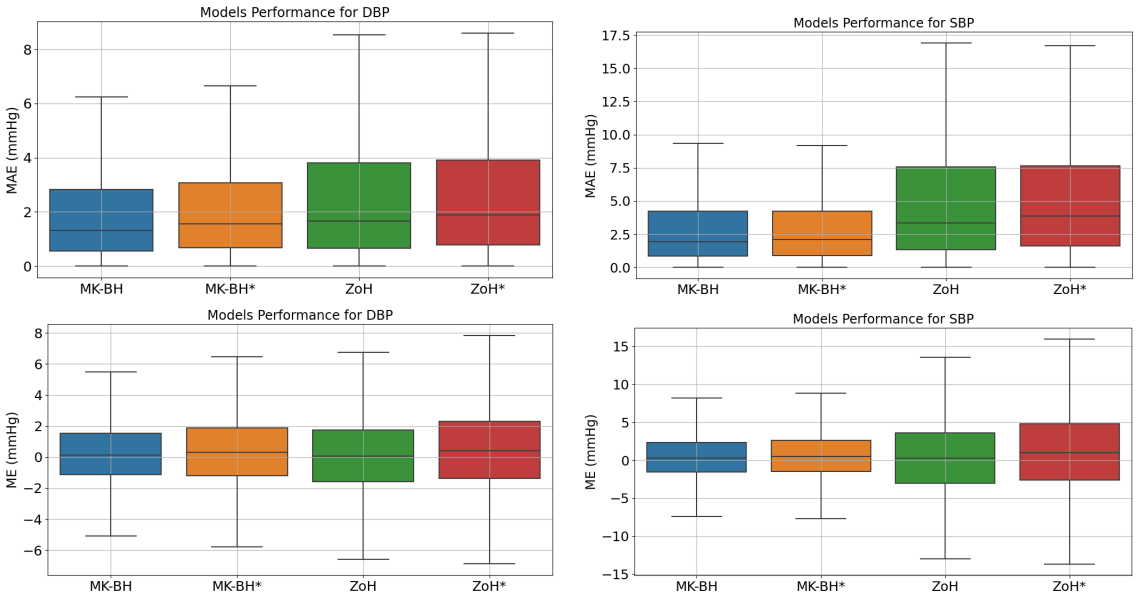

Figure 4.19: Boxplots showing distributions of absolute error (top) and error (bottom) for DBP (left) and SBP (right) for models with 5 minutes static and (*) dynamic recalibration.

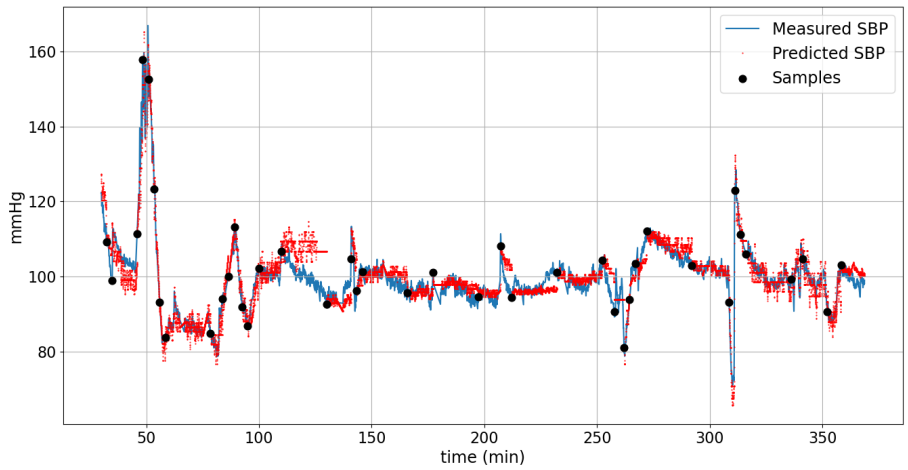

Figure 4.20: Example of one patient comparing ground truth SBP (blue) with MK-BH model's predictions with recalibration performed dynamically (red) with the samples identified with black dots.

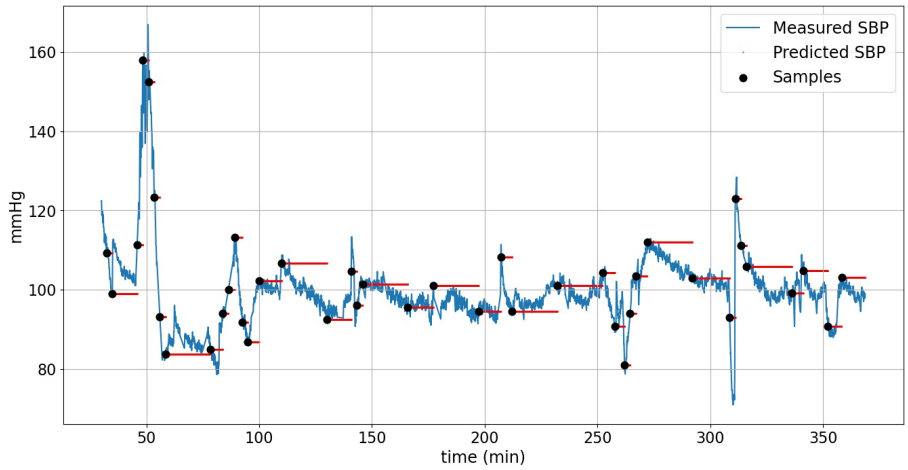

Figure 4.21: Example of one patient comparing ground truth SBP (blue) with ZoH predictions with samples extracted dynamically (red) with the samples identified with black dots.

4.4 Conclusion

In this chapter, the performance of different models for continuous BP estimation under distinct circumstances was analyzed, with the focus on real life application in the OR.
It started with an analysis of different proposed time-domain features for cardiac function evaluation that proved that the relationship between radial ABP and these features is conditional with low absolute global correlation coefficients, something that has been previously addressed in the literature [130, 49]. A screening of local correlation coefficients calculated inside 10 minutes windows with 50% overlape showed that the relationship between BP and HR, LVET, SI and RI is not linear, with local correlation coefficients ranging between positive and negative values. PAT_{onset} proved to be the best BP surrogate to correlate with ABP with R = -0.743 $\pm$ 0.220 for SBP, R = -0.730 $\pm$ 0.214 for MAP and R = -0.721 $\pm$ 0.228 for DBP.
Our assessment evolved around the test of 3 different BP estimation models against invasive ABP measurements (assumed as ground truth) and ZoH (intermittent NIBP measurements assumed as cuff measurements without associated errors) under different scenarios. First, different initial calibration settings, with a first initial calibration lasting 10 minutes (10 samples) and a second lasting 20 minutes (20 samples) were tested. The second calibration setting provided significantly better results, as shown in tables 4.6 and 4.7. The second analysis referred to different recalibration fixed intervals and opposed the mathematical models to the 5 minute sampling time ZoH, showing that the use of these models could highly improve the quality of BP monitoring in the OR with a continuous BP estimation solution that highly reduces the error between measured BP and ground truth BP, allowing a real-time BP monitoring and events detection. The MK-BH model proved to be the best mathematical model in terms of ME and MAE with the best error distribution, avoiding outliers and showing high versatility for adapting to changes in the cardiovascular structure properties during surgery, captured by recalibration samples. This is an extremely important feature, given that intraoperative hemodynamic perturbations are common due to the effects of anesthetic agents and techniques, surgical manipulations, and the patient's medical comorbidities. Also included in this analysis, one compares the performance of 5 minutes interval ZoH and the models with recalibration each 15 minutes, with the MK-BH model performing similarly to the ZoH. These promising results suggest that the MK-BH model might be used in less critical surgeries with less recalibration samplings, providing real-time BP estimation and detection of BP events while reducing the number of samples by almost an half.
The last step of this chapter includes the proposal of a dynamic sampling time that would adapt to BP variability, increasing the BP sampling in the presence of relevant events. For the definition of BP events, a simple approach that categorizes BP events based on $max - min$ differences inside 5 minutes windows is proposed. The idea behind this proposal is the utmost importance of detecting quick and wide BP changes of patients undergoing surgery aligned with the constant need for recalibration of the mathematical models that becomes more relevant in the presence of high cardiovascular instability. Also, one tests how the dynamic sampling would influence intermittent NIBP. The results support the idea that both continuous and intermittent NIBP would highly benefit from a dynamic BP sampling solution, with global ME and MAE dispersion highly reduced in the ZoH, in line with with the results presented by [12] in his *offline* analysis. Since the data being analyzed comes from patients undergoing delicate surgeries, such as cardiovascular interventions, the BP is highly unstable in some of the patients, and the dynamic approach considers the BP variability, resulting in an elevated number of BP samples. In a real-life application, this solution

would fit best in less critical interventions, as proposed by [95], resulting in less BP samples while maintaining a real-time BP monitoring and triggering increased number of samples only in the presence of relevant BP events. Also, this approach could fit to other scenarios such as the general ward, where BP measurements are often taken only every 4 to 6h and events of hypotension and hypertension are common, many of them going undetected [170]. With a solution like the one proposed, measurements could be triggered when a relevant BP change occurs.
Although the results for the dynamic sampling BP monitoring approach support the idea, the BP variability that is used to categorize BP events was extracted directly from the ABP signal, thus opening the door for a solution that would infer the BP variability non-invasively. This solution should be able to generalize for different patients, since there's no way to guarantee that relevant BP changes are captured during initial calibrations. In chapter 5, a solution for BP events detection and categorization is proposed based on the definition proposed here.
Overall, the analysis presented in this chapter suggests that the different mathematical models (L-MK, MK-EE and MK-BH), although very simple, are capable of estimating accurate real-time BP values compared with invasive measurements in the intraoperative environment, with a proper recalibration procedure requiring cuff measurements. The proposed strategy is described in figure 4.22. Since cuff-associated errors are not considered in this study, a future analysis is required in order to better estimate the performance of this models in real-life applications and compare with currently available continuous NIBP solutions such as the CNAP (CNSystems Medizintechnik AG, Graz, Austria). Different more complex models for BP estimation based on PWV have been proposed, as shown in table A.1, but non of them has been developed in an environment like the intraoperative scenario with continuous BP estimations compared with invasive ABP monitoring and designed for real-life applications.

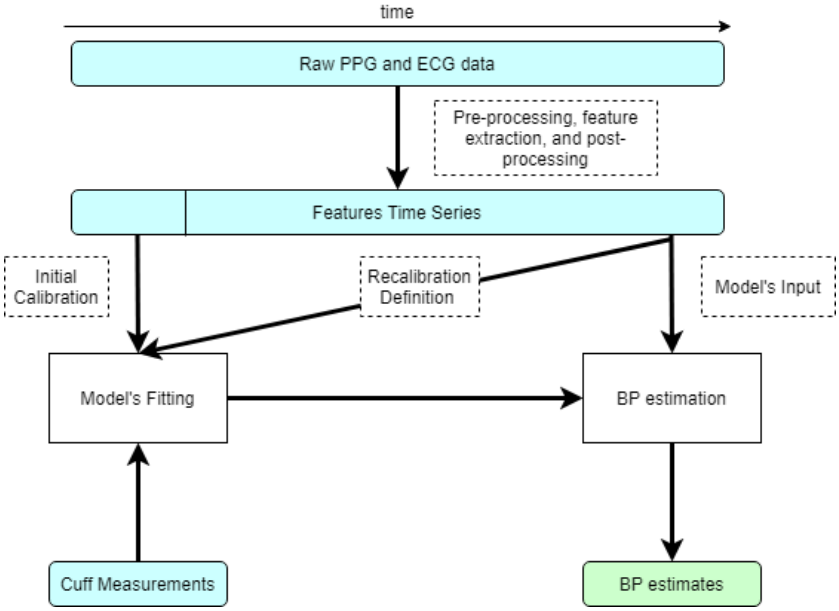

Figure 4.22: Diagram illustrating the proposed BP estimation algorithm.

5

Algorithm for Blood Pressure Fast Events Detection

5.1 Introduction

This thesis addresses the relevance of BP monitoring in clinical practice, showing that in the operative room (OR) or in the intensive care unit (ICU) the most accurate technique is the arterial line with a pressure transducer. This method provides a continuous ABP waveform signal that enables instantaneous analysis and allows quick clinical interventions with the major drawbacks being the fact that it is invasive, thus related to infections and requiring delicate procedures, and requires specially trained operators. The most common BP assessment method in the hospitals are cuff-based methods such as oscillometry or auscultation, which represent intermittent non-invasive BP (NIBP) monitoring solutions that are cheap and easy to employ. This methods are often used in situations of low to intermediate criticality and measurements can be triggered automatically in fixed time intervals ranging from several minutes (e.g., surgeries) to several hours (e.g., general ward) [146]. Given that the intermittent NIBP is such a widely available and simple application solution, an optimized non-uniform sampling solution could highly improve the intermittent NIBP monitoring performance [12].

In the previous chapter, continuous NIBP estimation solutions were addressed and the potential and limitations of some of the most simple mathematical models based on the pulse wave velocity (PWV) found in the literature were described, suggesting the need for several recalibrations during the procedure. One potentially interesting approach is the design of an events detection algorithm that triggers measurements based on the variability of BP, creating a personalized *online* solution that adapts to the patient condition at any given point in time. In fact, a recent study by Bresch et al. consisting of the analysis of an *offline* reconstruction of the ABP data as a ZoH with uniform *versus* optimized non-uniform sampling and evaluating the root mean squared error (RMSE) between the reconstruction and the original BP time series suggested improvements of approximately 50% with respect to the optimized non-uniform solution [12].

BP changes in a patient during the perioperative and intraoperative care can be either minor, but prolonged, or major, but brief, and both have impact in the surgery's outcome [98]. While the slower changes can be detected with a fixed interval cuff-based BP measurements and other monitoring techniques, faster and sharper BP changes can occur in a matter of seconds and drive the BP to certain values found to be correlated with worse outcomes, even if it lasts only a few minutes [103].

In this chapter, we propose a non-uniform sampling method based on the SBP variability inside 5 minutes windows and look at the $max - min$ SBP difference. Then, 3 thresholds were defined in order to categorize the BP instance as "No Event", "Small Event", "Medium Event" and "Big Event". Since this definition is based on the direct analysis of the BP time series, it was used as a target for a Logistic Regression classifier based on BP surrogates extracted with ECG and PPG signals, in order to create a non-invasive online solution for quick and sharp BP events detection. This solution would ideally provide real-time information to clinicians about relevant changes in a patient's hemodynamics that wouldn't be possible with traditional intermittent NIBP monitoring. Several features have been studied and analyzed in the previous chapter. The same features (PAT, HR, LVET, RI, SI) are expected to provide useful information in order to detect BP changes and will be analyzed.

5.2 Methods

5.2.1 Data Collection

Data collection was performed as described in 4.2.1.

5.2.2 Parameters Extraction

The different parameters used as BP surrogates (PAT, LVET, RI, SI and HR) were extracted as described in Sections 4.2.2, 4.2.3, 4.2.4 and 4.2.5. The chosen PAT definition was PAT_{onset} since it suggested the best relationship with BP from all the different PAT definitions.

5.2.3 Events Definition

The BP events definition consists of the categorization of the SBP in 4 classes (y), depending on it's variability as described in Algorithm 2.

Algorithm 2 Adaptive Recalibration Procedure with Class Definition.

for t in range(SurgeryDuration) **do**
  if $max(SBP[t-w:t]) - min(SBP[t-w:t]) > 20$ **then**
    y[t] = 3
  else if $15 < max(SBP[t-w:t]) - min(SBP[t-w:t]) < 20$ **then**
    y[t] = 2
  else if $10 < max(SBP[t-w:t]) - min(SBP[t-w:t]) < 15$ **then**
    y[t] = 1
  else
    y[t] = 0
  end if
end for

5.2.4 Feature Extraction

In order to extract features that reflect BP events as described, a similar approach as the events definition is taken and at each instance t one looks at each parameter for the last 5 minutes ($w = 5min$) $FT_i[t-w:t]$ and the $max - min$ difference is calculated and normalized by the mean

(5.1). In the following analysis FT_1 : HR, FT_2 : LVET, FT_3 : PAT, FT_4 : RI and FT_5 : SI.

$$FT_i[t] = (max(FT_i[t-w]) - min(FT_i[t-w]))/mean(FT_i[t-w]) \tag{5.1}$$

5.2.5 Features Evaluation

Features evaluation is performed with an analysis of its' distribution for the different defined classes. Also, a linear discriminant analysis (LDA) is performed. LDA is a well-known scheme for feature extraction and dimension reduction and projects the data onto a lower-dimensional vector space such that the ratio of the between-class distance to the within-class distance is maximized, thus achieving maximum discrimination. The optimal projection (transformation) can be readily computed by applying the eigen decomposition on the scatter matrices. LDA ends up creating one or more linear combinations of predictors, creating a new latent variable for each function. These functions are called discriminant functions. Here, the LDA is performed given all the features as inputs and one discriminant function maximizing the differences between groups is obtained.

5.2.6 Classification Model

The chosen statistical model for the events detection and classification is the multinomial logistic regression (MLR) that can be used to predict a nominal dependent variable given one or more independent variables. The logic of the MLR with a single predictor (X) and one categorical varaible (Y) is expressed as (5.2)

$$\text{logit}(Y) = \alpha + \beta X \tag{5.2}$$

Therefore (5.3),

$$\pi = \text{ Probability } (Y = y|X = x) = \frac{e^{\alpha+\beta X}}{1 + e^{\alpha+\beta X}} \tag{5.3}$$

where π is the probability of the event, α is the Y intercept, β is the regression coefficient, and X is the set of predictors. α and β are estimated by the negative log likelihood method. MLR, by default, is not effective with imbalanced classification so the optimization method (negative log likelihood) was modified in order to adjust the error penalty for the different targets based on their frequency, so that the more frequent classes have less weight, resulting in smaller error value thus less update to the model coefficients. The strategy to find the best weights is using the inverse of each class distribution in the training data set.

5.2.7 Model Evaluation

Since one of the goals for this analysis is to test a solution capable of generalizing for different patients, the chosen technique for the model evaluation is the 5-fold cross validation (5-CV). The 5-CV consists of 5 rounds involving the partitioning of each patient's data in 5 subsets and choosing 4 of them for training (fitting the MLR model) and the other for testing (evaluation). The training subsets of the different patients are merged and the same thing happens for the test subsets. At each round, one different test subset from each patient is chosen. At the end, the different evaluation metrics are averaged. Figure 5.1 illustrates the proposed algorithm and how it is evaluated.

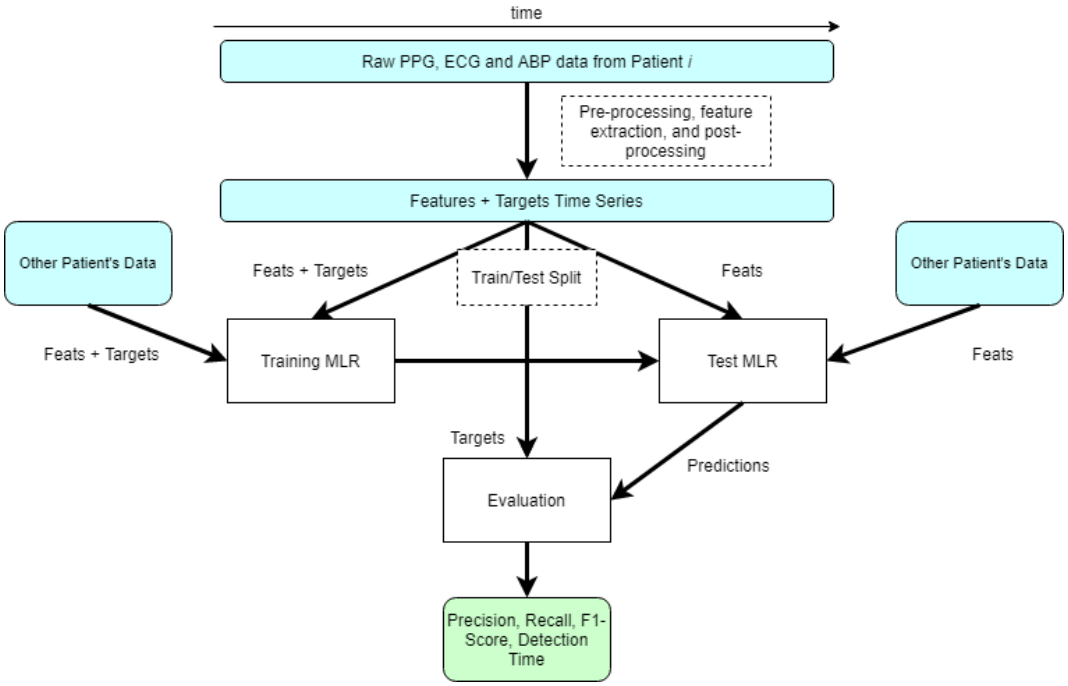

Figure 5.1: Diagram illustrating the proposed algorithm and evaluation.

The evaluation metrics include macro-average precision (maP), recall (maR) and F-score (maF), the precision (P), recall (R) and F-score (F) for each class. Ultimately, one looks at classes equal to zero ($C = 0$) and classes different than zero ($C \neq 0$) and calculate the precision (Pb), recall (Rb) and F-score (Fb) in order to evaluate the performance of this model in distinguishing between events and no-events and the time it takes the model to detect a transition between a no-event state ($C = 0$) to a event state ($C \neq 0$) is evaluated with the detection time (DT) metric. In the end, the confusion matrix for each of the 5-CV iterations are summed and presented.

5.3 Results and Discussion

5.3.1 Features Evaluation

Looking at each feature distribution ($FT_{1...5}$) in figure 5.2, one concludes that it is difficult to separate each feature in the different classes ($y = 0, 1, 2, 3, 4$, except for FT_3 extracted from PAT. Using the linear discriminant analysis, it was expected to obtain a discriminant function capable of maximize the differences between the different groups and a slight improve is observed (T1). This new feature will be used as input by the MLR. One important consideration in the following analysis is the frequency of each outcome ($y = 0, 1, 2, 3$) in the data available as shown in table 5.1. The data-set is unbalanced in terms of the different classes, thus the need for a modification in the MLR's optimization method as described in Section 5.2.6. Considering non-event ($y = 0$) and event ($y \neq 0$) states, the problem is attenuated with relative frequencies of 58.9% and 41.1%, respectively.

Class	**Relative Frequency (%)**
0	58.9
1	14.3
2	8.8
3	18.0

Table 5.1: Relative frequency of each class in the data

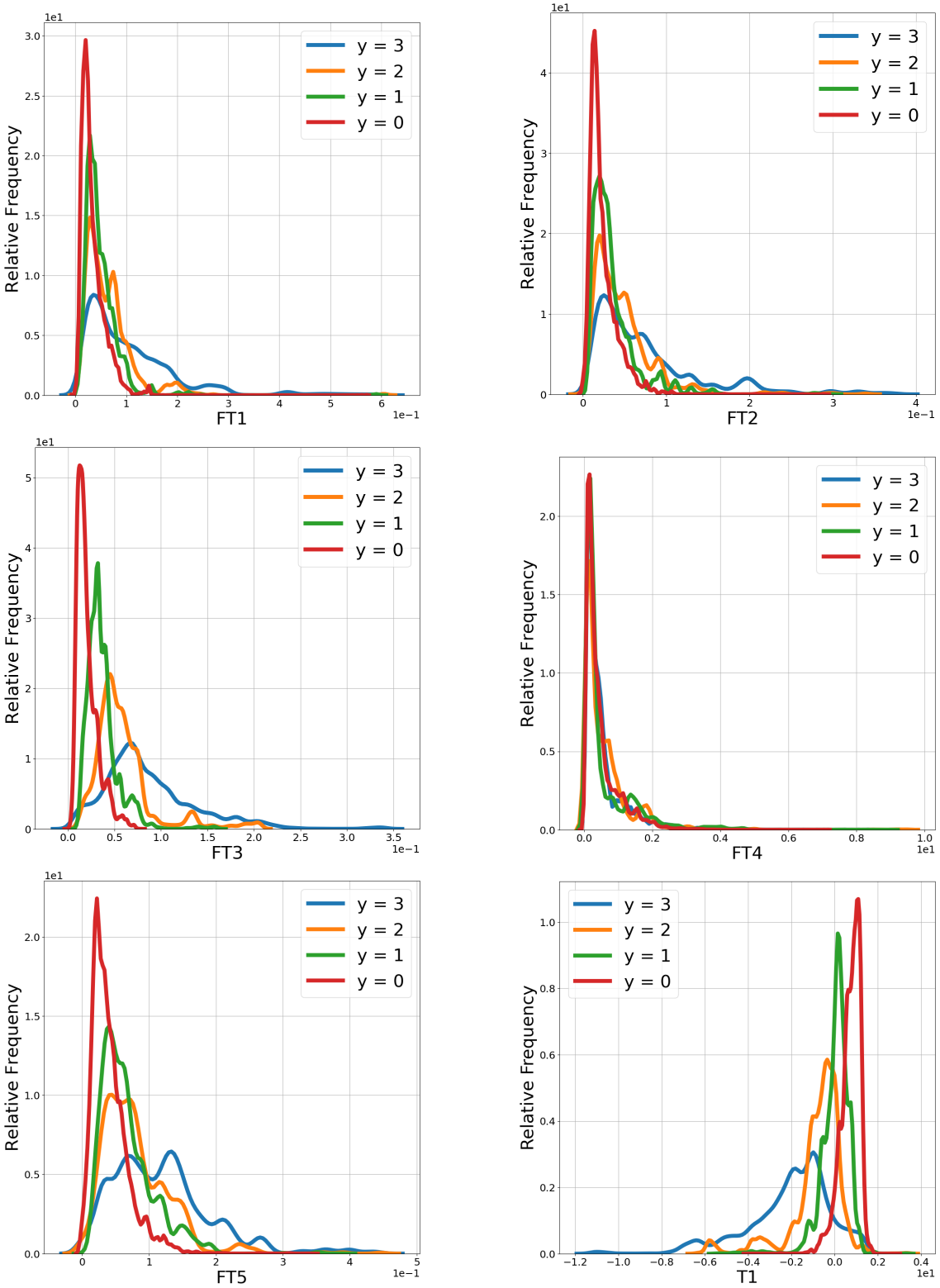

Figure 5.2: Features distributions (FT_1 : HR, FT_2 : LVET, FT_3 : PAT, FT_4 : RI and FT_5 : SI) and LDA (T1) for each class.

5.3.2 Models Performance

The MLR performance for each class and macro-average is shown in table 5.2. The results show that the model struggles to properly distinguish the different events with $y = 3$ being the event state, corresponding to SBP changes bigger than 20 mmHg inside 5 minutes windows, that is better classified. Looking at figure 5.4, corresponding to the normalized confusion matrix of the 5-CV test subsets merged, one concludes that each feature is often misclassified as one of it's neighbours and small events ($y = 1$) are misclassified as non-events ($y = 0$) 26.62% of the time while only 6.41% of medium and 7.50% of large events ($y = 2$ and $y = 3$) are misclassified as non-events. Also, only 23.05% of no-event states are misclassified as events, with 82.47% of these classified as small events ($y = 1$). Addressing this problem as a binary classification problem, considering non-event states ($y = 0$) and event states ($y \neq 0$), one can calculate the different evaluation metrics as shown in table 5.3. The results suggest that the MLR model can distinguish between the different states with accuracy of 80.7 ± 2.7 %, while struggling most to distinguish false positives with precision of 72.4 ± 6.5.

Transition between no-event states to event states is detected in 21.27 ± 54.17 seconds, suggesting that this tool would detect BP events in short time intervals, although it is difficult to compare this results with other available solutions, since there's no clear definition of BP events as the one presented here.

Figure 5.3 compares the categorical targets with the predictions from the 5 combined test subsets that results from the 5-CV in one of the patients. The results show that major events are detected, except for an event occurring between minutes 250-280. A wide region between minutes 100-200 defined as no-event are detected as small events (10 mmHg $< max - min <$ 15 mmHg).

Metric	**Class**				**Macro Average**
	0	**1**	**2**	**3**	
Precision (%)	88.9 ± 2.9	31.9 ± 5.4	26.5 ± 8.3	83.0 ± 7.0	57.4 ± 29.4
Recall (%)	76.6 ± 8.5	49.9 ± 11.3	38.3 ± 10.2	58.1 ± 13.0	55.7 ± 17.7
F1-Score (%)	81.9 ± 4.6	38.2 ± 7.4	30.9 ± 8.7	67.0 ± 8.4	54.5 ± 22.1

Table 5.2: Performance of 5-CV MLR with T1 as input.

Accuracy (%)	**Precision (%)**	**Recall (%)**	**F1-Score (%)**	**Detection Time (s)**
80.7 ± 2.7	72.4 ± 6.5	85.7 ± 4.4	78.2 ± 3.4	21.27 ± 54.17

Table 5.3: Performance for 5-CV MLR considering targets binary ($y = 0$ or $y \neq 0$). Detection time defined as transition from no-event state ($y = 0$) to event state ($y \neq 0$).

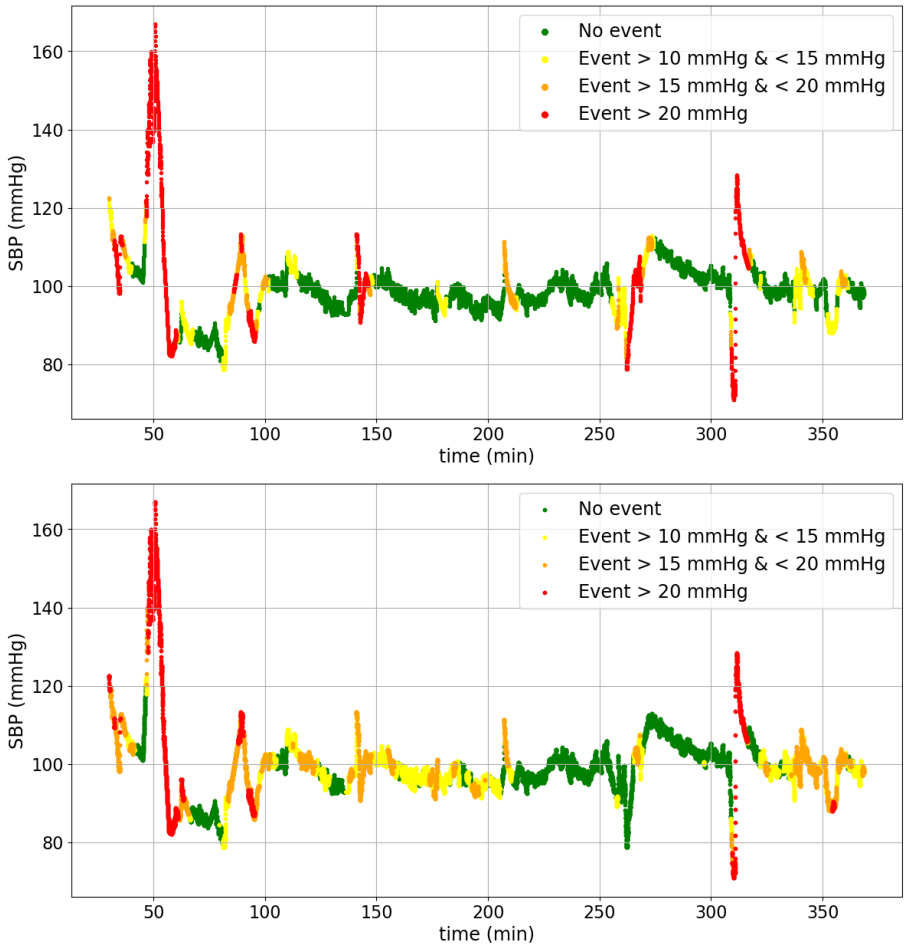

Figure 5.3: Example of events categorical targets (top) and the detection in one of the patients resulting from the 5 test subsets merged (bottom).

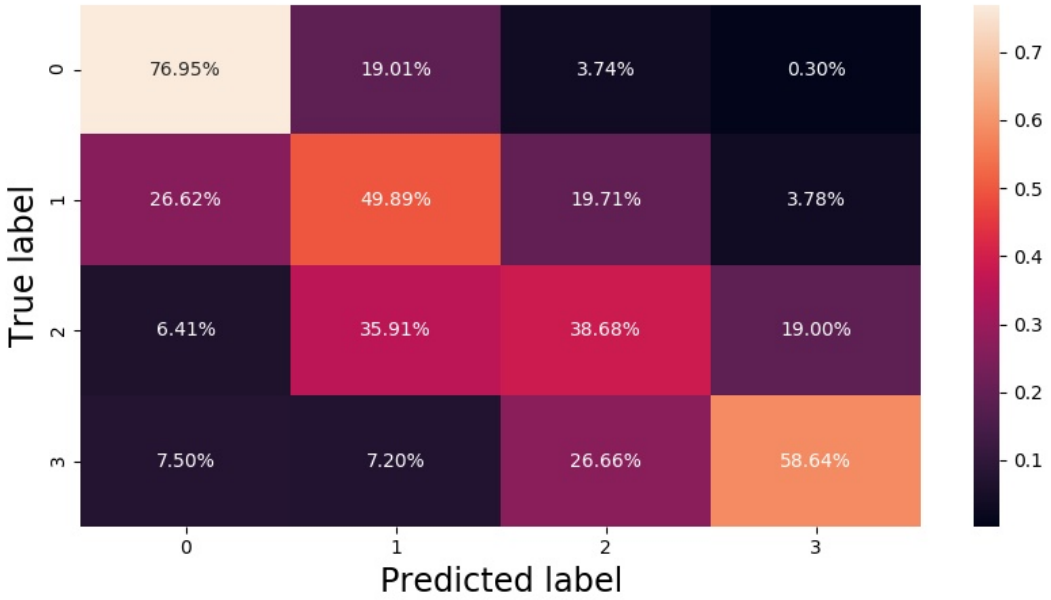

Figure 5.4: Normalized confusion matrix with all test subsets merged.

5.4 Conclusion

Along this chapter, an algorithm for blood pressure fast events detection is proposed. First, a definition of fast BP events is proposed, based on the previous description in chapter 4.2.8. As suggested by [98, 103], not only long lasting BP events can affect surgery outcomes, but also sharp and brief events. The definition of BP events here proposed is based on the SBP $max - min$ difference inside 5 minutes windows. In our data extracted from patients undergoing surgery, 5 out of 9 undergoing cardiovascular interventions, events bigger than 10 mmHg were found 41.1% of the time, while events bigger than 20 mmHg were found 18% the time, suggesting that sharp BP changes inside small time windows are common.

The approach for features extraction from non-invasive signals follows the strategy of the previous chapter, with the different parameters being PAT, HR, LVET, RI and SI. From each parameter, one applies a similar strategy as the BP the events definition, calculating the $max - min$ difference of each parameter inside 5 minutes windows. From here, a MLR model is tested with a 5-CV approach.

The results suggest that the simple MLR model can effectively distinguish between non-event and event states (table 5.3) while struggling to distinguish between the different event states (table 5.2). Also, one important conclusion is that this model is able to generalize for different patients, since it was tested with a 5-CV approach involving all the patients studied. Thus, it wouldn't require calibration procedures for each patient.

A model like the one described here could be applied in the OR, providing real-time variability-related information about BP with 3 different alarms and could be used in an optimized non-uniform BP sampling definition, triggering samples based on the amplitude of SBP change, as studied in chapter 4.

For future work, the study of different BP surrogates and different techniques for features extraction may provide useful insights about the BP events state. Also, since it was proved that the MLR model is able to generalize for different patients, no calibration procedures are required and more complex machine learning models can be used in order to classify BP events.

6

Conclusions

This thesis outlines the importance of accurate real-time BP monitoring of a patient during hospital stay, analyzed different BP surrogates extracted from PPG and ECG signals and proposes a simple yet effective solution based on the pulse wave velocity able to track BP even in the most critical scenarios (e.g., cardiovascular surgeries), while highlighting the major challenges. The continuous estimation of BP via surrogates (PAT) is compared with the invasive BP (A-line), the ground truth values, and intermittent fixed interval sampling from the invasive BP (zero-order hold (ZoH)) in order to simulate cuff measurements. The 5 minutes sampling interval was chosen for the ZoH to be used as reference, since it is the most common approach in less critical interventions where the A-line is not available [119].

With ECG and PPG signals from patients undergoing surgery, one could successfully extract relevant cardiovascular time intervals such as the pulse arrival time (PAT) that was highly correlated with invasive BP. The implementation of simple regression models (MK-EE, L-MK and MK-BH) revealed promising results for continuous BP estimation, but also the need for initial calibration and a systematic re-calibration strategy during the procedure for each patient. The first objective addressed in this thesis suggests that using 20 minutes (20 samples) initial calibration and 5 minutes fixed sampling time to extract new BP samples and update the regression models, would enable the models outperform the ZoH (reference NIBP) in terms of $ME \pm SD$ and MAE. The MK-BH model presented the best results achieving $ME \pm SD$ (mmHg) values of 0.55 ± 5.94 for SBP and 0.42 ± 4.17 for DBP while the ZoH achieved 0.10 ± 11.66 for SBP and -0.01 ± 5.44 for DBP. In terms of MAE, the MK-BH model achieved 3.50 for SBP and 2.39 for DBP while the ZoH obtained 6.58 for SBP and 3.20 for DBP. An analysis of the top 5% and 1% absolute errors suggested that this model is able to highly decrease the amplitude of outliers with only 5% of the MK-BH model SBP estimates with absolute errors above 11.9 mmHg while the ZoH resulted in 24.6 mmHg and only 1% of SBP estimates with absolute errors above 24.2 mmHg while the ZoH resulted in 50.2 mmHg. Increasing the sampling interval up to 15 minutes would still guarantee better performance from the MK-BH compared with the ZoH, suggesting that one could improve the patient's comfort while maintaining accurate BP estimations. This results suggest that a simple solution with widely available ECG and PPG signals, a simple real-time BP estimator like the MK-BH model and automatic cuff measurements could highly improve the BP monitoring during low and intermediate risk surgeries where only cuff measurements are usually performed. The use and implementation of this technology seems simple and reliable.

Furthermore, an optimized non-uniform BP sampling solution based on ground truth BP $max-min$ differences inside 5 minutes windows is proposed and it's impact on both regression models and ZoH is analyzed. The results showed once again that the MK-BH model performed best in terms of

$ME \pm SD$ and MAE. The MK-BH model with non-uniform BP sampling and calibration achieves $ME \pm SD$ (mmHg) of 0.68 ± 4.88 for SBP and 0.46 ± 3.86 for DBP while the ZoH achieved 0.69 ± 8.67 for SBP and 0.35 ± 4.28 for DBP. In terms of MAE, the MK-BH model achieved 3.23 for SBP and 2.40 for DBP while the ZoH obtained 5.72 for SBP and 2.88 for DBP. Both MK-BH model and ZoH seem to benefit from a non-uniform BP sampling solution and that also reflects on the top 5% of absolute errors that decrease from 11.9 mmHg to 10.0 mmHg for the MK-BH model and from 24.6 mmHg to 16.6 mmHg for the ZoH. Looking at the top 1% the errors, it decreased from 24.2 mmHg to 16.9 mmHg for the MK-BH model and from 50.2 mmHg to 34.0 mmHg for the ZoH.

The previous results show an improvement for both continuous BP estimator and ZoH with the non-uniform BP sampling solution, but the information about BP variability was extracted directly from the invasive BP data and the objective would be to have this information from non-invasive sources such as the PPG and ECG signals. Thus, one proposes an Algorithm for Blood Pressure Fast Events Detection consisting of several parameters (PAT, HR, LVET, RI and SI) where the $max - min$ difference inside 5 minutes windows is calculated and a Multinomial Logistic Regression (MLR) that fits the input data to the BP events targets defined previously. The MLR model is evaluated with 5-fold cross validation in order to ascertain if this solution would be able to generalize for different patients, therefore not needing calibration procedures for each patient. The results show that the MLR model struggles to distinguish between the different BP events categories, but is able to distinguish between no-event and event states, performing worst in terms of precision (72.4 ± 6.5 %) which means there are many false positives.

As the main suggestions for future improvements of the described work, one highlights the need to study the influence of cuff-related errors in both NIBP monitoring performance and regression models calibration and performance, the study of different BP surrogates and their relationship with BP, more complex regression models and the study of different BP sampling optimization techniques such as the locally adaptive sampling described by [43] with the help of BP surrogates such as PAT. Alongside the development of technological tools, a better understanding of the volatility of BP in the perioperative care and its impact in the outcomes is needed in order to create personalized BP management solutions that minimize the patients exposure to harmful hemodynamic conditions. Randomized controlled trials with low- and intermediate-risk patients during perioperative and primary care being monitored with continuous *versus* intermittent NIBP monitoring solutions should be performed in order to ascertain if the continuous BP estimation solution based on BP surrogates, via ECG and PPG, would improve outcomes. The reported analysis has a prototypical nature, meaning that these concepts and strategies are worth further study.

Bibliography

[1] Cardiac Muscle and Electrical Activity — Anatomy and Physiology II.

[2] Milton Abramowitz and Stegun Irene. Abramowitz_and_Stegun.Pdf, 1970.

[3] Christer Ahlstrom, Anders Johansson, Fredrik Uhlin, Toste Länne, and Per Ask. Noninvasive investigation of blood pressure changes using the pulse wave transit time: A novel approach in the monitoring of hemodialysis patients. *Journal of Artificial Organs*, 8(3):192–197, sep 2005.

[4] John Allen. Photoplethysmography and its application in clinical physiological measurement, mar 2007.

[5] Gregory C. Amberg and Manuel F. Navedo. Calcium Dynamics in Vascular Smooth Muscle. *Microcirculation*, 20(4):281–289, may 2013.

[6] Steven A. Atlas. The renin-angiotensin aldosterone system: Pathophysiological role and pharmacologic inhibition, sep 2007.

[7] Martin C. Baruch, Darren E.R. Warburton, Shannon S.D. Bredin, Anita Cote, David W. Gerdt, and Charles M. Adkins. Pulse Decomposition Analysis of the digital arterial pulse during hemorrhage simulation. *Nonlinear Biomedical Physics*, 5(1):1, jan 2011.

[8] Jan Benes, Alena Simanova, Tereza Tovarnicka, Silvie Sevcikova, Jakub Kletecka, Jan Zatloukal, Richard Pradl, Ivan Chytra, and Eduard Kasal. Continuous non-invasive monitoring improves blood pressure stability in upright position: randomized controlled trial. *Journal of Clinical Monitoring and Computing*, 29(1):11–17, 2014.

[9] Jilles B. Bijker, Suzanne Persoon, Linda M. Peelen, Karel G.M. Moons, Cor J. Kalkman, L. Jaap Kappelle, and Wilton A. Van Klei. Intraoperative hypotension and perioperative ischemic stroke after general surgery, a nested case-control study. *Anesthesiology*, 116(3):658–664, mar 2012.

[10] Jilles B. Bijker, Wilton A. Van Klei, Teus H. Kappen, Leo Van Wolfswinkel, Karel G.M. Moons, and Cor J. Kalkman. Incidence of intraoperative hypotension as a function of the chosen definition: Literature definitions applied to a retrospective cohort using automated data collection. *Anesthesiology*, 107(2):213–220, aug 2007.

[11] Jilles B. Bijker, Wilton A. Van Klei, Yvonne Vergouwe, Douglas J. Eleveld, Leo Van Wolfswinkel, Karel G.M. Moons, and Cor J. Kalkman. Intraoperative hypotension and 1-year mortality after noncardiac surgery. *Anesthesiology*, 111(6):1217–1226, 2009.

[12] E. Bresch, R. Derkx, I. Paulussen, E. Hornix, V. Davidoiu, G. J. Noordergraaf, and J. Muehlsteff. Optimized non-uniform sampling of blood pressure time series from the operating room. In *Proceedings of the Annual International Conference of the IEEE Engineering in Medicine and Biology Society, EMBS*, volume 2020-July, pages 2561–2564. Institute of Electrical and Electronics Engineers Inc., jul 2020.

[13] F. V. Brozovich, C. J. Nicholson, C. V. Degen, Yuan Z. Gao, M. Aggarwal, and Kathleen G. Morgan. Mechanisms of vascular smooth muscle contraction and the basis for pharmacologic treatment of smooth muscle disorders, apr 2016.

[14] Rosa M. Bruno, Lorenzo Ghiadoni, Gino Seravalle, Raffaella Dell'Oro, Stefano Taddei, and Guido Grassi. Sympathetic regulation of vascular function in health and disease. *Frontiers in Physiology*, 3 JUL:1–15, 2012.

[15] R. Busse, R. D. Bauer, A. Schabert, Y. Summa, P. Bumm, and E. Wetterer. The mechanical properties of exposed human common carotid arteries in vivo. *Basic Research in Cardiology*, 74(5):545–554, sep 1979.

[16] Messrs J C Bramwell, A V Hill, By J Crighton B ram ell, and A V H ill. The velocity of pulse wave in man. *Proceedings of the Royal Society of London. Series B, Containing Papers of a Biological Character*, 93(652):298–306, apr 1922.

[17] Maxime Cannesson, Gunther Pestel, Cameron Ricks, Andreas Hoeft, and Azriel Perel. Hemodynamic monitoring and management in patients undergoing high risk surgery: A survey among North American and European anesthesiologists. *Critical Care*, 15(4), aug 2011.

[18] Ana Castro, Paulo de Carvalho, Jens Muehlsteff, Sandra Mattos, and Miguel Coimbra. *A Review on Noninvasive Beat-to-Beat Systemic and Pulmonary Blood Pressure Estimation through Surrogate Cardiovascular Signals*. 01 2017.

[19] Federico S. Cattivelli and Harinath Garudadri. Noninvasive cuffless estimation of blood pressure from pulse arrival time and heart rate with adaptive calibration. In *Proceedings - 2009 6th International Workshop on Wearable and Implantable Body Sensor Networks, BSN 2009*, pages 114–119, 2009.

[20] David Chambers, Christopher Huang, and Gareth Matthews. *Basic Physiology for Anaesthetists*. Cambridge University Press, jul 2019.

[21] Gregory S.H. Chan, Paul M. Middleton, Branko G. Celler, Lu Wang, and Nigel H. Lovell. Automatic detection of left ventricular ejection time from a finger photoplethysmographic pulse oximetry waveform: Comparison with Doppler aortic measurement. *Physiological Measurement*, 28(4):439–452, 2007.

[22] Gregory S.H. Chan, Paul M. Middleton, Branko G. Celler, Lu Wang, and Nigel H. Lovell. Automatic detection of left ventricular ejection time from a finger photoplethysmographic pulse oximetry waveform: Comparison with Doppler aortic measurement. *Physiological Measurement*, 28(4):439–452, apr 2007.

[23] Anand Chandrasekhar, Chang Sei Kim, Mohammed Naji, Keerthana Natarajan, Jin Oh Hahn, and Ramakrishna Mukkamala. Smartphone-based blood pressure monitoring via the oscillometric finger-pressing method. *Science Translational Medicine*, 10(431), mar 2018.

[24] Mary E. Charlson, C. Ronald MacKenzie, Jeffrey P. Gold, Kathy L. Ales, Marjorie Topkins, and G. Tom Shires. Intraoperative blood pressure: What patterns identify patients at risk for postoperative complications? *Annals of Surgery*, 212(5):567–580, 1990.

[25] Arjun Chatterjee, Kirk Depriest, Russell Blair, David Bowton, and Robert Chin. Results of a survey of blood pressure monitoring by intensivists in critically ill patients: A preliminary study. *Critical Care Medicine*, 38(12):2335–2338, 2010.

[26] W. Chen, T. Kobayashi, S. Ichikawa, Y. Takeuchi, and T. Togawa. Continuous estimation of systolic blood pressure using the pulse arrival time and intermittent calibration. *Medical and Biological Engineering and Computing*, 38(5):569–574, 2000.

[27] Younhee Choi, Qiao Zhang, and Seokbum Ko. Noninvasive cuffless blood pressure estimation using pulse transit time and Hilbert-Huang transform. *Computers and Electrical Engineering*, 39(1):103–111, jan 2013.

[28] Anirban Dutta Choudhury, Rohan Banerjee, Aniruddha Sinha, and Shaswati Kundu. Estimating blood pressure using Windkessel model on photoplethysmogram. In *2014 36th Annual International Conference of the IEEE Engineering in Medicine and Biology Society, EMBC 2014*, volume 2014, pages 4567–4570. Institute of Electrical and Electronics Engineers Inc., nov 2014.

[29] Philip J. Chowienczyk, Ronan P. Kelly, Helen MacCallum, Sandrine C. Millasseau, Tomas L.G. Andersson, Raymond G. Gosling, James M. Ritter, and Erik E. Änggård. Photoplethysmographic assessment of pulse wave reflection: Blunted response to endothelium-dependent beta2-adrenergic vasodilation in type II diabetes mellitus. *Journal of the American College of Cardiology*, 34(7):2007–2014, dec 1999.

[30] C. P. Chua and C. Heneghan. Continuous blood pressure monitoring using ECG and finger photoplethysmogram. In *Annual International Conference of the IEEE Engineering in Medicine and Biology - Proceedings*, volume 2006, pages 5117–5120. Conf Proc IEEE Eng Med Biol Soc, 2006.

[31] L. B. Cook. Extracting arterial flow waveforms from pulse oximeter waveforms. *Anaesthesia*, 56(6):551–555, 2001.

[32] R. Couceiro. Cardiovascular Performance Assessment for p-Health Applications. *undefined*, 2015.

[33] R. Couceiro, P. Carvalho, R. P. Paiva, J. Henriques, M. Antunes, I. Quintal, and J. Muehlsteff. Multi-Gaussian fitting for the assessment of left ventricular ejection time from the Photoplethysmogram. In *Proceedings of the Annual International Conference of the IEEE Engineering in Medicine and Biology Society, EMBS*, pages 3951–3954, 2012.

[34] Paulo de Carvalho, Rui Pedro Paiva, Jorge Henriques, Manuel Antunes, I. Quintal, and Jens Muehlsteff. Robust characteristic points for icg - definition and comparative analysis. pages 161–168, 01 2011.

[35] Sujay Deb, Chinmayee Nanda, D. Goswami, J. Mukhopadhyay, and S. Chakrabarti. Cuff-Less Estimation of Blood Pressure Using Pulse Transit Time and Pre-ejection Period. pages 941–944. Institute of Electrical and Electronics Engineers (IEEE), apr 2008.

[36] Stephanie S. DeLoach and Raymond R. Townsend. Vascular Stiffness: Its measurement and significance for epidemiologic and outcome studies, jan 2008.

[37] Xiaorong Ding, Jing Liu, Wen-Xuan Dai, Paulo Carvalho, Ratko Magjarevic, and Yuan-Ting Zhang. *An Attempt to Define the Pulse Transit Time: ICBHI 2015, Haikou, China, 8-10 October 2015*, pages 219–221. 01 2019.

[38] C. Douniama, C. U. Sauter, and R. Couronne. Acquisition of Parameters for Noninvasive Continuous Blood Pressure Estimation – Review of the Literature and Clinical Trial. pages 2151–2154. Springer, Berlin, Heidelberg, 2009.

[39] Gary M. Drzewiecki, Julius Melbin, and Abraham Noordergraaf. Arterial tonometry: Review and analysis. *Journal of Biomechanics*, 16(2):141–152, jan 1983.

[40] Ron Dueck, Oliver Goedje, and Paul Clopton. Noninvasive continuous beat-to-beat radial artery pressure via TL-200 applanation tonometry. *Journal of Clinical Monitoring and Computing*, 26(2):75–83, jan 2012.

[41] Mohamed Elgendi, Richard Fletcher, Yongbo Liang, Newton Howard, Nigel H. Lovell, Derek Abbott, Kenneth Lim, and Rabab Ward. The use of photoplethysmography for assessing hypertension. *npj Digital Medicine*, 2(1):1–11, dec 2019.

[42] M. Esler. The autonomic nervous system and cardiac arrhythmias, apr 1992.

[43] Soheil Feizi, Vivek K Goyal, and Muriel Médard. Locally Adaptive Sampling. Technical report.

[44] Jong Yong A. Foo, Stephen J. Wilson, Gordon R. Williams, Margaret Anne Harris, and David M. Cooper. Pulse transit time changes observed with different limb positions. *Physiological Measurement*, 26(6):1093–1102, dec 2005.

[45] Parry Fung, Guy Dumont, Craig Ries, Chris Mott, and Mark Ansermino. Continuous noninvasive blood pressure measurement by pulse transit time. In *Annual International Conference of the IEEE Engineering in Medicine and Biology - Proceedings*, volume 26 I, pages 738–741. Conf Proc IEEE Eng Med Biol Soc, 2004.

[46] N. R. Gaddum, J. Alastruey, P. Beerbaum, P. Chowienczyk, and T. Schaeffter. A technical assessment of pulse wave velocity algorithms applied to non-invasive arterial waveforms. *Annals of Biomedical Engineering*, 41(12):2617–2629, 2013.

[47] L. A. Geddes, M. H. Voelz, C. F. Babbs, J. D. Bourland, and W. A. Tacker. Pulse Transit Time as an Indicator of Arterial Blood Pressure. *Psychophysiology*, 18(1):71–74, 1981.

[48] Thomas Geeraerts, Pierre Albaladejo, Adrien Descorps Declère, Jacques Duranteau, Jean Patrick Sales, and Dan Benhamou. Decrease in Left Ventricular Ejection Time on Digital Arterial Waveform during Simulated Hypovolemia in Normal Humans. *Journal of Trauma - Injury, Infection and Critical Care*, 56(4):845–849, 2004.

[49] Heiko Gesche, Detlef Grosskurth, Gert Küchler, and Andreas Patzak. Continuous blood pressure measurement by using the pulse transit time: Comparison to a cuff-based method. *European Journal of Applied Physiology*, 112(1):309–315, jan 2012.

[50] Brian Gribbin, Andrew Steptoe, and Peter Sleight. Pulse Wave Velocity as a Measure of Blood Pressure Change. *Psychophysiology*, 13(1):86–90, jan 1976.

[51] Ben Gupta. Monitoring in the ICU Anaesthesia Update in. *Update in Anaethesia*, 28:37–42, 2012.

[52] Patrice G. Guyenet. The sympathetic control of blood pressure, may 2006.

[53] Mark A Hamilton, Maurizio Cecconi, and Andrew Rhodes. A systematic review and meta-analysis on the use of preemptive hemodynamic intervention to improve postoperative outcomes in moderate and high-risk surgical patients. *Anesthesia and analgesia*, 112(6):1392–402, jun 2011.

[54] WILLARD S. HARRIS, NESET AYTAN, and JEAN M. POUGET. Effects of Nitroglycerin on Responses of the Systolic Time Intervals to Exercise. *Circulation*, 47(3):499–508, mar 1973.

[55] Junichiro Hashimoto, Wilmer W. Nichols, Michael F. O'Rourke, and Yutaka Imai. Association between wasted pressure effort and left ventricular hypertrophy in hypertension: Influence of arterial wave reflection. *American Journal of Hypertension*, 21(3):329–333, mar 2008.

[56] Rui He, Zhi Pei Huang, Lian Ying Ji, Jian Kang Wu, Huihui Li, and Zhi Qiang Zhang. Beat-to-beat ambulatory blood pressure estimation based on random forest. In *BSN 2016 - 13th Annual Body Sensor Networks Conference*, pages 194–198. Institute of Electrical and Electronics Engineers Inc., jul 2016.

[57] Alrick B. Hertzman. THE BLOOD SUPPLY OF VARIOUS SKIN AREAS AS ESTIMATED BY THE PHOTOELECTRIC PLETHYSMOGRAPH. *American Journal of Physiology-Legacy Content*, 124(2):328–340, oct 1938.

[58] HERTZMANN and AB. Observations on the finger volume pulse recorded photo-electrically. *Am J Physiol*, 119:334–335, 1937.

[59] Matthew Hoffman. Human Heart (Anatomy): Diagram, Function, Chambers, Location in Body, 2014.

[60] Zhongkui Hong, Kimberley J. Reeves, Zhe Sun, Zhaohui Li, Nicola J. Brown, and Gerald A. Meininger. Vascular smooth muscle cell stiffness and adhesion to collagen I modified by vasoactive agonists. *PLoS ONE*, 10(3), mar 2015.

[61] H. Hosaka, H. Sakata, Y. Sugo, T. Sohma, and H. Kasuya. Pulse-wave propagation time basis blood pressure monitor. *US patent*, 5:649,543,.

[62] D Hughes. Measurements of Young's modulus of elasticity of the canine aorta with ultrasound. *Ultrasonic Imaging*, 1(4):356–367, oct 1979.

[63] C. Ilies, H. Kiskalt, D. Siedenhans, P. Meybohm, M. Steinfath, B. Bein, and R. Hanss. Detection of hypotension during Caesarean section with continuous non-invasive arterial pressure device or intermittent oscillometric arterial pressure measurement. *British Journal of Anaesthesia*, 109(3):413–419, 2012.

[64] J. R. Jago and A. Murray. Repeatability of peripheral pulse measurements on ears, fingers and toes using photoelectric plethysmography. *Clinical Physics and Physiological Measurement*, 9(4):319–329, nov 1988.

[65] Yi Kim Jung, Hwan Cho Baek, Mi Im Soo, Ju Jeon Myoung, Young Kim In, and I. Kim Sun. Comparative study on artificial neural network with multiple regressions for continuous estimation of blood pressure. In *Annual International Conference of the IEEE Engineering in Medicine and Biology - Proceedings*, volume 7 VOLS, pages 6942–6945, 2005.

[66] Mohamad Kachuee, Mohammad Mahdi Kiani, Hoda Mohammadzade, and Mahdi Shabany. Cuff-less high-accuracy calibration-free blood pressure estimation using pulse transit time. In *Proceedings - IEEE International Symposium on Circuits and Systems*, volume 2015-July, pages 1006–1009. Institute of Electrical and Electronics Engineers Inc., jul 2015.

[67] Mohammad Kachuee, Mohammad Mahdi Kiani, Hoda Mohammadzade, and Mahdi Shabany. Cuffless Blood Pressure Estimation Algorithms for Continuous Health-Care Monitoring. *IEEE Transactions on Biomedical Engineering*, 64(4):859–869, apr 2017.

[68] M. Karamanoglu, D. E. Gallagher, A. P. Avolio, and M. F. O'Rourke. Functional origin of reflected pressure waves in a multibranched model of the human arterial system. *American Journal of Physiology - Heart and Circulatory Physiology*, 267(5 36-5), 1994.

[69] Sang Hyun Kim, Marc Lilot, Kulraj S. Sidhu, Joseph Rinehart, Zhaoxia Yu, Cecilia Canales, and Maxime Cannesson. Accuracy and precision of continuous noninvasive arterial pressure monitoring compared with invasive arterial pressure: A systematic review and meta-analysis. *Anesthesiology*, 120(5):1080–1097, may 2014.

[70] Jesper Kjaergaard, Christian Hassager, Jae K. Oh, Jens H. Kristensen, Jens Berning, and Peter Sogaard. Measurement of cardiac time intervals by Doppler tissue M-Mode imaging of the anterior mitral leaflet. *Journal of the American Society of Echocardiography*, 18(10):1058–1065, oct 2005.

[71] D. J. Korteweg. Ueber die Fortpflanzungsgeschwindigkeit des Schalles in elastischen Röhren. *Annalen der Physik*, 241(12):525–542, jan 1878.

[72] Steen Dalby Kristensen, Juhani Knuuti, Antti Saraste, Stefan Anker, Hans Erik Bøtker, Stefan De Hert, Ian Ford, Jose Ramón Gonzalez-Juanatey, Bulent Gorenek, Guy Robert Heyndrickx, Andreas Hoeft, Kurt Huber, Bernard Iung, Keld Per Kjeldsen, Thomas F. Lüscher, Luc Pierard, Stuart Pocock, Susanna Price, Marco Roffi, Per Anton Sirnes, Miguel Sousa-Uva, Vasilis Voudris, Christian Funck-Brentano, Jose Luis Zamorano, Stephan Achenbach, Helmut Baumgartner, Jeroen J. Bax, Héctor Bueno, Veronica Dean, Christi Deaton, Cetin Erol, Robert Fagard, Roberto Ferrari, David Hasdai, Arno W. Hoes, Paulus Kirchhof, Philippe Kolh, Patrizio Lancellotti, Ales Linhart, Petros Nihoyannopoulos, Massimo F. Piepoli, Piotr Ponikowski, Juan Luis Tamargo, Michal Tendera, Adam Torbicki, William Wijns, Stephan Windecker, Maurizio Solca, Jean François Brichant, Edoardo De Robertis, Dan Longrois, Sibylle Kozek Langenecker, and Josef Wichelewski. 2014 ESC/ESA Guidelines on non-cardiac surgery: Cardiovascular assessment and management: The Joint Task Force on non-cardiac surgery: Cardiovascular assessment and management of the European Society of Cardiology (ESC) and the European Society of Anaesth. *European Heart Journal*, 35(35):2383–2431, 2014.

[73] Yuriy Kurylyak, Francesco Lamonaca, and Domenico Grimaldi. A Neural Network-based method for continuous blood pressure estimation from a PPG signal. In *Conference Record - IEEE Instrumentation and Measurement Technology Conference*, pages 280–283, 2013.

[74] M C Kyle and E D Freis. Serial measurements of systolic time intervals: effects of propranolol alone and combined with other agents in hypertensive patients. *Hypertension*, 2(1):111–117, jan 1980.

[75] Jan Kříž and Petr Šeba. Force plate monitoring of human hemodynamics. *Nonlinear Biomedical Physics*, 2(1), feb 2008.

[76] James D. Lane, Lisa Greenstadt, David Shapiro, and Eduardo Rubinstein. Pulse Transit Time and Blood Pressure: An Intensive Analysis. *Psychophysiology*, 20(1):45–49, 1983.

[77] J. Lass, K. Meigas, D. Karai, R. Kattai, J. Kaik, and M. Rossmann. Continuous blood pressure monitoring during exercise using pulse wave transit time measurement. In *Annual International Conference of the IEEE Engineering in Medicine and Biology - Proceedings*, volume 26 III, pages 2239–2242. Conf Proc IEEE Eng Med Biol Soc, 2004.

[78] R. D. Latham, N. Westerhof, P. Sipkema, B. J. Rubal, P. Reuderink, and J. P. Murgo. Regional wave travel and reflections along the human aorta: A study with six simultaneous micromanometric pressures. *Circulation*, 72(6):1257–1269, 1985.

[79] Hyeonwoo Lee, Eunhye Kim, Yongsu Lee, Hoyeon Kim, Jaeho Lee, Mincheol Kim, Hoi Jun Yoo, and Seunghyup Yoo. Toward all-day wearable health monitoring: An ultralow-power, reflective organic pulse oximetry sensing patch. *Science Advances*, 4(11):eaas9530, nov 2018.

[80] Li Wei H. Lehman, Mohammed Saeed, Daniel Talmor, Roger Mark, and Atul Malhotra. Methods of blood pressure measurement in the ICU. *Critical Care Medicine*, 41(1):34–40, jan 2013.

[81] Jian Qiang Li, Rui Li, Zhuang Zhuang Chen, Gen Qiang Deng, Huihui Wang, Constandinos X. Mavromoustakis, Houbing Song, and Zhong Ming. Design of a Continuous Blood Pressure Measurement System Based on Pulse Wave and ECG Signals. *IEEE Journal of Translational Engineering in Health and Medicine*, 6:1–14, jan 2018.

[82] Peng Li, Ming Liu, Xu Zhang, Xiaohui Hu, Bo Pang, Zhaolin Yao, and Hongda Chen. Novel wavelet neural network algorithm for continuous and noninvasive dynamic estimation of blood pressure from photoplethysmography. *Science China Information Sciences*, 59(4):1–10, apr 2016.

[83] Yongbo Liang, Zhencheng Chen, Rabab Ward, and Mohamed Elgendi. Hypertension Assessment Using Photoplethysmography: A Risk Stratification Approach. *Journal of Clinical Medicine*, 8(1):12, dec 2018.

[84] Yongbo Liang, Zhencheng Chen, Rabab Ward, and Mohamed Elgendi. Photoplethysmography and Deep Learning: Enhancing Hypertension Risk Stratification. *Biosensors*, 8(4):101, oct 2018.

[85] Yongbo Liang, Mohamed Elgendi, Zhencheng Chen, and Rabab Ward. Analysis: An optimal filter for short photoplethysmogram signals. *Scientific Data*, 5(1):1–12, may 2018.

[86] L. G. Lindberg, T. Tamura, and P. Å Öberg. Photoplethysmography - Part 1 Comparison with laser Doppler flowmetry. *Medical & Biological Engineering & Computing*, 29(1):40–47, jan 1991.

[87] Yinbo Liu and Yuan-Ting Zhang. Pulse transit time and arterial blood pressure at different vertical wrist positions. 01 2006.

[88] Gérard M. London, Jacques Blacher, Bruno Pannier, Alain P. Guérin, Sylvain J. Marchais, and Michel E. Safar. Arterial Wave Reflections and Survival in End-Stage Renal Failure. *Hypertension*, 38(3):434–438, sep 2001.

[89] Joseph Loscalzo and George Welch. Nitric oxide and its role in the cardiovascular system. *Progress in Cardiovascular Diseases*, 38(2):87–104, sep 1995.

[90] A. Luchner and H. Schunkert. Interactions between the sympathetic nervous system and the cardiac natriuretic peptide system, aug 2004.

[91] Nashat Maher, G. A. Elsheikh, Wagdy R. Anis, and Tamer Emara. Non-invasive Calibration-Free Blood Pressure Estimation Based on Artificial Neural Network. In *Advances in Intelligent Systems and Computing*, volume 921, pages 701–711. Springer Verlag, 2020.

[92] Nephtali Marina, Ana P.L. Abdala, Alla Korsak, Annabel E. Simms, Andrew M. Allen, Julian F.R. Paton, and Alexander V. Gourine. Control of sympathetic vasomotor tone by catecholaminergic C1 neurones of the rostral ventrolateral medulla oblongata. *Cardiovascular Research*, 91(4):703–710, sep 2011.

[93] Devin B. McCombie, Phillip A. Shaltis, Andrew T. Reisner, and H. Harry Asada. Adaptive hydrostatic blood pressure calibration: Development of a wearable, autonomous pulse wave velocity blood pressure monitor. In *Annual International Conference of the IEEE Engineering in Medicine and Biology - Proceedings*, volume 2007, pages 370–373. Conf Proc IEEE Eng Med Biol Soc, 2007.

[94] Michigan Medicine. Anatomy of a Human Heart, 2019.

[95] Agnes S. Meidert, Wolfgang Huber, Alexander Hapfelmeier, Miriam Schöfthaler, Johannes N. Müller, Nicolas Langwieser, Julia Y. Wagner, Roland M. Schmid, and Bernd Saugel. Evaluation of the radial artery applanation tonometry technology for continuous noninvasive blood pressure monitoring compared with central aortic blood pressure measurements in patients with multiple organ dysfunction syndrome. *Journal of Critical Care*, 28(6):908–912, dec 2013.

[96] Agnes S. Meidert and Bernd Saugel. Techniques for non-invasive monitoring of arterial blood pressure, 2017.

[97] Kalju Meigas, Rain Kattai, and Jaanus Lass. Continuous blood pressure monitoring using pulse wave delay. In *Annual Reports of the Research Reactor Institute, Kyoto University*, volume 4, pages 3171–3174, 2001.

[98] Lingzhong Meng, Weifeng Yu, Tianlong Wang, Lina Zhang, Paul M. Heerdt, and Adrian W. Gelb. Blood Pressure Targets in Perioperative Care. *Hypertension*, 72(4):806–817, oct 2018.

[99] Christian Meyer, Paulo Carvalho, Christoph Brinkmeyer, Malte Kelm, Ricardo Couceiro, and Jens Mühlsteff. Wearable sensors in syncope management, jan 2015.

[100] S. C. Millasseau, R. P. Kelly, J. M. Ritter, and P. J. Chowienczyk. Determination of age-related increases in large artery stiffness by digital pulse contour analysis. *Clinical Science*, 103(4):371–377, 2002.

[101] Sandrine C. Millasseau, James M. Ritter, Kenji Takazawa, and Philip J. Chowienczyk. Contour analysis of the photoplethysmographic pulse measured at the finger, 2006.

[102] Gary F. Mitchell, Yves Lacourcière, J. Malcolm O. Arnold, Mark E. Dunlap, Paul R. Conlin, and Joseph L. Izzo. Changes in aortic stiffness and augmentation index after acute converting enzyme or vasopeptidase inhibition. *Hypertension*, 46(5):1111–1117, nov 2005.

[103] Terri G. Monk, Michael R. Bronsert, William G. Henderson, Michael P. Mangione, S. T.John Sum-Ping, Deyne R. Bentt, Jennifer D. Nguyen, Joshua S. Richman, Robert A. Meguid, and Karl E. Hammermeister. Association between intraoperative hypotension and hypertension and 30-day postoperative mortality in noncardiac surgery. *Anesthesiology*, 123(2):307–319, aug 2015.

[104] Seyedeh Somayyeh Mousavi, Mohammad Firouzmand, Mostafa Charmi, Mohammad Hemmati, Maryam Moghadam, and Yadollah Ghorbani. Blood pressure estimation from appropriate and inappropriate PPG signals using A whole-based method. *Biomedical Signal Processing and Control*, 47:196–206, jan 2019.

[105] IM Moxham. Understanding Arterial Pressure Waveforms. *Southern African Journal of Anaesthesia and Analgesia*, 9(1):40–42, feb 2003.

[106] J. Muehlsteff, X. A. Aubert, and G. Morren. Continuous cuff-less blood pressure monitoring based on the pulse arrival time approach: The impact of posture. In *Proceedings of the 30th Annual International Conference of the IEEE Engineering in Medicine and Biology Society, EMBS'08 - "Personalized Healthcare through Technology"*, volume 2008, pages 1691–1694. IEEE Computer Society, 2008.

[107] J. Muehlsteff, X. L. Aubert, and M. Schuett. Cuffless estimation of systolic blood pressure for short effort bicycle tests: The prominent role of the pre-ejection period. In *Annual International Conference of the IEEE Engineering in Medicine and Biology - Proceedings*, volume 2006, pages 5088–5092. Conf Proc IEEE Eng Med Biol Soc, 2006.

[108] J Muehlsteff, M Kelm, and C Meyer. Experiences with Pulse Arrival Time as Surrogate for Systolic Blood Pressure. *Biomedical Engineering / Biomedizinische Technik*, 58 Suppl 1, oct 2013.

[109] Ramtanu Mukherjee, Sanchita Ghosh, Bharat Gupta, and Tapas Chakravarty. A Literature Review on Current and Proposed Technologies of Noninvasive Blood Pressure Measurement. *Telemedicine and e-Health*, 24(3):185–193, mar 2018.

[110] Ramakrishna Mukkamala, Jin Oh Hahn, Omer T. Inan, Lalit K. Mestha, Chang Sei Kim, Hakan Toreyin, and Survi Kyal. Toward Ubiquitous Blood Pressure Monitoring via Pulse Transit Time: Theory and Practice. *IEEE Transactions on Biomedical Engineering*, 62(8):1879–1901, aug 2015.

[111] Jochanan E. Naschitz, Stanislas Bezobchuk, Renata Mussafia-Priselac, Scott Sundick, Daniel Dreyfuss, Igal Khorshidi, Argyro Karidis, Hagit Manor, Mihael Nagar, Elisabeth Rubin Peck,

Shannon Peck, Shimon Storch, Itzhak Rosner, and Luis Gaitini. Pulse transit time by r-wave-gated infrared photoplethysmography: Review of the literature and personal experience, dec 2004.

[112] Amanda J. Naylor, Daniel I. Sessler, Kamal Maheshwari, Ashish K. Khanna, Dongsheng Yang, Edward J. Mascha, Iman Suleiman, Eric M. Reville, Devan Cote, Matthew T. Hutcherson, Bianka M. Nguyen, Hesham Elsharkawy, and Andrea Kurz. Arterial Catheters for Early Detection and Treatment of Hypotension During Major Noncardiac Surgery. *Anesthesia & Analgesia*, Publish Ah(Xxx):1–9, 2019.

[113] Matthew R. Nelson, Jan Stepanek, Michael Cevette, Michael Covalciuc, R. Todd Hurst, and A. Jamil Tajik. Noninvasive measurement of central vascular pressures with arterial tonometry: Clinical revival of the pulse pressure waveform?, 2010.

[114] M. Nitzan, B. Khanokh, and Y. Slovik. The difference in pulse transit time to the toe and finger measured by photoplethysmography. *Physiological Measurement*, 23(1):85–93, 2002.

[115] E. R. NYE. THE EFFECT OF BLOOD PRESSURE ALTERATION ON THE PULSE WAVE VELOCITY. *British heart journal*, 26(2):261–265, 1964.

[116] A. Ochagavía, F. Baigorri, J. Mesquida, J.M. Ayuela, A. Ferrándiz, X. García, M.I. Monge, L. Mateu, C. Sabatier, F. Clau-Terré, R. Vicho, L. Zapata, J. Maynar, and A. Gil. Hemodynamic monitoring in the critically patient. Recommendations of the Cardiological Intensive Care and CPR Working Group of the Spanish Society of Intensive Care and Coronary Units. *Medicina Intensiva (English Edition)*, 38(3):154–169, apr 2014.

[117] Openstax. *Concepts of Biology*. CreateSpace Independent Publishing Platform, 2013.

[118] World Health Organization. Global Pulse Oximetry Project. Technical report, 2008.

[119] World Health Organization. *WHO — WHO guidelines for safe surgery: safe surgery saves lives*. World Health Organization, 2009.

[120] M. F. O'Rourke and T. Yaginuma. Wave reflections and the arterial pulse, 1984.

[121] Michael F. O'Rourke and Junichiro Hashimoto. Mechanical Factors in Arterial Aging. A Clinical Perspective, jul 2007.

[122] Michael F. O'Rourke and Alfredo Pauca Xiong Jing Jiang. Pulse wave analysis, 2001.

[123] Toshiaki Otsuka, Tomoyuki Kawada, Masao Katsumata, and Chikao Ibuki. Utility of second derivative of the finger photoplethysmogram for the estimation of the risk of coronary heart disease in the general population. *Circulation Journal*, 70(3):304–310, 2006.

[124] Rui Pedro Paiva, Paulo de Carvalho, Xavier Aubert, Jens Muehlsteff, Jorge Henriques, and Manuel Antunes. Assessing pep and lvet from heart sounds: Algorithms and evaluation. *Conference proceedings : ... Annual International Conference of the IEEE Engineering in Medicine and Biology Society. IEEE Engineering in Medicine and Biology Society. Conference*, 2009:3129–33, 09 2009.

[125] Jiapu Pan and Willis J. Tompkins. A Real-Time QRS Detection Algorithm. *IEEE Transactions on Biomedical Engineering*, BME-32(3):230–236, 1985.

[126] R. A. Payne, C. N. Symeonides, D. J. Webb, and S. R.J. Maxwell. Pulse transit time measured from the ECG: An unreliable marker of beat-to-beat blood pressure. *Journal of Applied Physiology*, 100(1):136–141, jan 2006.

[127] J Penáz, A Voigt, and W Teichmann. [Contribution to the continuous indirect blood pressure measurement]. *Zeitschrift fur die gesamte innere Medizin und ihre Grenzgebiete*, 31(24):1030–3, dec 1976.

[128] Michael R. Pinsky. Functional hemodynamic monitoring, jan 2015.

[129] C. C.Y. Poon and Y. T. Zhang. Cuff-less and noninvasive measurements of arterial blood pressure by pulse transit time. In *Annual International Conference of the IEEE Engineering in Medicine and Biology - Proceedings*, volume 7 VOLS, pages 5877–5880. Institute of Electrical and Electronics Engineers Inc., 2005.

[130] Carmen C.Y. Poon and Y. T. Zhang. Using the changes in hydrostatic pressure and pulse transit time to measure arterial blood pressure. In *Annual International Conference of the IEEE Engineering in Medicine and Biology - Proceedings*, volume 2007, pages 2336–2337. Conf Proc IEEE Eng Med Biol Soc, 2007.

[131] G. L. Pressman and P. M. Newgard. A Transducer for the Continuous External Measurement of Arterial Blood Pressure. *IEEE Transactions on Bio-medical Electronics*, 10(2):73–81, 1963.

[132] Jorge Proença, Jens Muehlsteff, Xavier Aubert, and Paulo Carvalho. Is Pulse Transit Time a good indicator of blood pressure changes during short physical exercise in a young population? In *2010 Annual International Conference of the IEEE Engineering in Medicine and Biology Society, EMBC'10*, pages 598–601, 2010.

[133] VERONICA QUARRY-PIGOTT, RAUL CHIRIFE, and DAVID H. SPODICK. Ejection Time by Ear Densitogram and Its Derivative. *Circulation*, 48(2):239–246, aug 1973.

[134] Christopher M. Quick, David S. Berger, and Abraham Noordergraaf. Constructive and destructive addition of forward and reflected arterial pulse waves. *American Journal of Physiology - Heart and Circulatory Physiology*, 280(4 49-4), 2001.

[135] G. Rådegran and B. Saltin. Nitric oxide in the regulation of vasomotor tone in human skeletal muscle. *American Journal of Physiology - Heart and Circulatory Physiology*, 276(6 45-6), 1999.

[136] D Robertson, G A Johnson, R M Robertson, A S Nies, D G Shand, and J A Oates. Comparative assessment of stimuli that release neuronal and adrenomedullary catecholamines in man. *Circulation*, 59(4):637–643, apr 1979.

[137] T. Rocha, S. Paredes, P. Carvalho, J. Henriques, and M. Harris. Wavelet based time series forecast with application to acute hypotensive episodes prediction. In *2010 Annual International Conference of the IEEE Engineering in Medicine and Biology Society, EMBC'10*, pages 2403–2406. IEEE, aug 2010.

[138] Mary J. Roman, Peter M. Okin, Jorge R. Kizer, Elisa T. Lee, Barbara V. Howard, and Richard B. Devereux. Relations of central and brachial blood pressure to left ventricular hypertrophy and geometry: The Strong Heart Study. *Journal of Hypertension*, 28(2):384–388, 2010.

[139] Uldis Rubins. Finger and ear photoplethysmogram waveform analysis by fitting with Gaussians. *Medical and Biological Engineering and Computing*, 46(12):1271–1276, 2008.

[140] Francesco Rundo, Sabrina Conoci, Alessandro Ortis, and Sebastiano Battiato. An advanced bio-inspired photoplethysmography (PPG) and ECG pattern recognition system for medical assessment. *Sensors (Switzerland)*, 18(2), feb 2018.

[141] Francesco Rundo, Alessandro Ortis, Sebastiano Battiato, and Sabrina Conoci. Advanced Bio-Inspired System for Noninvasive Cuff-Less Blood Pressure Estimation from Physiological Signal Analysis. *Computation*, 6(3):46, aug 2018.

[142] Michel E. Safar. Peripheral pulse pressure, large arteries, and microvessels, aug 2004.

[143] Osman Salem, Yaning Liu, and Ahmed Mehaoua. A lightweight anomaly detection framework for medical wireless sensor networks. In *IEEE Wireless Communications and Networking Conference, WCNC*, pages 4358–4363, 2013.

[144] Rohan Samria, Ridhi Jain, Ankita Jha, Sandeep Saini, and Shubhajit Roy Chowdhury. Noninvasive cuffless estimation of blood pressure using photoplethysmography without electrocardiograph measurement. In *IEEE TENSYMP 2014 - 2014 IEEE Region 10 Symposium*, pages 254–257. Institute of Electrical and Electronics Engineers Inc., jul 2014.

[145] M. Sandberg, Q. Zhang, J. Styf, B. Gerdle, and L. G. Lindberg. Non-invasive monitoring of muscle blood perfusion by photoplethysmography: Evaluation of a new application. *Acta Physiologica Scandinavica*, 183(4):335–343, apr 2005.

[146] Robert D. Sanders, Fintan Hughes, Andrew Shaw, Annemarie Thompson, Angela Bader, Andreas Hoeft, David A. Williams, Michael P.W. Grocott, Monty G. Mythen, Timothy E. Miller, Mark R. Edwards, Michael PW Grocott, Gareth L. Ackland, Charles S. Brudney, Maurizio Cecconi, Can Ince, Michael G. Irwin, Jonathan Lacey, Michael R. Pinsky, Robert Sanders, Finton Hughes, David Williams, Andrew D. Shaw, Daniel I. Sessler, Sol Aronson, Colin Berry, Tong J. Gan, John Kellum, James Plumb, Joshua Bloomstone, Matthew D. McEvoy, Julie K.M. Thacker, Ruchir Gupta, Elena Koepke, Aarne Feldheiser, Denny Levett, Frederic Michard, and Mark Hamilton. Perioperative Quality Initiative consensus statement on preoperative blood pressure, risk and outcomes for elective surgery. *British Journal of Anaesthesia*, 122(5):552–562, may 2019.

[147] Bernd Saugel, Ron Dueck, and Julia Y. Wagner. Measurement of blood pressure, 2014.

[148] Bernd Saugel, Karim Kouz, Agnes S. Meidert, Leonie Schulte-Uentrop, and Stefano Romagnoli. How to measure blood pressure using an arterial catheter: A systematic 5-step approach, apr 2020.

[149] Bernd Volker Scheer, Azrie Perel, and Ulrich J. Pfeiffer. Clinical review: Complications and risk factors of peripheral arterial catheters used for haemodynamic monitoring in anaesthesia and intensive care medicine, 2002.

[150] James S. Shahoud and Narothama Reddy Aeddula. *Physiology, Arterial Pressure Regulation.* StatPearls Publishing, feb 2019.

[151] P. Shaltis, A. Reisner, and H. Asada. A hydrostatic pressure approach to cuffless blood pressure monitoring. In *Annual International Conference of the IEEE Engineering in Medicine*

and Biology - Proceedings, volume 26 III, pages 2173–2176. Conf Proc IEEE Eng Med Biol Soc, 2004.

[152] Jiang Shao, Ping Shi, Sijung Hu, Yang Liu, and Hongliu Yu. An Optimization Study of Estimating Blood Pressure Models Based on Pulse Arrival Time for Continuous Monitoring. *Journal of Healthcare Engineering*, 2020, 2020.

[153] Zixiao Shen, Fen Miao, Qinghan Meng, and Ye Li. Cuffless and continuous blood pressure estimation based on multiple regression analysis. In *2015 5th International Conference on Information Science and Technology, ICIST 2015*, pages 117–120. Institute of Electrical and Electronics Engineers Inc., oct 2015.

[154] J Šimek, D Wichterle, V Melenovský, J Malík, Š Svačina, and J Widimský. Second Derivative of the Finger Arterial Pressure Waveform: An Insight into Dynamics of the Peripheral Arterial Pressure Pulse. *Physiol. Res*, 54:505–513, 2005.

[155] K. M. Spyer. Annual review prize lecture. Central nervous mechanisms contributing to cardiovascular control. *The Journal of Physiology*, 474(1):1–19, jan 1994.

[156] S Sü Dfeld, S Brechnitz, J Y Wagner, P C Reese, H O Pinnschmidt, D A Reuter, and B Saugel. Post-induction hypotension and early intraoperative hypotension associated with general anaesthesia. *British Journal of Anaesthesia*, 119:57–64, 2017.

[157] J. Abdul Sukor, S. J. Redmond, and N. H. Lovell. Signal quality measures for pulse oximetry through waveform morphology analysis. *Physiological Measurement*, 32(3):369–384, mar 2011.

[158] Yan Sun, Kap Luk Chan, and Shankar Muthu Krishnan. Characteristic wave detection in ECG signal using morphological transform. *BMC Cardiovascular Disorders*, 5(1):28, sep 2005.

[159] Kenji Takazawa. Clinical usefulness of the second derivative of a plethysmogram (acceleration plethysmogram). 1993.

[160] Kenji Takazawa, Nobuhiro Tanaka, Masami Fujita, Osamu Matsuoka, Tokuyu Saiki, Masaru Aikawa, Sinobu Tamura, and Chiharu Ibukiyama. Assessment of vasoactive agents and vascular aging by the second derivative of photoplethysmogram waveform. In *Hypertension*, volume 32, pages 365–370. Lippincott Williams and Wilkins, 1998.

[161] Toshiyo Tamura, Yuka Maeda, Masaki Sekine, and Masaki Yoshida. Wearable Photoplethysmographic Sensors—Past and Present. *Electronics*, 3(2):282–302, apr 2014.

[162] Hideshi Tanaka, Katsuyuki Sakamoto, and Hiroshi Kanai. Indirect Blood Pressure Measurement by the Pulse Wave Velocity Method. *Japanese journal of medical electronics and biological engineering*, 22(1):13–18, feb 1984.

[163] Zunyi Tang, Toshiyo Tamura, Masaki Sekine, Ming Huang, Wenxi Chen, Masaki Yoshida, Kaoru Sakatani, Hiroshi Kobayashi, and Shigehiko Kanaya. A Chair-Based Unobtrusive Cuffless Blood Pressure Monitoring System Based on Pulse Arrival Time. *IEEE Journal of Biomedical and Health Informatics*, 21(5):1194–1205, sep 2017.

[164] M. G. Taylor. Hemodynamics., 1973.

[165] Mohamed Temmar, Piotr Jankowski, Marcel Peltier, Vincent Mouquet, Dorota Debicka-DÄbrowska, Farah Hamida, Kalina Kawecka-Jaszcz, and Michel E. Safar. Intraaortic pulse pressure amplification in subjects at high coronary risk. *Hypertension*, 55(2):327–332, feb 2010.

[166] X. F. Teng and Y. T. Zhang. Continuous and Noninvasive Estimation of Arterial Blood Pressure Using a Photoplethysmographic Approach. In *Annual International Conference of the IEEE Engineering in Medicine and Biology - Proceedings*, volume 4, pages 3153–3156, 2003.

[167] X. F. Teng and Y. T. Zhang. An evaluation of a PTT-based method for noninvasive and cuffless estimation of arterial blood pressure. In *Annual International Conference of the IEEE Engineering in Medicine and Biology - Proceedings*, volume 2006, pages 6049–6052. Conf Proc IEEE Eng Med Biol Soc, 2006.

[168] X. F. Teng and Y. T. Zhang. The effect of applied sensor contact force on pulse transit time. *Physiological Measurement*, 27(8):675–684, aug 2006.

[169] C. T. Ting, M. S. Chang, S. P. Wang, B. N. Chiang, and Frank C.P. Yin. Regional pulse wave velocities in hypertensive and normotensive humans, nov 1990.

[170] Alparslan Turan, Christine Chang, Barak Cohen, Wael Saasouh, Hani Essber, Dongsheng Yang, Chao Ma, Karen Hovsepyan, Ashish K. Khanna, Joseph Vitale, Ami Shah, Kurt Ruetzler, Kamal Maheshwari, and Daniel I. Sessler. Incidence, Severity, and Detection of Blood Pressure Perturbations after Abdominal Surgery: A Prospective Blinded Observational Study. *Anesthesiology*, 130(4):550–559, apr 2019.

[171] Nedya Utami, Agung W. Setiawan, Hasballah Zakaria, Tati R. Mengko, and Richard Mengko. Extracting blood flow parameters from Photoplethysmograph signals: A review. In *Proc. of 2013 3rd Int. Conf. on Instrumentation, Communications, Information Technol., and Biomedical Engineering: Science and Technol. for Improvement of Health, Safety, and Environ., ICICI-BME 2013*, pages 403–407. IEEE Computer Society, 2013.

[172] Judith A.R. Van Waes, Wilton A. Van Klei, Duminda N. Wijeysundera, Leo Van Wolfswinkel, Thomas F. Lindsay, and W. Scott Beattie. Association between intraoperative hypotension and myocardial injury after vascular surgery. *Anesthesiology*, 124(1):35–44, jan 2016.

[173] Orestis Vardoulis, Theodore G. Papaioannou, and Nikolaos Stergiopulos. Validation of a novel and existing algorithms for the estimation of pulse transit time: Advancing the accuracy in pulse wave velocity measurement. *American Journal of Physiology - Heart and Circulatory Physiology*, 304(11), 2013.

[174] S. T. Veerabhadrappa, Anoop Lal Vyas, and Sneh Anand. Estimation of pulse transit time using time delay estimation techniques. In *Proceedings - 2011 4th International Conference on Biomedical Engineering and Informatics, BMEI 2011*, volume 2, pages 739–743, 2011.

[175] Charalambos Vlachopoulos, Konstantinos Aznaouridis, Michael F. O'Rourke, Michel E. Safar, Katerina Baou, and Christodoulos Stefanadis. Prediction of cardiovascular events and all-cause mortality with central haemodynamics: A systematic review and meta-analysis. *European Heart Journal*, 31(15):1865–1871, aug 2010.

[176] Charalambos Vlachopoulos, Konstantinos Aznaouridis, and Christodoulos Stefanadis. Prediction of Cardiovascular Events and All-Cause Mortality With Arterial Stiffness. A Systematic Review and Meta-Analysis. *Journal of the American College of Cardiology*, 55(13):1318–1327, mar 2010.

[177] Mitul Vyas, Joseph L. Izzo, Yves Lacourcière, J. Malcolm O. Arnold, Mark E. Dunlap, Jennifer L. Amato, Marc A. Pfeffer, and Gary F. Mitchell. Augmentation Index and Central Aortic Stiffness in Middle-Aged to Elderly Individuals. *American Journal of Hypertension*, 20(6):642–647, jun 2007.

[178] Michael Walsh, Philip J. Devereaux, Amit X. Garg, Andrea Kurz, Alparslan Turan, Reitze N. Rodseth, Jacek Cywinski, Lehana Thabane, and Daniel I. Sessler. Relationship between intraoperative mean arterial pressure and clinical outcomes after noncardiac surgery: Toward an empirical definition of hypotension. *Anesthesiology*, 119(3):507–515, 2013.

[179] Michael Walsh, Philip J. Devereaux, Amit X. Garg, Andrea Kurz, Alparslan Turan, Reitze N. Rodseth, Jacek Cywinski, Lehana Thabane, and Daniel I. Sessler. Relationship between intraoperative mean arterial pressure and clinical outcomes after noncardiac surgery: Toward an empirical definition of hypotension. *Anesthesiology*, 119(3):507–515, 2013.

[180] Ludi Wang, Wei Zhou, Ying Xing, and Xiaoguang Zhou. A novel neural network model for blood pressure estimation using photoplethesmography without electrocardiogram. *Journal of Healthcare Engineering*, 2018, 2018.

[181] David B. Wax, Hung Mo Lin, and Andrew B. Leibowitz. Invasive and concomitant noninvasive intraoperative blood pressure monitoring: Observed differences in measurements and associated therapeutic interventions. *Anesthesiology*, 115(5):973–978, nov 2011.

[182] Anthony J. Weinhaus. Anatomy of the human heart. In *Handbook of Cardiac Anatomy, Physiology, and Devices, Third Edition*, pages 61–88. Springer International Publishing, jan 2015.

[183] Carl F. Wippermann, Dietmar Schranz, and Ralph G. Huth. Evaluation of the pulse wave arrival time as a marker for blood pressure changes in critically ill infants and children. *Journal of Clinical Monitoring*, 11(5):324–328, sep 1995.

[184] N. A. Wisely and L. B. Cook. Arterial flow waveforms from pulse oximetry compared with measured Doppler flow waveforms. *Anaesthesia*, 56(6):556–561, 2001.

[185] M. Y.M. Wong and Y. T. Zhang. The effects of pre-ejection period on the blood pressure estimation using pulse transit time. In *Proc. 5th Int. Workshop on Wearable and Implantable Body Sensor Networks, BSN2008, in conjunction with the 5th Int. Summer School and Symp. on Medical Devices and Biosensors, ISSS-MDBS 2008*, pages 254–255, 2008.

[186] Mico Yee Man Wong, Emma Pickwell-Macpherson, Yuan Ting Zhang, and Jack C.Y. Cheng. The effects of pre-ejection period on post-exercise systolic blood pressure estimation using the pulse arrival time technique. *European Journal of Applied Physiology*, 111(1):135–144, jan 2011.

[187] Mico Yee Man Wong, Carmen Chung Yan Poon, and Yuan Ting Zhang. An evaluation of the

cuffless blood pressure estimation based on pulse transit time technique: A half year study on normotensive subjects. *Cardiovascular Engineering*, 9(1):32–38, 2009.

[188] Y. M. Wong and Y. T. Zhang. Effects of exercise on the pulse transit time. In *2004 2nd IEEE/EMBS International Summer School on Medical Devices and Biosensors, ISSS-MDBS 2004*, pages 101–102, 2004.

[189] Y. M. Wong and Y. T. Zhang. The effects of exercises on the relationship between pulse transit time and arterial blood pressure. In *Annual International Conference of the IEEE Engineering in Medicine and Biology - Proceedings*, volume 7 VOLS, pages 5576–5578. Institute of Electrical and Electronics Engineers Inc., 2005.

[190] Xiaoman Xing and Mingshan Sun. Optical blood pressure estimation with photoplethysmography and FFT-based neural networks. *Biomedical Optics Express*, 7(8):3007, aug 2016.

[191] Guanqun Zhang, Mingwu Gao, and Ramakrishna Mukkamala. Robust, beat-to-beat estimation of the true pulse transit time from central and peripheral blood pressure or flow waveforms using an arterial tube-load model. In *Proceedings of the Annual International Conference of the IEEE Engineering in Medicine and Biology Society, EMBS*, volume 2011, pages 4291–4294. Conf Proc IEEE Eng Med Biol Soc, 2011.

[192] J. M. Zhang, P. F. Wei, and Y. Li. A LabVIEW based measure system for pulse wave transit time. In *5th Int. Conference on Information Technology and Applications in Biomedicine, ITAB 2008 in conjunction with 2nd Int. Symposium and Summer School on Biomedical and Health Engineering, IS3BHE 2008*, pages 477–480, 2008.

[193] Yue Zhang and Zhimeng Feng. A SVM method for continuous blood pressure estimation from a PPG signal. In *ACM International Conference Proceeding Series*, volume Part F1283, pages 128–132, New York, New York, USA, feb 2017. Association for Computing Machinery.

[194] Yali Zheng, Carmen C.Y. Poon, Bryan P. Yan, and James Y.W. Lau. Pulse Arrival Time Based Cuff-Less and 24-H Wearable Blood Pressure Monitoring and its Diagnostic Value in Hypertension. *Journal of Medical Systems*, 40(9), sep 2016.

Appendices

A

Appendix A

Table A.1: Description of several papers found in the literature.

Year	Features	Model/Method	BP Confidence Interval in mmHg	Sample Size	Subjects/Environment Characteristics	Ref	Notes
2018	Whole-based	AdaBoostR	DBP: -0.05 ± 8.90; SBP: 0.19 ± 4.17	441 subjects (MIMIC) (1323 x 15 seconds recordings)	ICU	[104]	Discrete (15s interval); No Recalibration
2018	41 Features	ANNs	DBP: 2; SBP: 2 (MAE)	42 subjects	Poor information about data aquisition; BP data aquired with sphygmomanomether	[140]	No recalibration
2018	22 Features	ANNs	DBP: 0.10 ± 2.91; SBP: -0.02 ± 4.90	72 subjects (MIMIC)	ICU	[180]	No recalibration
2018	PAT	Linear Regression	DBP: 4 ± 3; SBP: 3 ± 2.5 (MAE)	15 subjects (x 10 measures)	pre and after exercise data acquisiton; BP data aquired with sphygmomanomether	[81]	No recalibration
2016	18 Features	Random Forest	DBP: 4.44 ± 3.72; SBP: 8.29 ± 5.84	285 subjects (MIMIC)	ICU	[56]	Beat-to-Beat; No recalibration
2016	Systolic Amplitude of PPG (150 data points)	ANNs	DBP: 0.01 ± 3.69; SBP: 0.06 ± 5.57	69 subjects (MIMIC)	ICU	[190]	No recalibration; Features and averaged for several seconds
2016	Whole-based	Wavelet Neural Network	DBP: 1.92 ± 2.47; SBP: 2.32 ± 2.91 (MAE)	No information	ICU; Poor information about data aquisition;	[82]	Training/Testing poorly explained; No Recalibration
2016	7 features	AdaBoostR	DBP: 5.35 ± 6.14; SBP: 11.17 ± 10.09 (MAE)	3663 records (∼= 1000 subjects)	ICU	[67]	Calibration-based Model is addressed (improved results); AdaBoostR performed slightly better than Random Forest, SVM, RLR); Parameter-based performed better than whole-based
2015	PAT, HR, ppgSystolicTime, ppgDiastolicTime, ppgK	Stepwise Regression	DBP: 4.01 ± 3.83; SBP: 5.68 ± 6.09 (MAE)	10 subjects	healthy young adults (age ∼= 25); BP data aquired with Finapres-1000 (finger cuff)	[153]	Training/Testing poorly explained; No Recalibration
2015	7 features	SVM	DBP: 6.34 ± 8.45; SBP: 12.38 ± 16.17 (MAE)	No information	ICU; Poor information about data aquisition	[66]	SVM performed better than ANNs; No recalibration
2014	ppgSystolicTime, ppgDiastolicTime, T1	Linear Regression	Complex	22 subjects	young (18-25) vs old (26-50) adults; Poor information about data aquisition; BP data aquired with sphygmomanomether	[144]	No recalibration
2014	ppgSystolicTime, ppgDiastolicTime	Linear Regression + Windkessel Model	DBP: 0.59 ± 10.2; SBP: 0.78 ± 13.1	32 subjects	surgical patients; BP data aquired with sphygmomanomether	[28]	No recalibration; Arithmetic mode over 5 minutes window for features
2013	21 Features	ANNs	DBP: 3.90 ± 3.51; SBP: 3.80 ± 3.46	15000 heartbeats (MIMIC)	ICU; Poor information about data aquisition	[73]	No recalibration
2013	PAT	Linear Regression	DBP: -0.93 ± 1.84; SBP: -0.44 ± 3.85	33 records (25 subjects)	ICU	[27]	Hilbert–Huang transform for ECG/PPG processing; Calibration each hour
2009	PAT, HR	Linear Regression + Adaptive Re-calibration	DBP: -0.07 ± 4.96; SBP: -0.41 ± 7.77 (Tcal = 1 h)	34 records (25 subjects)	ICU	[19]	Different Calibration intervals addressed
2009	PAT	Linear Regression	DBP: 0.0 ± 3.5; SBP: 0.0 ± 4.0	41 subjects	BP data aquired with sphygmomanomether; pre and after exercise data acquisiton	[187]	No recalibration
2008	PAT	Linear Regression	Max SBP error: 8.26; Min SBP error: 1.58	14 subjects (x 5 minutes)	healthy people; BP data aquired with sphygmomanomether;	[192]	No recalibration
2005	PAT, Weight, Arm length	ANNs	SBP: 4.53 ± 2.68	45 subjects (x 4 measures)	healthy men aged between 22 and 32; Poor information about data aquisition	[65]	No recalibration
2005	PAT	Non-Linear Regression	DBP: 0.9 ± 5.6; SBP: 0.6 ± 9.8	85 subjects	BP data aquired with sphygmomanomether;	[129]	Trained with 1 day of data and tested for weeks; No recalibration
2003	ppgDiastolicTime	Linear Regression	DBP: 0.02 ± 4.39; SBP: 0.21 ± 7.32	15 subjects	healthy male subjects; pre, during and after exercise; BP data aquired with oscillometry;	[166]	PPG processing with Continuous Wavelet Transform; Individual Calibration is applied